INJECTABLE POLYURETHANE SCAFFOLDS WITH DELIVERY OF BIOLOGICS FOR SKIN WOUND HEALING

By

Elizabeth Jean Adolph

Dissertation

Submitted to the Faculty of the

Graduate School of Vanderbilt University

in partial fulfillment of the requirements

for the degree of

DOCTOR OF PHILOSOPHY

in

Chemical Engineering

August, 2014

Nashville, Tennessee

Approved:

Professor Scott A. Guelcher

Professor G. Kane Jennings

Professor Jamey D. Young

Professor Jeffrey M. Davidson

To my parents and my sisters

for their love and support

as I completed my PhD

ACKNOWLEDGEMENTS

I would like to begin by acknowledging the funding sources that supported my research, including the National Institutes of Health, the Philanthropic Educational Organization, the Department of Education, and the Vanderbilt Graduate School.

I would like to thank my advisor Dr. Scott Guelcher for his mentorship, guidance, and support throughout my graduate school experience. Thank you for providing me opportunities to work on exciting interdisciplinary research projects and allowing me to participate in programs to enhance my teaching skills. I would also like to thank my continuing committee for their insight and support of my dissertation research: Dr. Kane Jennings, Dr. Jamey Young, and Dr. Jeffrey Davidson.

Thank you to all of my collaborators who have contributed to my research projects. I would especially like to thank the Regeneration Team, including Dr. Jeffrey Davidson, Dr. Lillian Nanney, Dr. Susan Opalenik, Dr. Fang Yu, Dr. Craig Duvall, and Dr. Christopher Nelson, for their guidance and feedback on my research. Thank you to Katarzyna Zienkiewicz, our lab manager who works so hard to keep the lab running smoothly, for help with developing polyurethane formulations over the years.

I want to thank all of the graduate students in the Guelcher lab for their friendship, support, and help with research projects: Dr. Andrea Hafeman, Dr. Jerald Dumas, Dr. Bing Li, Dr. Nazanin Ruppender, Dr. Margarita Prieto-Ballengee, Dr. Jonathan Page, Ruijing Guo, Drew Harmata, Anne Talley, Ushashi Dadwal, and Sichang Lu. I would also like to acknowledge the undergraduate and high school students who have worked on research projects with me, including Courtney Smith, Sally Ingham, Alex Anderson,

Laura Moribe, and Michelle Lu. Furthermore, I want to thank all of my friends, especially my fellow chemical engineering graduate students.

Finally, I would like to thank my family (Anne, Randy, Lisa, and Sara Adolph) for supporting me as I moved out of the great state of Texas to attend graduate school at Vanderbilt.

TABLE OF CONTENTS

Page

LIST OF TABLES

LIST OF FIGURES

Figure Page

LIST OF ABBREVIATIONS

ANOVA	Analysis of variance
αSMA	α-Smooth muscle actin
ATR-FTIR	Attenuated total reflectance-Fourier transform infrared spectroscopy
BMA	Butyl methacrylate
CMC	Carboxymethylcellulose
CTA	Chain transfer agent
DLS	Dynamic light scattering
DMA	Dynamic mechanical analyzer
DMAEE	Bis(2-dimethylaminoethyl)ether
DMAEMA	2-(Dimethylamino)ethyl methacrylate
DMEM	Dulbecco's Modified Eagle Medium
DPBS	Dulbecco's phosphate buffered saline
FBS	Fetal bovine serum
G'	Shear storage modulus
G"	Shear loss modulus
HA	Hyaluronic acid
HPBCD	Hydroxyprolyl β-cyclodextrin
LCST	Lower critical solution temperature
LTI	Lysine triisocyanate
LTIPEG	Lysine triisocyanate-poly(ethylene glycol)
NCO	Isocyanate group
N/P	Amine/phosphate ratio
OH	Hydroxyl group
PAA	Propylacrylic acid
pDNA	Plasmid DNA
PEG	Polyethylene glycol
PEI	Polyethylenimine
PnBA	Poly(n-butyl acrylate)
pNIPAAM	Poly(N-isopropylacrylamide)
PPF	Polypropylene fumarate
pphp	Parts per hundred parts polyol
PUR	Polyurethane
RAFT	Reversible addition fragmentation chain transfer
rhPDGF	Recombinant human platelet-derived growth factor
SEM	Scanning electron microscopy
sFRP2	Secreted Frizzled-related protein-2
siRNA	Short interfering RNA
T_g	Glass transition temperature

CHAPTER I

INTRODUCTION

It is estimated that 35 million cases of significant skin loss occur in the United States each year, of which 7 million become chronic [1]. Furthermore, the aging of the population and the rising incidence of diabetes and vascular disease have resulted in a higher prevalence of chronic wounds. In addition, approximately one million burns require hospital visits each year [2]. These and other cutaneous defects create a need for cost-effective wound care products that restore tissue function. The gold standard for treatment of skin wounds is autograft skin, but it is in limited supply and introduces complications of a second surgery and potential for donor site morbidity [1-3]. Natural and synthetic scaffolds that are currently available, such as Alloderm™ and Integra™, are thin sheets that provide a temporary wound covering but do not fill deep tissue defects [1-4]. Other biomaterials such as hydrogels and nanofibrous scaffolds are biocompatible and biodegradable; however, hydrogels lack sufficient pore structure and mechanical properties, and nanofibrous scaffolds must be pre-formed and cannot conform to irregular defects [3, 5, 6].

Lysine-derived polyurethane (PUR) scaffolds have been used in a variety of tissue engineering applications including bone regeneration and skin wound healing [7-13]. These scaffolds have previously been shown to be biocompatible and biodegradable, and they have tunable physical and mechanical properties. Furthermore, PUR scaffolds have potential for injectability [7, 8]. Injectable scaffolds are advantageous because they allow for site-specific customization, require minimally invasive surgical techniques, and can

conform to fill irregularly shaped wounds [5]. In addition, PUR scaffolds have been used to deliver biologics such as antibiotics and growth factors in animal wound models [9, 10].

In a previous study, implantable PUR scaffolds with delivery of platelet-derived growth factor accelerated tissue infiltration and scaffold degradation in a mouse subcutaneous model [9]. However, injectable PUR scaffolds have not been investigated previously in skin wound healing applications. In addition, PUR scaffolds delivering biologics other than drugs and proteins, such as nucleic acids, have not been studied. Therapeutic proteins are often expensive and difficult to manufacture, but plasmid DNA can be produced more cheaply and efficiently than proteins [14]. Therefore, delivery of plasmid DNA encoding genes for regenerative factors from PUR scaffolds is a promising approach for regenerative medicine applications. In addition, a PUR delivery system for plasmid DNA has potential for use as a screening tool to test the ability of newly discovered regenerative factors to facilitate wound healing.

The goal of this dissertation was to develop an injectable PUR delivery system for biologics such as plasmid DNA. In order to accomplish this goal, the research was focused on two main objectives: developing an injectable PUR scaffold for skin wound healing applications, and delivering plasmid DNA from PUR scaffolds. Chapters III – V discuss the investigation of the effects of injectable and implantable polyurethane scaffolds on skin wound healing in rats and pigs. Chapter VI describes the development of a PUR plasmid delivery system that can be used for local gene therapy applications.

In Chapter III, the development of injectable PUR scaffolds for use in skin wound healing applications is described. Injectable scaffolds are a promising approach for

healing skin defects because they can conform to irregularly shaped defects, allow for patient-specific customization, and be applied with minimally invasive surgical techniques [5]. However, there are many challenges associated with injectable biomaterials. They must be flowable for a sufficient time (the working time) to enable injection and cure within minutes of injection (the setting time) to avoid long surgical procedures. The injected material should not have adverse effects on surrounding host tissue due to the reactivity of specific components or to the release of heat through a reaction exotherm [15]. Porous biomaterials must have suitable pore structure and mechanical properties for cell migration, nutrient exchange, and tissue ingrowth [16].

In this study, the properties of injectable PUR biocomposite scaffolds were characterized *in vitro*, and their capacity to facilitate wound healing was investigated using a rat excisional model. Carboxymethylcellulose or hyaluronic acid was added to the injectable scaffolds as a filler to control the foaming reaction and absorb excess moisture in the wound bed. The scaffolds had a minimal reaction exotherm and clinically relevant working and setting times. Moreover, the mechanical and thermal properties of the scaffolds were consistent with rubbery elastomers. In the rat excisional wound model, injection of settable biocomposite scaffolds stented the wounds at early time points, resulting in a regenerative rather than a scarring phenotype at later time points. Measurements of wound length and thickness revealed that the scaffold-treated wounds were significantly less contracted at day 7 compared to blank wounds. Analysis of cell proliferation and apoptosis showed that the scaffolds were biocompatible and supported tissue ingrowth. Myofibroblast formation and collagen fiber organization provided evidence that the scaffolds had a positive effect on extracellular matrix remodeling by

disrupting the formation of an aligned matrix under elevated tension. In summary, an injectable biodegradable PUR biocomposite scaffold that enhances cutaneous wound healing in a rat model was developed.

Although PUR scaffolds successfully promoted wound healing in a small animal model, large animal models with similarities to human skin needed to be tested to prove scaffold compatibility in a clinically relevant model. Chapter IV describes the investigation of the capacity of implantable lysine-derived PUR scaffolds to support wound healing in a porcine excisional wound model. This model was chosen because pig skin is physiologically and anatomically similar to human skin [17]. To improve cellular infiltration into and attachment to the scaffolds, carboxymethylcellulose was added as a porogen to increase interconnectivity (CMC), and plasma treatment was applied to decrease surface hydrophobicity (Plasma). All three types of PUR scaffolds supported cellular infiltration and were biodegradable. Scaffolds stented the wounds hence reducing unwanted wound contraction compared to untreated wounds at day 15. Wounds treated with CMC and Plasma scaffolds for 15 days showed higher macrophage presence than untreated wounds, a finding that was consistent with macrophage-mediated scaffold degradation via an oxidative mechanism. Cell proliferation decreased from day 8 to day 15 in untreated and scaffold-treated wounds, and scaffolds had no significant effects on apoptosis or blood vessel area density compared to untreated wounds. These results provide further evidence that PUR scaffolds had no adverse effects on the wound healing process. To summarize, PUR scaffolds in porcine excisional wounds supported tissue infiltration, underwent biodegradation, and stented wounds to prevent unwanted contraction.

Chapter V describes the use of injectable PUR scaffolds in a porcine excisional wound model. As described above, injectable scaffolds are advantageous compared to preformed implants due to their abilities to fill the contours of irregularly shaped defects and allow for patient-specific customization [5]. In this study, sucrose was added as a filler to control the PUR foaming reaction through absorption of excess moisture from the wound bed. The physical, mechanical, and rheological properties of the scaffolds were characterized *in vitro*, and injectable and implantable PUR scaffolds were applied in a porcine excisional wound model. Scaffolds had working and setting times of 4.8 ± 1.2 min and 16 ± 3 min, respectively, which are appropriate for the clinical environment. The permeability of the scaffolds ranged from 10^{-10} to 10^{-9} m^2 and was comparable to the permeability of rigid open-cell foams reported elsewhere [18].

In porcine excisional wounds, implantable and injectable scaffolds stented wounds and reduced unwanted contraction at early time points. Although epithelialization was delayed at early time points in scaffold-treated wounds, there were no differences in epithelialization between untreated and scaffold-treated wounds by day 30. The amount of PUR remaining in the wounds decreased over time with only a few fragments remaining after 30 days, providing evidence that the scaffolds underwent biodegradation. There were no differences in fractional area of PUR remaining in the wounds between implantable and injectable treatment groups. The number of proliferating cells decreased from day 9 to day 13 in all treatment groups, and there were no significant differences in apoptosis among scaffold treatment groups. Although the injectable group had fewer macrophages at day 9 and more blood vessels at day 13 compared to the implant group, blood vessel density and macrophage presence decreased

from day 9 to day 13 in all treatment groups. Overall, these results provide evidence that applying PUR scaffolds by injection rather than implantation did not adversely affect the wound healing process or scaffold persistence. In this study, injectable and implantable PUR scaffolds were shown to be biocompatible and biodegradable, reduce wound contraction, and support wound healing in a porcine excisional model.

In Chapter VI, the research focus shifts from the development and testing of injectable PUR scaffolds to the delivery of plasmid DNA from PUR scaffolds. Nonviral gene therapy has potential for safely promoting tissue restoration and treating diseases [14]. One current limitation is that conventional transfection reagents such as polyethylenimine (PEI) form polyplexes with plasmid DNA that suffer from colloidal instability during storage or incorporation into biomaterial scaffolds [19-21]. In this study, a library of poly(ethylene glycol-*b*-(dimethylaminoethyl methacrylate-*co*-butyl methacrylate)) [poly(EG-*b*-(DMAEMA-*co*-BMA))] polymers were synthesized and screened for improved stability and nucleic acid transfection following lyophilization and incorporation into PUR scaffolds. When added to plasmid DNA, the DMAEMA moieties initiate formation of electrostatic polyplexes that are further stabilized by both hydrophobic interactions of the core BMA and steric shielding from the PEG corona. The BMA content in the second block of the copolymer was varied from 0 mol% to 60 mol% in order to optimally tune the balance of electrostatic and hydrophobic interactions in the polyplex core. Polymers with 40% and 50% BMA achieved the highest transfection efficiency.

Diblock copolymers aggregated more slowly than PEI in physiologic buffers, leading to slower aggregation that was reaction-controlled rather than diffusion-

controlled. Polymers with 40% BMA did not aggregate significantly after lyophilization and had higher transfection efficiency than PEI polyplexes both before and after lyophilization. Furthermore, poly(EG-*b*-(DMAEMA-*co*-BMA)) polyplexes exhibited pH-dependent membrane disruption in a red blood cell hemolysis assay and endosomal escape as observed by confocal microscopy. When incorporated into PUR scaffolds as a lyophilized powder, poly(EG-*b*-(DMAEMA-*co*-BMA))-pDNA polyplexes achieved higher transfection than fresh polyplexes injected into the scaffold pores for up to three days. In summary, poly(EG-*b*-(DMAEMA-*co*-BMA))-pDNA polyplexes have the potential to be incorporated into PUR scaffolds for local gene therapy applications due to their colloidal stability, endosomal escape, and resultant high transfection efficiency.

In conclusion, Chapter VII summarizes the results of this dissertation, and Chapter VIII presents suggestions for future studies to build on this work. Overall, this dissertation shows that the use of injectable PUR scaffolds with delivery of biologics is a promising approach for treatment of skin wounds.

References

[1] Clark RAF, Ghosh K, Tonnesen MG. Tissue engineering for cutaneous wounds. Journal of Investigative Dermatology 2007;127:1018-29.
[2] Supp DM, Boyce ST. Engineered skin substitutes: practices and potentials. Clinics in Dermatology 2005;23:403-12.
[3] Lim CT, Zhong SP, Zhang YZ. Tissue scaffolds for skin wound healing and dermal reconstruction. Wiley Interdisciplinary Reviews-Nanomedicine and Nanobiotechnology 2010;2:510-25.
[4] Eccleston GM, Boateng JS, Matthews KH, Stevens HNE. Wound healing dressings and drug delivery systems: A review. Journal of Pharmaceutical Sciences 2008;97:2892-923.
[5] Mikos AG, Kretlow JD, Klouda L. Injectable matrices and scaffolds for drug delivery in tissue engineering. Advanced Drug Delivery Reviews 2007;59:263-73.
[6] Ferguson MWJ, Metcalfe AD. Bioengineering skin using mechanisms of regeneration and repair. Biomaterials 2007;28:5100-13.
[7] Dumas JE, BrownBaer PB, Prieto EM, Guda T, Hale RG, Wenke JC, et al. Injectable reactive biocomposites for bone healing in critical-size rabbit calvarial defects. Biomedical materials (Bristol, England) 2012;7:024112.
[8] Guelcher SA, Dumas JE, Zienkiewicz K, Tanner SA, Prieto EM, Bhattacharyya S. Synthesis and Characterization of an Injectable Allograft Bone/Polymer Composite Bone Void Filler with Tunable Mechanical Properties. Tissue Engineering Part A 2010;16:2505-18.
[9] Guelcher SA, Li B, Davidson JM. The effect of the local delivery of platelet-derived growth factor from reactive two-component polyurethane scaffolds on the healing in rat skin excisional wounds. Biomaterials 2009;30:3486-94.
[10] Guelcher SA, Li B, Brown KV, Wenke JC. Sustained release of vancomycin from polyurethane scaffolds inhibits infection of bone wounds in a rat femoral segmental defect model. Journal of Controlled Release 2010;145:221-30.
[11] Guelcher SA. Biodegradable polyurethanes: Synthesis and applications in regenerative medicine. Tissue Engineering Part B-Reviews 2008;14:3-17.
[12] Guelcher SA, Hafeman AE, Zienkiewicz KJ, Zachman AL, Sung HJ, Nanney LB, et al. Characterization of the degradation mechanisms of lysine-derived aliphatic poly(ester urethane) scaffolds. Biomaterials 2011;32:419-29.
[13] Guelcher SA, Patel V, Gallagher KM, Connolly S, Didier JE, Doctor JS, et al. Synthesis and in vitro biocompatibility of injectable polyurethane foam scaffolds. Tissue Engineering 2006;12:1247-59.
[14] Kim SW, Park TG, Jeong JH. Current status of polymeric gene delivery systems. Advanced Drug Delivery Reviews 2006;58:467-86.
[15] Belkoff SM, Deramond H, Wright NT. Temperature elevation caused by bone cement polymerization during vertebroplasty. Bone 1999;25:17s-21s.
[16] Laurencin CT, Khan Y, Yaszemski MJ, Mikos AG. Tissue engineering of bone: Material and matrix considerations. Journal of Bone and Joint Surgery-American Volume 2008;90A:36-42.

[17] Sullivan TP, Eaglstein WH, Davis SC, Mertz P. The pig as a model for human wound healing. Wound repair and regeneration : official publication of the Wound Healing Society [and] the European Tissue Repair Society 2001;9:66-76.
[18] Zhao W, Pizzi A, Fierro V, Du G, Celzard A. Effect of composition and processing parameters on the characteristics of tannin-based rigid foams. Part I: Cell structure. Materials Chemistry and Physics 2010;122:175-82.
[19] Segura T, Lei YG, Huang SX, Sharif-Kashani P, Chen Y, Kavehpour P. Incorporation of active DNA/cationic polymer polyplexes into hydrogel scaffolds. Biomaterials 2010;31:9106-16.
[20] Kichler A, Chillon M, Leborgne C, Danos O, Frisch B. Intranasal gene delivery with a polyethylenimine-PEG conjugate. Journal of controlled release : official journal of the Controlled Release Society 2002;81:379-88.
[21] Mooney DJ, Hahn LD, Kong H. Polycation Structure Mediates Expression of Lyophilized Polycation/pDNA Complexes. Macromolecular Bioscience 2010;10:1210-5.

CHAPTER II

BACKGROUND

Wound Healing

Skin functions as a barrier against infectious agents, prevents dehydration, and performs immune surveillance and self-healing [1]. When skin is wounded, healing progresses through several stages to restore tissue function: (1) hemostasis and inflammation, (2) proliferation and granulation tissue formation, and (3) remodeling. Hemostasis, characterized by vasoconstriction and fibrin clot formation, occurs within minutes of injury to restrict blood loss. Neutrophils and later macrophages infiltrate the wound site to phagocytose microorganisms and secrete growth factors. In the proliferative phase, granulation tissue containing fibroblasts, macrophages, new blood vessels, and extracellular matrix (ECM) components is formed within days after injury. After migrating to the wound site in response to growth factor signals, fibroblasts proliferate and produce ECM components such as collagen. Tensile forces and growth factors stimulate fibroblasts to differentiate into myofibroblasts, which have a highly contractile and synthetic phenotype. Angiogenesis, the sprouting of new blood vessels from existing ones, occurs in order to supply oxygen and nutrients to the wound site. Keratinocytes in adjacent skin proliferate and begin migrating over the wound site. During the remodeling phase, which occurs from weeks to months after injury, the cellular granulation tissue is replaced by relatively acellular scar tissue. The number of fibroblasts and myofibroblasts decreases due to apoptosis. Angiogenesis ceases, and the number of blood vessels declines. Fibroblasts remodel the ECM, rearranging collagen fibers so that they support the tensile strength of skin. The healing process restores the

functions of the skin, but it does not result in regeneration. Rather, scarring occurs, and the tensile strength of healed skin never reaches that of native skin [1-7].

Abnormal Healing

Wound healing is a complex process involving coordinated interactions among different cell types, growth factors, and ECM components. When this process is disrupted, abnormal healing can result. Estimates suggest that 35 million cases of significant skin loss occur in the United States each year, of which 7 million become chronic and infected [8]. Over 2 million Americans suffer from chronic ulcers, requiring treatment costs of approximately $8 billion per year [8]. Chronic wounds are characterized by prolongation of the inflammatory phase, abnormal levels of growth factors, increased levels of proteases, and decreased ECM production [2-4]. Moreover, approximately one million burns require hospital visits each year, and hypertrophic scarring occurs in 90% of these injuries [9]. Hypertrophic scars result from increased myofibroblast formation, decreased protease levels, and excessive production of collagen [2-4]. These and other cutaneous defects create a need for cost-effective wound care products that restore skin function.

Current Standard of Care

Autograft skin, which is transplanted from an uninjured location on the patient's body, is the current gold standard for treatment of burns and traumatic injuries [8]. However, autografts are in limited supply. Autograft transplantation requires additional surgery to harvest the skin, which causes pain and can result in donor site morbidity [8].

Allograft skin (usually taken from cadavers) avoids the complications of a second surgery, but it introduces the risk of immune rejection and is also in limited supply [8, 9]. Alloskin™ is a cellular graft containing both epidermis and dermis that is used for acute and chronic wound therapy [10]. In order to retain the benefits of autografts and allografts while avoiding some of the risks, cellular skin substitute products that incorporate autologous keratinocytes in a natural or synthetic matrix, such as EpiCel® and Bioseed™, have been developed [8, 9, 11]. A small punch biopsy is used to obtain the cells, so expensive and invasive surgery is not needed [9]. Since the cells are autologous, immune rejection is avoided. EpiCel® has served as a permanent wound coverage that reduced the appearance of scarring in burns and diabetic ulcers [2, 8, 9]. However, disadvantages of these treatments include high costs, long time needed to culture cells (2-3 weeks), labor intensive procedures, and scaffold fragility [2, 9].

Natural and Synthetic Scaffolds

A variety of acellular scaffolds comprising natural and/or synthetic polymers have been developed in order to overcome the challenges associated with autograft and allograft skin. Alloderm™ is a scaffold comprising decellularized allograft tissue that has been used to treat chronic wounds and burns [1, 8, 9, 11]. Integra™, a scaffold composed of both natural (bovine collagen-glycosaminoglycan) and synthetic (silicone) components, has been used to treat burns [1, 8, 9, 11]. Oasis™, a skin substitute derived from porcine small intestinal submucosa, has accelerated healing in chronic leg ulcers [8, 12]. Although over 200,000 people have been treated with tissue-engineered skin substitutes, none of these products fully restores the functions of native skin [8]. Skin

substitutes currently only lead to a 25% increase in healing of chronic leg ulcers compared to standard of care [8]. These scaffolds are thin sheets that do not function as void fillers for deep tissue defects. They often serve as temporary skin substitutes that require additional treatments such as autografts [1].

Research on other tissue engineered scaffolds, such as hydrogels and nanofibrous scaffolds, focuses on providing molecular cues for tissue repair. Hydrogels composed of natural or synthetic polymers such as polyethylene glycol, alginate, hyaluronic acid, and chitosan have been used successfully in drug and growth factor delivery applications in a variety of tissues, including skin and bone [1, 13-18]. Hydrogels are advantageous due to their biodegradability and injectability. Furthermore, many hydrogels are "smart" biomaterials that undergo a phase transition in response to environmental stimuli such as temperature, pH, or ionic strength. However, their small pore size and low porosity can result in delayed infiltration and vascularization, and their low strength and stiffness do not provide mechanical support for tissue infiltration and matrix remodeling [1, 14, 16, 18].

Nanofibrous meshes have been used as wound dressings and as three-dimensional tissue engineering scaffolds. They mimic the structure and function of natural ECM, and their high surface area to volume ratio and high porosity (up to 90%) result in excellent permeability for oxygen and nutrients [1, 14]. A study by Scherer et al. showed that poly-N-acetyl-glucosamine nanofibrous membranes enhanced keratinocyte migration, cell proliferation, and angiogenesis in cutaneous wounds in diabetic mice [19]. In another study, nanofibrous meshes used as wound dressings were shown to promote hemostasis and cell respiration while preventing infection [20]. However, nanofibrous scaffolds must

be pre-formed using techniques such as electrospinning [1, 14]. Thus, they must be implanted rather than injected, and they cannot conform to large irregularly shaped wounds.

Injectable Scaffolds

Injectable scaffolds are advantageous due to their abilities to incorporate and deliver biologics at the point of care, allow for patient specific customization, conform to fill irregular tissue defects, and be applied with minimally invasive surgical techniques. Several techniques are being investigated for fabrication of injectable scaffolds, including ionic crosslinking, self-assembly, thermogelling, and *in situ* polymerization and crosslinking [18]. Examples of each of these systems are discussed below.

Alginate and chitosan are naturally derived biomaterials that can undergo ionic crosslinking with divalent cations such as calcium [11, 18, 21]. These biomaterials are beneficial for use in drug delivery due to their biocompatibility, tunable degradation rate, stabilizing effects on drugs, and ability to target specific tissues. One approach to creating injectable drug delivery systems using ionic crosslinking systems involves mixing a solution of alginate or chitosan, an anionic drug, and lipid vesicles containing calcium ions into the targeted tissue [21]. The vesicles are disrupted upon the temperature increase to 37˚C, resulting in rapid release of calcium and formation of an alginate or chitosan gel incorporating the drug. The drug is encapsulated and stabilized in the biomaterial matrix due to electrostatic interactions.

Self-assembling systems are commonly used for drug delivery applications. They are advantageous because they do not involve potentially cytotoxic compounds such as

catalysts and initiators, but they have weak mechanical properties due to the absence of covalent crosslinking [18, 22]. One approach to creating self-assembling systems is phase separation. In these systems, a water insoluble polymer is dissolved in a biocompatible organic solvent such as dimethyl sulfoxide. When injected in a physiologic environment, the polymer precipitates to form a gel. A study by Tae et al. demonstrated that a fluorocarbon-functionalized poly(ethylene glycol) phase separation system delivered therapeutic proteins with diffusion-controlled release kinetics [22].

Poly(N-isopropylacrylamide) (pNIPAAM) is a synthetic thermogelling polymer. It is advantageous for use as an injectable drug delivery system due to its lower critical solution temperature (LCST) of 32˚C, which is between room temperature and physiologic temperature. An aqueous solution containing pNIPAAM can be mixed with the drug and injected into the targeted tissue, where it forms a gel. However, pNIPAAM exhibits cytotoxicity and has a slow degradation rate. Therefore, it is incorporated into a copolymer or blended with a biocompatible polymer when used in drug delivery applications. Liposomes and nanoparticles incorporating pNIPAAM have been used to deliver doxorubicin, a drug for cancer therapy [23, 24]. When the temperature is increased above pNIPAAM's LCST, pNIPAAM disrupts the liposomal membrane [23] or collapses the nanoparticles [24], resulting in a burst release of the drug. Sustained delivery of the drugs dexamethasone and ascorbate from pNIPAAM hydrogels successfully promoted chondrocyte differentiation when injected in mice subcutaneous wounds. Furthermore, copolymers of pNIPAAM are widely used due to their thermosensitivity. An injectable poly(NIPAAM-co-propylacrylic acid (PAA)) copolymer has been developed for use as a delivery vehicle for angiogenic factors to sites of

ischemia, such as diabetic ulcers [25]. The copolymer is temperature-sensitive (due to NIPAAM) and pH-sensitive (due to PAA). It forms a gel at physiologic temperature and low pH, which are the conditions present in an ischemic site. The gel has been shown to release the encapsulated angiogenic drug in a sustained manner [25]. When ischemia is eliminated and the tissue returns to physiologic pH, the polymer quickly degrades due to the phase transition of the PAA component from a gel to a solution [25].

Although they are beneficial for drug delivery systems, self-assembling and thermogelling systems are not well-suited for tissue engineering applications due to their weak mechanical properties (low modulus, low strength, and high fragility). *In situ* polymerizable scaffolds can achieve robust mechanical properties due to polymerization and crosslinking. However, they must meet several requirements in order to be used in biomedical applications: they must have nontoxic reactants and intermediates, minimal reaction exotherm, reproducible and robust mechanical properties, and clinically relevant working and setting times (on the order of minutes) [18]. Two biocompatible and biodegradable polymers that meet these requirements are polypropylene fumarate and polyurethane.

Polypropylene fumarate (PPF) is a viscous liquid with unsaturated carbon-carbon double bonds that can be crosslinked to form a solid polymeric network. Due to its high strength and stiffness, PPF is well-suited for use in hard tissue applications such as bone regeneration [26]. PPF is biodegradable to noncytotoxic degradation products (fumaric acid and propylene glycol) via hydrolysis of its ester bonds [26]. Furthermore, PPF can be combined with crosslinking agents such as diethyl fumarate, poly(ethylene glycol), polycaprolactone, or N-vinyl pyrrolidinone to form a copolymer with tunable physical

and mechanical properties [27]. In several injectable delivery systems, PPF is mixed with an initiator and crosslinking agent and injected into the targeted tissue. The polymer is then crosslinked *in situ* to form a solid polymeric network. Injectable scaffolds incorporating PPF have been used to deliver osteogenic peptides and transforming growth factor-β1 in bone tissue engineering applications and the drugs acetazolamide, dichlorphenamide, and timolol maleate in ophthalmic applications [26-28].

Polyurethane Scaffolds

Polyurethane (PUR) has been used in biodegradable medical devices since the 1980s [29]. It is advantageous for the field of tissue engineering due to its biocompatibility, biodegradability to nontoxic decomposition products, tunable mechanical and degradation properties, reproducible pore structure, and potential for injectability and use as a delivery vehicle [30-33]. Polyurethane is synthesized from the reaction of a polyol and an isocyanate. Hydroxyl groups from the polyol react with isocyanates to form urethane bonds. In addition, water can be added to the reaction. Water reacts with isocyanates to from carbamic acid, an unstable compound that quickly decomposes to an amine and carbon dioxide. The amine can further react with an isocyanate to form a disubstituted urea. In the Guelcher lab, we use polyols comprising glycolide, lactide and caprolactone [30, 32, 33]. These compounds have been commonly used in tissue engineering and drug delivery applications [18, 34-37]. We use lysine-derived aliphatic polyisocyanates such as lysine triisocyanate (LTI) because they are biocompatible and degrade to nontoxic decomposition products [30, 31]. By adjusting the composition and molecular weight of the polyol and isocyanate and the amount of water,

the physical, mechanical, and degradation properties of PUR can be tuned [30-32]. As a result, PUR is a versatile biomaterial that is suitable for use with both soft tissues (such as skin) and hard tissues (such as bone).

Our lab has used PUR scaffolds to enhance bone regeneration and skin wound healing in several animal models. One study demonstrated that injectable allograft bone/PUR composite scaffolds supported tissue infiltration and new bone formation in femoral plug defects in rats [38]. Another study showed that compression-molded mineralized bone particle/PUR composites exhibited cellular infiltration, resorption, and new bone formation in femoral plug defects in rabbits [39]. Injectable allograft bone/PUR composite scaffolds supported ingrowth of new bone in a critical-size rabbit calvarial defect model, and delivery of bone morphogenetic protein-2 from the biocomposites enhanced new bone formation [40].

Furthermore, PUR scaffolds have been tested in several studies investigating skin wound healing. Pre-formed PUR implants developed for cutaneous healing supported cellular infiltration and ECM synthesis in both subcutaneous and excisional wounds in rats [41, 42]. Although they serve as a provisional ECM and support cellular infiltration and remodeling, PUR scaffolds alone are not enough to accelerate wound healing. PUR scaffolds also have the potential to serve as delivery vehicles for growth factors, nucleic acids, and small molecule drugs to enhance wound healing. For example, a study by Li et al. showed that delivery of platelet-derived growth factor from PUR implants resulted in increased fibroblast infiltration and accelerated granulation tissue formation and scaffold degradation compared to blank PUR scaffolds in rat excisional wounds [42].

Porcine Wound Model

Animal models are advantageous for studying wound healing because there is less variation than in the clinical setting, there are few limits to obtaining tissue samples, and different treatments can be compared in the same animal [43]. Small animal models are useful when a large number of animals or certain characteristics (such as a compromised immune system or transgenic animals) are required [43]. Several previous studies on the use of PUR scaffolds in wound healing applications have used rat wound models [31, 41, 42]. However, rat skin differs from human skin physiologically and anatomically. The dermis and epidermis are thinner in rats than in humans, rat skin has lower vascular density than human skin, and rats heal primarily through contraction rather than through epithelialization and production of granulation tissue [44]. In contrast, pig skin is physiologically and anatomically similar to human skin [44]. Pig skin and human skin have similar density and distribution of blood vessels, sweat glands, and hair follicles [44]. Furthermore, pigs and humans have similar epidermal thickness and close primarily through epithelialization rather than contraction [44]. In addition, the porcine wound model is advantageous because each animal has a large area of skin available for experimentation. Therefore, several treatments can be applied on the same animal, which reduces variability [43].

Previous studies have investigated the use of void-filling scaffolds in porcine wound models, but this research has been limited to preformed implants and does not include injectable scaffolds [45-48]. A study by Huang et al. treated full-thickness porcine wounds with a bilayer dressing comprising an external PUR layer and an internal gelatin sponge layer incorporating basic fibroblast growth factor-loaded microspheres

[45]. After 21 days, wounds treated with these dressings had smaller areas, thicker epidermis, and better collagen organization than control wounds treated with Vaseline gauze. Studies by Greenwood and Dearman investigated the use of biodegradable PUR foams and spun mats as a temporizing matrix prior to skin graft surgery [46, 47]. Porcine excisional wounds treated with a PUR foam sealed with a microporous PUR membrane had no signs of infection and delayed contraction compared to wounds treated with Integra after 28 days. However, wounds treated with unsealed foams exhibited significant contraction and had thick scar layers above the implants. No studies have shown that single-layer void filling scaffolds without the use of protective membranes facilitate dermal wound healing in a full-thickness porcine excisional wound model. Furthermore, the use of injectable scaffolds in porcine cutaneous wound models has not been investigated.

Gene Therapy

One advantage of PUR scaffolds is their ability to incorporate and deliver biologics. A promising strategy for delivering regenerative factors from PUR scaffolds is to release plasmid DNA (pDNA) encoding genes for growth factors that enhance wound healing. Proteins are often expensive and difficult to manufacture, and gene therapy is an alternative to conventional protein therapy that avoids these problems [49]. Nonviral gene therapy has potential for use in accelerating restoration of tissue defects and treatment of myriad diseases. Plasmid production is efficient and relatively inexpensive, and DNA therapy avoids the immunogenic risk associated with viral vectors.

Naked pDNA uptake and utilization is inefficient; however, synthetic polymer- and lipid-based carriers face several *in vivo* challenges, and there has been limited translation of efficient and nontoxic nonviral options for pDNA delivery. An ideal transfection reagent for pDNA delivery *in vivo* should condense pDNA into stable nanoparticles, minimize aggregation in physiological conditions (i.e., presence of proteins and salts), and protect the plasmid from nuclease degradation in the extracellular environment. After endocytosis, the vectors must escape the endo-lysosomal pathways to avoid degradation or exocytosis, and the plasmid must be unpackaged and trafficked to the nucleus.

Electrostatic condensation of plasmids into nanoparticles using cationic polymers or lipids is a promising approach for overcoming *in vivo* barriers to nonviral gene therapy. Lipofectamine2000 is a cationic lipid that achieves high transfection efficiency in a wide range of cell lines *in vitro*, but several studies have reported high cytotoxicity [50, 51]. Polyethylenimine (PEI) is one of the most commonly used polymeric vectors for DNA delivery due to its low immunogenicity, high transfection efficiency, and low manufacturing cost [49, 52-55]. After entering cells through endocytosis, polyplexes made from amine-containing polymers with pKa in the range 5.0 – 7.4 (such as PEI) are presumed to buffer the acidification of the vesicles of the endo-lysosomal trafficking pathways. This "proton sponge" behavior increases proton and counterion influx and causes osmotic swelling and rupture of endosomes, enabling pDNA cytoplasmic entry [56]. While direct injection of PEI-pDNA polyplexes has been used successfully *in vivo* for a number of tissue types, effective delivery of polyplexes from tissue engineering scaffolds has been challenging due to aggregation of the polyplex nanoparticles [52, 53,

57-59]. Recently, lyophilization of PEI-pDNA polyplexes with excipients such as sucrose has reduced polyplex aggregation and increased transfection efficiency [53, 60]. However, approaches to improve the inherent stability of the polymer-pDNA polyplexes and studies on the contribution of colloidal stability to transfection efficiency have not been extensively investigated.

Block copolymers are a promising strategy to improve colloidal stability, increase transfection efficiency, and decrease cytotoxicity of nonviral carriers. Complexation of pDNA with block copolymers comprising polycations and polyethylene glycol (PEG) has been reported to enhance steric stability of the resulting polyplexes by formation of a PEG corona [61-63]. Furthermore, adding hydrophobic components into the cationic, pDNA-condensing polymer block has also been investigated as a strategy for reducing charge density, increasing stability, decreasing toxicity, and enhancing endosomal escape of polycations. For example, increasing hydrophobicity and decreasing charge density through the modification of poly(amido amines) with benzoyl groups was found to increase polyplex stability, decrease cytotoxicity, and increase transfection efficiency [64, 65]. In other studies, the ratio of cationic DMAEMA to hydrophobic butyl methacrylate (BMA) or propylacrylic acid (PPAA) has been optimized to achieve pH-dependent membrane disruptive properties ideally tuned for endosomal escape [66-68]. Recently, Nelson et al. investigated a PEG-stabilized polyplex system in which siRNA cargo was loaded into the poly(BMA-*co*-DMAEMA) particle core and yielded enhanced performance following intravenous injection *in vivo* [69]. Due to their high transfection efficiency and stability *in vivo*, these polymers have potential for use as transfection reagents in PUR nucleic acid delivery systems for wound healing applications.

Conclusion

In summary, the research on skin wound healing and tissue engineering scaffolds supports the need for an injectable, biodegradable polyurethane scaffold that serves as a delivery system for biologics such as nucleic acids. My research is divided into aims that address different aspects of developing this scaffold: (1) creating an injectable PUR scaffold and applying it in a rat wound model, (2) investigating the effects of implantable PUR scaffolds on porcine wound healing, (3) testing the use of injectable PUR scaffolds in porcine wounds, and (4) developing a PUR delivery system for nucleic acids. Chapters III – VI discuss each of these aims.

References

[1] Lim CT, Zhong SP, Zhang YZ. Tissue scaffolds for skin wound healing and dermal reconstruction. Wiley Interdisciplinary Reviews-Nanomedicine and Nanobiotechnology 2010;2:510-25.
[2] Singer AJ, Clark RAF. Mechanisms of disease - Cutaneous wound healing. New England Journal of Medicine 1999;341:738-46.
[3] Schultz GS, Wysocki A. Interactions between extracellular matrix and growth factors in wound healing. Wound Repair and Regeneration 2009;17:153-62.
[4] Kahari VM, Toriseva M. Proteinases in cutaneous wound healing. Cellular and Molecular Life Sciences 2009;66:203-24.
[5] Gurtner GC, Werner S, Barrandon Y, Longaker MT. Wound repair and regeneration. Nature 2008;453:314-21.
[6] Hinz B. The myofibroblast: Paradigm for a mechanically active cell. Journal of Biomechanics 2010;43:146-55.
[7] Herman IM, Schultz GS, Davidson JM, Kirsner RS, Bornstein P. Dynamic reciprocity in the wound microenvironment. Wound Repair and Regeneration 2011;19:134-48.
[8] Clark RAF, Ghosh K, Tonnesen MG. Tissue engineering for cutaneous wounds. Journal of Investigative Dermatology 2007;127:1018-29.
[9] Supp DM, Boyce ST. Engineered skin substitutes: practices and potentials. Clinics in Dermatology 2005;23:403-12.
[10] Wound Care. AlloSource 2013. Accessed April 2014 from allosource.org/products/alloskin-2/
[11] Eccleston GM, Boateng JS, Matthews KH, Stevens HNE. Wound healing dressings and drug delivery systems: A review. Journal of Pharmaceutical Sciences 2008;97:2892-923.
[12] Mostow EN, Haraway GD, Dalsing M, Hodde JP, King D, Grp OVUS, et al. Effectiveness of an extracellular matrix graft (OASIS Wound Matrix) in the treatment of chronic leg ulcers: A randomized clinical trial. Journal of Vascular Surgery 2005;41:837-43.
[13] Friess W. Collagen--biomaterial for drug delivery. European journal of pharmaceutics and biopharmaceutics : official journal of Arbeitsgemeinschaft fur Pharmazeutische Verfahrenstechnik eV 1998;45:113-36.
[14] Ferguson MWJ, Metcalfe AD. Bioengineering skin using mechanisms of regeneration and repair. Biomaterials 2007;28:5100-13.
[15] Augst AD, Kong HJ, Mooney DJ. Alginate hydrogels as biomaterials. Macromolecular Bioscience 2006;6:623-33.
[16] Mooney DJ, Chen RR. Polymeric growth factor delivery strategies for tissue engineering. Pharmaceutical research 2003;20:1103-12.
[17] Mizuno K, Yamamura K, Yano K, Osada T, Saeki S, Takimoto N, et al. Effect of chitosan film containing basic fibroblast growth factor on wound healing in genetically diabetic mice. Journal of Biomedical Materials Research Part A 2003;64A:177-81.
[18] Mikos AG, Kretlow JD, Klouda L. Injectable matrices and scaffolds for drug delivery in tissue engineering. Advanced Drug Delivery Reviews 2007;59:263-73.

[19] Scherer SS, Pietramaggiori G, Matthews J, Perry S, Assmann A, Seth A, et al. Biodegradable poly-n-acetyl glucosamine (pglcnac) nanofibers enhance wound healing by activating cell migration, angiogenesis and cell proliferation. Wound Repair and Regeneration 2008;16:A78-A.
[20] Abrigo M, McArthur SL, Kingshott P. Electrospun Nanofibers as Dressings for Chronic Wound Care: Advances, Challenges, and Future Prospects. Macromolecular Bioscience 2014:n/a-n/a.
[21] Wang JJ, Zeng ZW, Xiao RZ, Xie T, Zhou GL, Zhan XR, et al. Recent advances of chitosan nanoparticles as drug carriers. International journal of nanomedicine 2011;6:765-74.
[22] Tae G, Kornfield JA, Hubbell JA. Sustained release of human growth hormone from in situ forming hydrogels using self-assembly of fluoroalkyl-ended poly(ethylene glycol). Biomaterials 2005;26:5259-66.
[23] Ta T, Convertine AJ, Reyes CR, Stayton PS, Porter TM. Thermosensitive liposomes modified with poly(N-isopropylacrylamide-co-propylacrylic acid) copolymers for triggered release of doxorubicin. Biomacromolecules 2010;11:1915-20.
[24] Rahimi M, Kilaru S, Sleiman GE, Saleh A, Rudkevich D, Nguyen K. Synthesis and Characterization of Thermo-Sensitive Nanoparticles for Drug Delivery Applications. Journal of biomedical nanotechnology 2008;4:482-90.
[25] Garbern JC, Hoffman AS, Stayton PS. Injectable pH- and temperature-responsive poly(N-isopropylacrylamide-co-propylacrylic acid) copolymers for delivery of angiogenic growth factors. Biomacromolecules 2010;11:1833-9.
[26] Kasper FK, Tanahashi K, Fisher JP, Mikos AG. Synthesis of poly(propylene fumarate). Nature protocols 2009;4:518-25.
[27] Fisher JP, Dean D, Mikos AG. Photocrosslinking characteristics and mechanical properties of diethyl fumarate/poly(propylene fumarate) biomaterials. Biomaterials 2002;23:4333-43.
[28] Hacker MC, Haesslein A, Ueda H, Foster WJ, Garcia CA, Ammon DM, et al. Biodegradable fumarate-based drug-delivery systems for ophthalmic applications. Journal of biomedical materials research Part A 2009;88:976-89.
[29] Guelcher SA. Biodegradable polyurethanes: Synthesis and applications in regenerative medicine. Tissue Engineering Part B-Reviews 2008;14:3-17.
[30] Guelcher SA, Srinivasan A, Dumas JE, Didier JE, McBride S, Hollinger JO. Synthesis, mechanical properties, biocompatibility, and biodegradation of polyurethane networks from lysine polyisocyanates. Biomaterials 2008;29:1762-75.
[31] Guelcher SA, Hafeman AE, Zienkiewicz KJ, Zachman AL, Sung HJ, Nanney LB, et al. Characterization of the degradation mechanisms of lysine-derived aliphatic poly(ester urethane) scaffolds. Biomaterials 2011;32:419-29.
[32] Guelcher S, Srinivasan A, Hafeman A, Gallagher K, Doctor J, Khetan S, et al. Synthesis, In vitro degradation, and mechanical properties of two-component poly(ester urethane)urea scaffolds: Effects of water and polyol composition. Tissue Engineering 2007;13:2321-33.
[33] Guelcher SA, Patel V, Gallagher KM, Connolly S, Didier JE, Doctor JS, et al. Synthesis and in vitro biocompatibility of injectable polyurethane foam scaffolds. Tissue Engineering 2006;12:1247-59.

[34] Taira M, Araki Y, Takahashi J. Scaffold consisting of poly (lactide-caprolactone) sponge, collagen gel and bone marrow stromal cells for tissue engineering. Journal of Materials Science Letters 2001;20:1773-4.
[35] Wang SG, Yang J, Shi GX, Bei JZ, Cao YL, Shang QX, et al. Fabrication and surface modification of macroporous poly(L-lactic acid) and poly(L-lactic-co-glycolic acid) (70/30) cell scaffolds for human skin fibroblast cell culture. Journal of Biomedical Materials Research 2002;62:438-46.
[36] Kim SH, Lee SH, Kim BS, Choi SW, Jeong SI, Kwon IK, et al. Elastic biodegradable poly(glycolide-co-caprolactone) scaffold for tissue engineering. Journal of Biomedical Materials Research Part A 2003;66A:29-37.
[37] Vaquette C, Frochot C, Rahouadj R, Muller S, Wang X. Mechanical and biological characterization of a porous poly-L-lactic acid-co-epsilon-caprolactone scaffold for tissue engineering. Soft Materials 2008;6:25-33.
[38] Guelcher SA, Dumas JE, Zienkiewicz K, Tanner SA, Prieto EM, Bhattacharyya S. Synthesis and Characterization of an Injectable Allograft Bone/Polymer Composite Bone Void Filler with Tunable Mechanical Properties. Tissue Engineering Part A 2010;16:2505-18.
[39] Guelcher SA, Dumas JE, Davis T, Holt GE, Yoshii T, Perrien DS, et al. Synthesis, characterization, and remodeling of weight-bearing allograft bone/polyurethane composites in the rabbit. Acta Biomaterialia 2010;6:2394-406.
[40] Dumas JE, BrownBaer PB, Prieto EM, Guda T, Hale RG, Wenke JC, et al. Injectable reactive biocomposites for bone healing in critical-size rabbit calvarial defects. Biomedical materials (Bristol, England) 2012;7:024112.
[41] Guelcher SA, Hafeman AE, Li B, Yoshii T, Zienkiewicz K, Davidson JM. Injectable biodegradable polyurethane scaffolds with release of platelet-derived growth factor for tissue repair and regeneration. Pharmaceutical research 2008;25:2387-99.
[42] Guelcher SA, Li B, Davidson JM. The effect of the local delivery of platelet-derived growth factor from reactive two-component polyurethane scaffolds on the healing in rat skin excisional wounds. Biomaterials 2009;30:3486-94.
[43] Middelkoop E, van den Bogaerdt AJ, Lamme EN, Hoekstra MJ, Brandsma K, Ulrich MMW. Porcine wound models for skin substitution and burn treatment. Biomaterials 2004;25:1559-67.
[44] Sullivan TP, Eaglstein WH, Davis SC, Mertz P. The pig as a model for human wound healing. Wound repair and regeneration : official publication of the Wound Healing Society [and] the European Tissue Repair Society 2001;9:66-76.
[45] Huang S, Deng T, Wu H, Chen F, Jin Y. Wound dressings containing bFGF-impregnated microspheres. Journal of Microencapsulation 2006;23:277-90.
[46] Greenwood JE, Dearman BL. Split skin graft application over an integrating, biodegradable temporizing polymer matrix: immediate and delayed. Journal of burn care & research : official publication of the American Burn Association 2012;33:7-19.
[47] Greenwood JE, Dearman BL. Comparison of a sealed, polymer foam biodegradable temporizing matrix against Integra(R) dermal regeneration template in a porcine wound model. Journal of burn care & research : official publication of the American Burn Association 2012;33:163-73.
[48] van der Veen VC, van der Wal MBA, van Leeuwen MCE, Ulrich MMW, Middelkoop E. Biological background of dermal substitutes. Burns 2010;36:305-21.

[49] Kim SW, Park TG, Jeong JH. Current status of polymeric gene delivery systems. Advanced Drug Delivery Reviews 2006;58:467-86.
[50] Fujii Y, Kachi S, Ito A, Kawasumi T, Honda H, Terasaki H. Transfer of gene to human retinal pigment epithelial cells using magnetite cationic liposomes. The British journal of ophthalmology 2010;94:1074-7.
[51] Li P, Liu D, Sun X, Liu C, Liu Y, Zhang N. A novel cationic liposome formulation for efficient gene delivery via a pulmonary route. Nanotechnology 2011;22:245104.
[52] Mooney DJ, Hahn LD, Kong H. Polycation Structure Mediates Expression of Lyophilized Polycation/pDNA Complexes. Macromolecular Bioscience 2010;10:1210-5.
[53] Segura T, Lei YG, Huang SX, Sharif-Kashani P, Chen Y, Kavehpour P. Incorporation of active DNA/cationic polymer polyplexes into hydrogel scaffolds. Biomaterials 2010;31:9106-16.
[54] Otsuka M, Ito T, Koyama Y. Analysis of the surface structure of DNA/polycation/hyaluronic acid ternary complex by Raman microscopy. Journal of Pharmaceutical and Biomedical Analysis 2010;51:268-72.
[55] Koyama Y, Ito T, Iida-Tanaka N. Efficient in vivo gene transfection by stable DNA/PEI complexes coated by hyaluronic acid. Journal of Drug Targeting 2008;16:276-81.
[56] Behr J-P. The Proton Sponge: a Trick to Enter Cells the Viruses Did Not Exploit. CHIMIA International Journal for Chemistry 1997;51:34-6.
[57] Aoki K, Furuhata S, Hatanaka K, Maeda M, Remy JS, Behr JP, et al. Polyethylenimine-mediated gene transfer into pancreatic tumor dissemination in the murine peritoneal cavity. Gene therapy 2001;8:508-14.
[58] Kichler A, Chillon M, Leborgne C, Danos O, Frisch B. Intranasal gene delivery with a polyethylenimine-PEG conjugate. Journal of controlled release : official journal of the Controlled Release Society 2002;81:379-88.
[59] Wang S, Ma N, Gao SJ, Yu H, Leong KW. Transgene expression in the brain stem effected by intramuscular injection of polyethylenimine/DNA complexes. Molecular therapy : the journal of the American Society of Gene Therapy 2001;3:658-64.
[60] Lei Y, Rahim M, Ng Q, Segura T. Hyaluronic acid and fibrin hydrogels with concentrated DNA/PEI polyplexes for local gene delivery. Journal of controlled release : official journal of the Controlled Release Society 2011;153:255-61.
[61] Itaka K, Yamauchi K, Harada A, Nakamura K, Kawaguchi H, Kataoka K. Polyion complex micelles from plasmid DNA and poly(ethylene glycol)-poly(L-lysine) block copolymer as serum-tolerable polyplex system: physicochemical properties of micelles relevant to gene transfection efficiency. Biomaterials 2003;24:4495-506.
[62] Vader P, van der Aa LJ, Engbersen JF, Storm G, Schiffelers RM. Physicochemical and biological evaluation of siRNA polyplexes based on PEGylated Poly(amido amine)s. Pharmaceutical research 2012;29:352-61.
[63] Verbaan FJ, Oussoren C, Snel CJ, Crommelin DJ, Hennink WE, Storm G. Steric stabilization of poly(2-(dimethylamino)ethyl methacrylate)-based polyplexes mediates prolonged circulation and tumor targeting in mice. The journal of gene medicine 2004;6:64-75.
[64] Piest M, Engbersen JF. Effects of charge density and hydrophobicity of poly(amido amine)s for non-viral gene delivery. Journal of controlled release : official journal of the Controlled Release Society 2010;148:83-90.

[65] Liu Z, Zhang Z, Zhou C, Jiao Y. Hydrophobic modifications of cationic polymers for gene delivery. Progress in Polymer Science 2010;35:1144-62.
[66] Convertine AJ, Benoit DS, Duvall CL, Hoffman AS, Stayton PS. Development of a novel endosomolytic diblock copolymer for siRNA delivery. Journal of controlled release : official journal of the Controlled Release Society 2009;133:221-9.
[67] Duvall CL, Convertine AJ, Benoit DS, Hoffman AS, Stayton PS. Intracellular delivery of a proapoptotic peptide via conjugation to a RAFT synthesized endosomolytic polymer. Molecular pharmaceutics 2010;7:468-76.
[68] Manganiello MJ, Cheng C, Convertine AJ, Bryers JD, Stayton PS. Diblock copolymers with tunable pH transitions for gene delivery. Biomaterials 2012;33:2301-9.
[69] Nelson CE, Kintzing JR, Hanna A, Shannon JM, Gupta MK, Duvall CL. Balancing cationic and hydrophobic content of PEGylated siRNA polyplexes enhances endosome escape, stability, blood circulation time, and bioactivity in vivo. ACS nano 2013;7:8870-80.

CHAPTER III

INJECTABLE POLYURETHANE COMPOSITE SCAFFOLDS DELAY WOUND CONTRACTION AND SUPPORT CELLULAR INFILTRATION AND REMODELING IN RAT EXCISIONAL WOUNDS

Introduction

The increases in immobile aging, diabetic amputee, and paralyzed patients afflicted with large, chronic wounds and fistulas as well as trauma victims with large cutaneous defects create a need for development of injectable biomaterials to promote restoration of tissue integrity. Such scaffolds could offer new options for both cutaneous and fascial indications while adding options for site-specific customization [1]. Furthermore, a biomaterial that is applied as a liquid and cures *in situ* can flow to fill the contours of irregularly shaped defects that may not conform to a preformed implant. Maximizing the contact surface area between the material and surrounding tissue should enhance cellular infiltration and integration of the scaffold.

Several requirements are critical to the success of injectable biomaterials, such as flowability for a sufficient time (the working time) to enable injection and curing within minutes of injection (the setting time) thus avoiding long surgical procedures. The injected material should not have adverse effects on surrounding host tissue due to the reactivity of specific components or to the release of heat through a reaction exotherm [2]. The viscosity of the injected material should be high enough to be retained at the injection site and to minimize extravasation into surrounding tissues where it may have an adverse effect [3]. The reproducibility of properties such as porosity, degradation, and setting time in the clinical environment is also a significant challenge. Injectable porous

biomaterials must have a suitable pore structure for cell migration, nutrient exchange, and tissue ingrowth [4].

Injectable hydrogels, such as poly(ethylene glycol) (PEG), collagen, fibrin, chitosan, alginate, and hyaluronan, have been shown to support bone ingrowth *in vivo*, particularly when combined with angiogenic or osteogenic growth factors [5-11]. However, hydrogels lack the tough, elastomeric properties of thermoplastic polymers that are appropriate for cutaneous applications. Furthermore, the microstructure of synthetic hydrogels is typically smaller than the average size of cellular populations (5-15 μm) [12], thus requiring resorption or displacement of the matrix by cells that results in slow infiltration of the scaffold. We have recently developed injectable, allograft bone/polyurethane (PUR) composite scaffolds for bone regeneration with tunable working and setting times of 5 and 15 minutes [13]. Materials were prepared by mixing allograft bone particles, a flowable lysine triisocyanate (LTI)-PEG prepolymer, a flowable polyester triol, and triethylene diamine catalyst. An LTI-PEG prepolymer was used in the scaffold synthesis rather than monomeric LTI because it has been shown previously that injection of LTI *in vivo* could be toxic [13]. The porosity of the cured scaffolds varied from 30 – 70%, and the pore size ranged from 177 – 700 μm. When injected into 3-mm femoral condylar plug defects in rats, the composites exhibited cellular infiltration and new bone formation at 3 weeks. While these composites are not suitable for cutaneous wound healing due to the allograft bone component, our previous studies have shown that pre-formed PUR scaffolds implanted in both subcutaneous [14] and excisional [15] wounds in Sprague-Dawley rats supported cellular infiltration and ingrowth of new tissue.

In the present study, we have synthesized injectable PUR composite scaffolds incorporating polysaccharide particles and evaluated their performance *in vitro* and *in vivo*. We hypothesized that the degradable scaffolds would function as an initial temporary matrix that both provides a surface for attachment and proliferation of cells and also stents the wound to minimize the undesirable outcomes of contraction and scarring. Either hyaluronic acid (HA), a 1,500 – 2,200 kDa glycosaminoglycan found in the extracellular matrix, or carboxymethylcellulose (CMC), a plant-derived 90 kDa polysaccharide, was added to the reactive PUR to control the foaming reaction through absorption of excess moisture from the wound bed. Rheological and physical properties of the scaffolds were measured *in vitro*, and their potential to support cellular infiltration and new tissue ingrowth were evaluated in excisional wounds in Sprague-Dawley rats.

Methods

Materials

Glycolide and D,L-lactide were purchased from Polysciences (Warrington, PA). TEGOAMIN33, a tertiary amine catalyst composed of 33 wt% triethylene diamine (TEDA) in dipropylene glycol, was obtained from Goldschmidt (Hopewell, VA). Polyethylene glycol (PEG, 200 Da) was supplied by Alfa Aesar (Ward Hill, MA). Glycerol and the sodium salts of carboxymethylcellulose (CMC; 90 kDa) and hyaluronic acid (HA; 1,500 – 2,200 kDa) were purchased from Acros Organics (Morris Plains, NJ). Lysine triisocyanate (LTI) was obtained from Kyowa Hakko USA (New York), and stannous octoate catalyst was obtained from Nusil technology (Overland Park, KS). All other reagents were purchased from Sigma-Aldrich (St. Louis, MO). Prior to use,

glycerol and PEG were dried at 10 mm Hg for 3 h at 80ºC, and ε-caprolactone was dried over anhydrous magnesium sulfate. All other materials were used as received.

Synthesis of PUR scaffolds and reactive intermediates

PEG (200 Da) was reacted with an excess of LTI (NCO:OH equivalent ratio = 3:1) to form an LTI-PEG prepolymer (21,000 cP) in which the PEG molecules were end-capped with LTI [13]. PEG with molecular weight > 200 Da did not yield a flowable prepolymer, and thus could not be injected. PEG was added dropwise to LTI in a 100 mL reaction flask with stirring under argon for 24 h at 45°C. The prepolymer was then dried under vacuum at 80°C for 14 h. A polyester triol (900 Da) with a backbone comprising 60% caprolactone, 30% glycolide, and 10% lactide was synthesized by reacting the monomers (ε-caprolactone, glycolide, and D,L-lactide) with a glycerol starter in the presence of stannous octoate catalyst [16]. This polyester triol composition and molecular weight were chosen to maintain both good flowability of the reactive mixture as well as a favorable degradation rate of the cured PUR scaffold *in vivo* [17]. The reaction was carried out under dry argon at 140ºC for 48 h, and the resulting polyester triol was dried under vacuum at 80ºC for 24 h.

PUR scaffolds were synthesized by reactive liquid molding of the LTI-PEG prepolymer with a hardener component [13, 14] and a polysaccharide filler (CMC or HA). The hardener comprised 100 parts polyester triol (polyol), 1.5 parts per hundred parts polyol (pphp) water, 0.625 pphp TEGOAMIN33 catalyst, 0.375 pphp 30% bis(2-dimethylaminoethyl)ether (DMAEE) blowing catalyst in poly(propylene glycol), and 4.0 pphp calcium stearate pore opener. The polysaccharide was combined with the hardener

and mixed by hand for 30 s. The prepolymer was added to the hardener and polysaccharide and mixed by hand for 1 min. The resulting mixture then rose freely for 10 – 20 min and cured. The targeted index (the ratio of NCO to OH equivalents times 100) was 115.

Scaffold characterization

Core densities and porosities were determined from mass and volume measurements of triplicate cylindrical foam cores [14, 18]. The scaffold pore size distribution was assessed by scanning electron microscopy (Hitachi S-4200 SEM, Finchampstead, UK) after gold sputter coating with a Cressington Sputter Coater. Temperature profiles of the reactive mixtures during foaming were measured using a digital thermocouple at the centers of the rising foams. Scaffold degradation was evaluated by incubating triplicate 20 mg samples in 1 ml phosphate buffered saline (PBS) (pH 7.4) at 37°C for up to 24 weeks. At various time points, the samples were rinsed in deionized water, dried under vacuum for 48 h at room temperature, and weighed.

Reactivity of scaffold components

The reactivities of the LTI-PEG prepolymer with the polyester triol, HA, and CMC were measured using attenuated total reflectance fourier transform infrared spectroscopy (ATR-FTIR; Bruker Tensor 27 FTIR, Billerica, MA). Prepolymer; TEGOAMIN33 and DMAEE catalyst; and either polyol, HA, or CMC were mixed together for 1 min and then placed in contact with the ATR crystal. The area of the isocyanate peak (wavelength 2150 – 2350 cm) was monitored as a function of time.

Mechanical properties

Mechanical properties were measured using a TA Instruments Q800 Dynamic Mechanical Analyzer (DMA) in compression mode (New Castle, DE). Samples were soaked in water for a few minutes or 7 days prior to mechanical testing. Stress-strain curves were generated by compressing wet cylindrical 7 x 6 mm samples at 37°C at a rate of 0.1 N/min until they reached 50% strain. The Young's modulus was determined from the slope of the initial linear region of each stress-strain curve. The scaffolds could not be compressed to failure due to their elasticity, so the compressive stress was measured one minute after the application of 50% strain [14].

Rheological properties during cure

The cure profiles of the HA and CMC scaffolds were measured using a TA Instruments parallel plate AR 2000ex rheometer operating in dynamic mode with 25 mm disposable aluminum plates (New Castle, DE). LTI-PEG prepolymer was added to a mixture of hardener and polysaccharide (0, 15, or 30 wt%) and mixed by hand using a spatula for 1 min. The sample was then loaded onto the bottom plate of the rheometer. An oscillation time sweep was run with a controlled strain of 1% and a frequency of 6.28 rad/s in order to obtain the cure profile of each PUR scaffold. The storage modulus (G') and loss modulus (G") were determined as a function of time. The working time was determined to be the G-crossover point. To measure the setting time, the surface of the foam was contacted with a spatula at regular intervals of 30 sec. The tack-free time, which approximates the setting time, was determined to be the time at which the foam did not stick to the spatula.

In vivo cutaneous repair in rats

All surgical procedures were reviewed and approved by the local Institutional Animal Care and Use Committee. NIH guidelines for the care and use of laboratory animals (NIH Publication #85-23 Rev. 1985) have been observed. The capacity of the scaffolds to facilitate dermal wound healing was evaluated in an excisional wound model (6.25cm^2 square wounds) in adult male Sprague-Dawley rats. All materials were sterilized by gamma irradiation at 5 kGy prior to surgery. The treatment groups investigated were untreated wounds (negative control) and PUR scaffolds with 15 wt% HA or CMC polysaccharide. We have previously observed that PUR scaffolds without polysaccharide fillers over-expanded and formed large voids *in vivo*, so this treatment group was not investigated in the rat study. Preliminary experiments showed that 15% polysaccharide was sufficient to control foaming, and no additional benefits were observed at 30%. To investigate the effects of the bioactivity of the polysaccharide on healing, both HA (which was anticipated to possibly have biological effects and enhance healing) and CMC (which was considered a relatively inert material) were tested. For the HA and CMC treatment groups, the materials were applied as a reactive liquid immediately after mixing the LTI-PEG prepolymer with the hardener and polysaccharide. The polyurethane expanded by gas foaming to fill the defects and cured *in situ*. When the scaffolds expanded beyond the wound dimensions, they were trimmed to be flush with the skin surface. Each wound and scaffold was covered with nonadherent, absorbent, Release gauze (Johnson & Johnson) and covered with a Tegaderm outer dressing (3M, St. Paul, MN). Wounds were harvested at days 7, 17, 26, and 35 after surgery. Four replicates of each treatment group were harvested at each time point. The wounds were

fixed in neutral buffered formalin for 24 h, transferred into 70% ethanol for 48 h, embedded in paraffin, and sectioned at 5 μm. Hematoxylin & eosin (H&E), Gomori's trichrome, picrosirius red, TUNEL, myeloperoxidase, Ki67, α-SMA, and procollagen I immunostaining were performed on the tissue sections.

Statistical analysis

Single factor analysis of variance (ANOVA) was used to evaluate the statistical significance of results. P values less than 0.05 were considered statistically significant. Data are plotted as mean ± standard error unless otherwise indicated.

Results

Setting properties of PUR foams

The specific reaction rates for the second order reactions between LTI-PEG prepolymer and water, polyol, HA, and CMC were determined using ATR-FTIR (Figure 3.1B). Water was the most reactive, with a rate constant of 600 g mol^{-1} min^{-1} (data not shown). The rate constant measured for the polyester triol (9.14 g mol^{-1} min^{-1}) was 21 times larger than that measured for CMC (0.438 g mol^{-1} min^{-1}) and 7 times larger than that measured for HA (1.29 g mol^{-1} min^{-1}). These data show that the water and polyester triol components are the most reactive in the system and considerably more reactive than the polysaccharides. The higher reactivity of HA compared to CMC is consistent with the structures shown in Figure 3.1A. Each repeat unit of HA has one primary OH group, while CMC has only carboxylic acids and secondary OH groups, which are at least 2 – 4 times less reactive than primary OH groups [19].

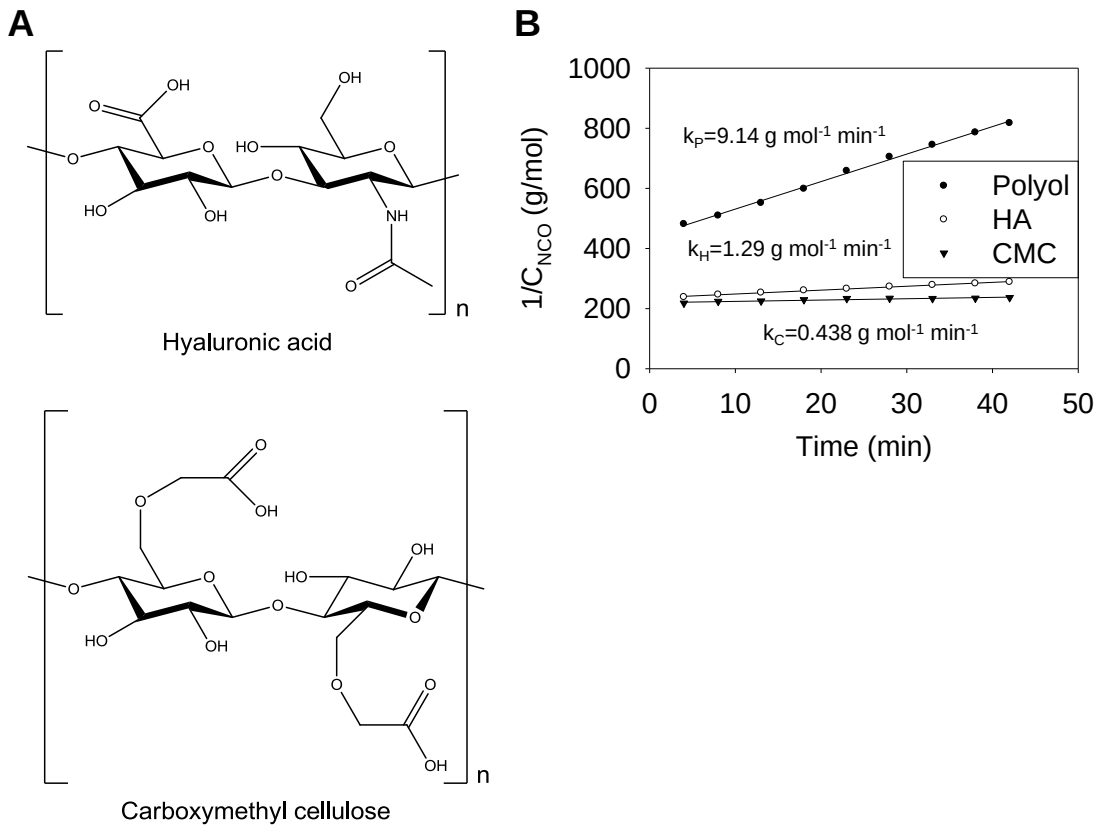

Figure 3.1. Reactivities of polyester triol, HA, and CMC with LTI-PEG prepolymer. (A) Chemical structures of HA and CMC. HA contains one primary hydroxyl group per repeat unit while CMC has no primary hydroxyl groups. (B) Determination of second-order rate constants for the reactions of polyester triol, HA, and CMC with LTI-PEG prepolymer.

The rheological properties of PUR, PUR + 15% CMC, and PUR + 15% HA scaffolds are shown in Figure 3.2A-C. The G-crossover point was considered to be the gel point and thus the working time of the foam. The working time was 5.8 ± 0.7 min for the PUR foam, 6.2 ± 0.5 min for the PUR + 15% CMC foam, and 5.5 ± 0.6 min for the PUR + 15% HA foam. Although the working time can be adjusted by altering the concentrations of the catalysts, it was maintained constant in the present study. The tack-free time was 16 ± 3 min for the PUR foam, 19 ± 3 min for the PUR + 15% CMC foam,

and 15 ± 4 min for the PUR + 15% HA foam. The addition of the polysaccharide had no significant effect on either the working or tack-free time.

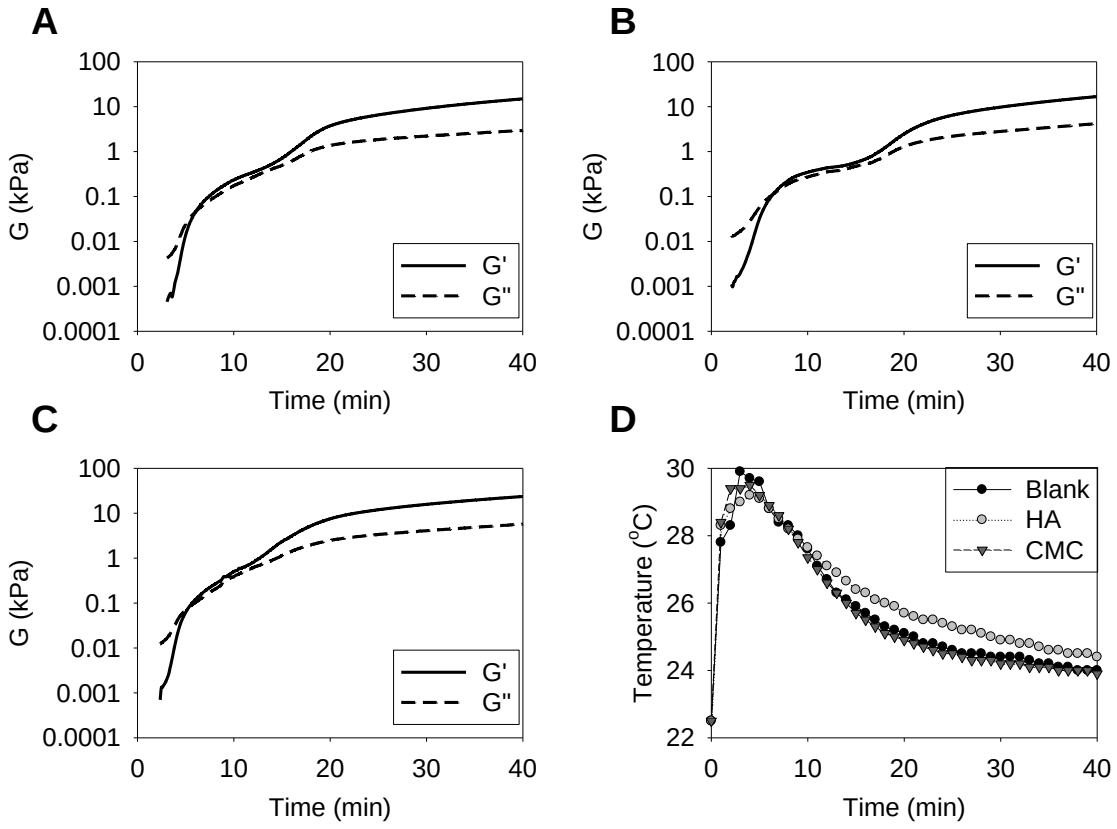

Figure 3.2. Rheological properties of injectable PUR scaffolds. (A) PUR, (B) PUR + 15% CMC, (C) PUR + 15% HA. (D) Temperature profile during cure.

The temperature profiles of PUR, PUR + 15% CMC, and PUR + 15% HA foams are shown in Figure 3.2D. The temperature within the reactive mixture was recorded with a digital thermocouple at the center of the rising foams, which were insulated to minimize the effects of heat loss from the exterior surface. Starting at room temperature, the maximum increase in temperature was 7.3 ± 1.7 °C for the PUR foam, 7.1 ± 1.4 °C for

the PUR + 15% CMC foam, and 6.7 ± 1.1 °C for the PUR + 15% HA foam. The addition of the polysaccharide did not significantly affect the temperature profile.

Physical properties of PUR scaffolds

Physical properties of the PUR scaffolds before and after incubating in an aqueous environment for 7 days are shown in Table 3.1. On day 0, the properties of PUR + 15% HA and PUR + 15% CMC scaffolds were not significantly different from each other, but both had significantly higher densities (45%), lower porosities (4%), and smaller pore sizes (13%) than the blank PUR scaffolds. However, by day 7 there were no significant differences in porosity or density between the three groups, presumably due to dissolution of the polysaccharides.

Table 3.1. Physical properties of PUR scaffolds.

PUR Sample	Day 0			Day 7		
	Density (kg/m^3)	**Porosity (vol %)**	**Pore Size (μm)**	**Density (kg/m^3)**	**Porosity (vol %)**	**Pore Size (μm)**
Blank	110 ± 2	90.9 ± 0.1	370 ± 90	105 ± 2	91.4 ± 0.1	320 ± 70
PUR + HA	158 ± 9	87.0 ± 0.7	330 ± 70	100 ± 7	91.8 ± 0.6	330 ± 80
PUR + CMC	161 ± 8	86.7 ± 0.6	320 ± 80	116 ± 18	90.4 ± 1.5	340 ± 90

Degradation of PUR scaffolds

A representative SEM image of a PUR + HA scaffold is shown in Figure 3.3A.1. The interconnected pores of the scaffolds permit cellular infiltration [14]. Panels A.2 and A.3 show images of 100 – 200 μm particles embedded in a PUR + HA scaffold at low and high magnification, respectively. As shown in Panel A.4, the particles were almost completely dissolved after 24 h *in vitro* incubation time in buffer, resulting in the formation of additional pores. Alcian blue staining was used to confirm the presence of

HA particles embedded in the scaffolds. PUR (negative control) and PUR + HA scaffolds were stained with Alcian blue at pH 2.5 and pH 1.0. At pH 1.0, Alcian blue only stains highly sulfated glycosaminoglycans, while at pH 2.5 the dye stains HA blue. While PUR scaffolds did not stain at either pH and PUR + HA scaffolds did not stain at pH 1.0, PUR + HA scaffolds stained blue at pH 2.5, thereby confirming the presence of HA in the scaffolds. Taken together, these data suggest that dissolution of HA (or CMC) can create additional pores in the scaffold *in vivo*. To investigate the effects of polysaccharide loading on scaffold degradation, the degradation rates of the PUR and PUR + CMC (15 and 30%) scaffolds in PBS at 37°C were recorded for up to 24 weeks (Figure 3.3B). Under *in vitro* conditions, the primary mechanism of degradation was hydrolysis of the ester bonds within the polyester soft segment [17]. The polysaccharides caused a high initial mass loss within the first few days, which is consistent with the SEM data in Figure 3.3A. After this time period, the rates of polymer degradation were similar.

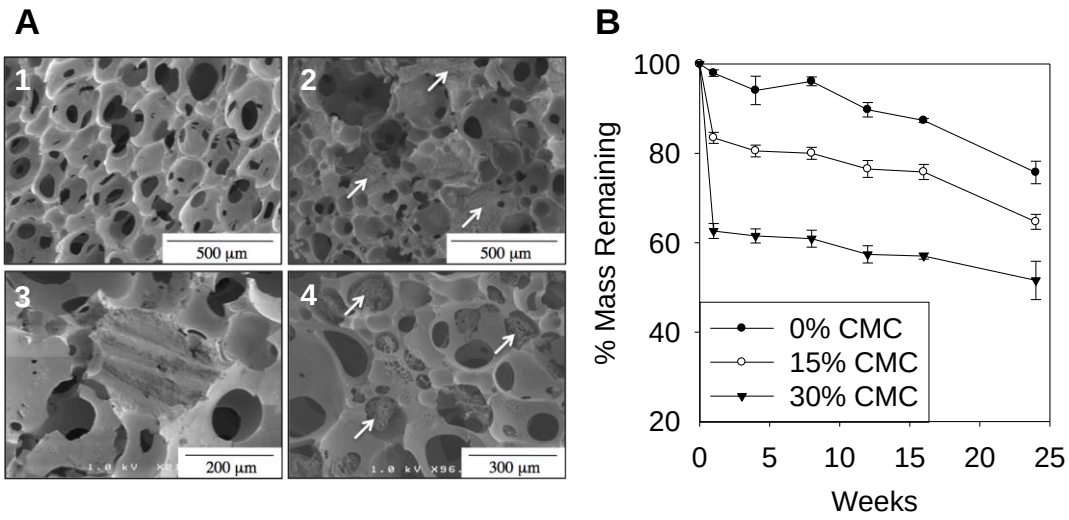

Figure 3.3. (A) SEM images of injectable LTI-PEG PUR scaffolds with no additive (top left) and 30 wt% HA (top right). The HA (or CMC) granules rise with the foam and become bridged in the pore walls, as indicated by the arrows and magnified at bottom left. Some of the HA dissolved (arrows) when the PUR was foamed in a high-moisture environment, as would occur *in vivo* (bottom right). (B) Degradation of injectable PUR scaffolds in PBS at 37 °C. The wt% polysaccharide affects the rate of degradation due to the rapid rate of dissolution of the polysaccharide (n = 3).

Mechanical properties of PUR scaffolds

The compressive Young's modulus and compressive stress of the scaffolds under physiological conditions (wet at 37^{o}C) before and after incubation for 7 days are summarized in Table 3.2. When compressed for extended periods of time, the scaffolds exhibited less than 5% permanent deformation, which is consistent with the properties of rubbery elastomers. Furthermore, the materials did not fail under compression, so compressive stress-strain tests were carried out to 50% strain, where the compressive stress was measured as reported previously [20]. The initial modulus and strength of scaffolds containing filler were higher (but not significantly) than those of blank scaffolds. After incubating 7 days, the modulus and strength of all three scaffolds

decreased, but only the changes in the modulus of the polysaccharide-filled scaffolds were significant ($p < 0.005$ for PUR + HA and $p < 0.02$ for PUR + CMC).

Table 3.2. Mechanical properties of PUR scaffolds.

PUR Sample	Day 0		Day 7	
	Young's Modulus (kPa)	**Compressive Stress (kPa)**	**Young's Modulus (kPa)**	**Compressive Stress (kPa)**
Blank	30 ± 4	7.7 ± 1.0	19 ± 8	6.8 ± 0.6
PUR + HA	50 ± 20	10 ± 2	11 ± 4	8 ± 3
PUR + CMC	60 ± 30	10 ± 7	14 ± 4	9 ± 3

Measurements of excisional wounds

Injectable PUR scaffolds with 15% CMC or HA were tested for their effects upon dermal wound healing in a rat excisional wound model. No frank necrosis of the surrounding tissue was seen at the early time points, suggesting that the mild exotherm resulting from the PUR reaction did not adversely affect the host tissue. In addition, the level of apoptosis in the scaffold-treated groups was not greater than in the blank wounds at any of the time points (Figure 3.5B). The average length of the wound gap, granulation tissue thickness, and percent re-epithelialization of the wounds in the three treatment groups at each time point are summarized in Figure 3.4. At days 7 and 17, the thickness of the wounds in the HA and CMC treatment groups was less than the thickness of the blank wounds; however, only the thickness of the wounds in the HA group at day 17 was significantly less than the blank ($p < 0.015$). At day 7, the length of the blank wounds was significantly less than those of the HA and CMC groups ($p < 0.045$, $p < 0.015$, respectively), providing evidence that the PUR scaffolds stented the wound. Blank (contracted) wounds were fully epithelialized by day 26, while HA and CMC treatment groups (stented) were not fully epithelialized by day 35.

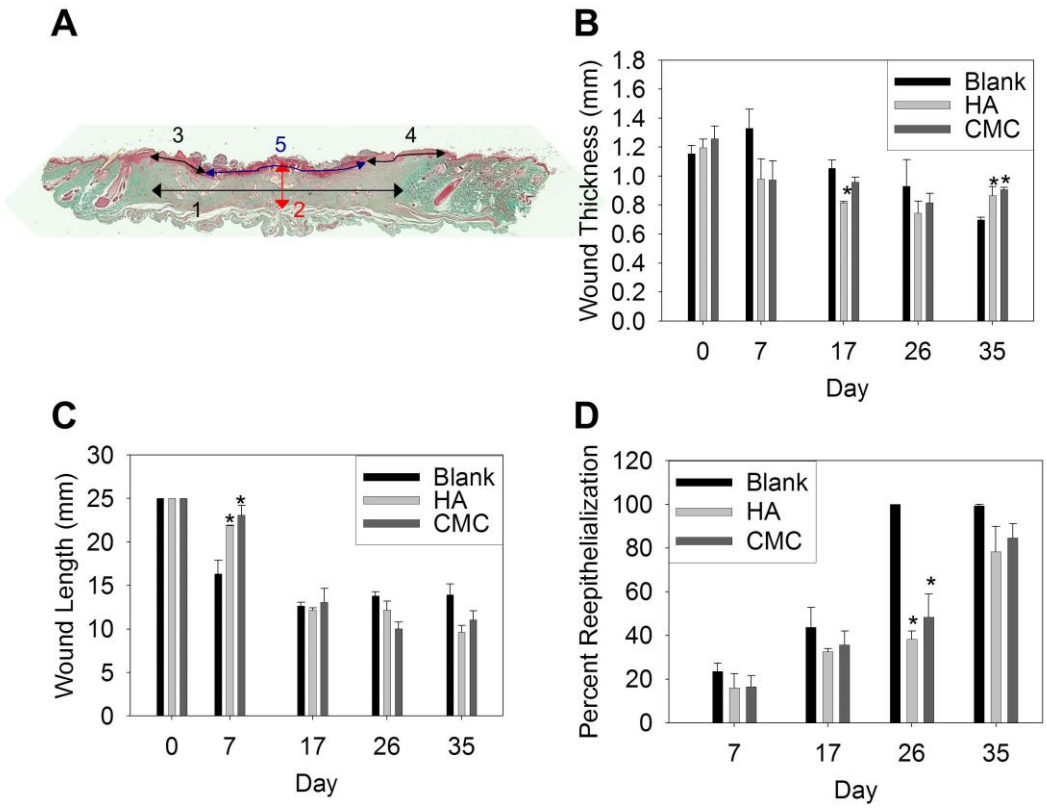

Figure 3.4. Measurements of wounds from the blank, HA, and CMC treatment groups at days 7, 17, 26, and 35. (A) Schematic summarizing measured dimensions using a representative image of PUR + HA at day 26 as an example. Line 1 represents wound gap length and line 2 represents wound thickness. Percent reepithelialization was calculated by dividing the length of the epidermis on either side of the wound (sum of lines 3 and 4) by the total length of the wound surface (sum of lines 3, 4, and 5). (B) Wound thickness. (C) Wound length. (D) Percentage of reepithelialization. Asterisks indicate statistically significant differences from the blank treatment group.

Analysis of proliferating and apoptotic cells in an excisional wound model

Ki67 staining was performed to assess the level of cell proliferation within the wound bed (Figure 3.5A). After 7 days, we found no difference in the number of $Ki67^{+}$ cells in the blank wounds compared to the scaffold treatment groups. From day 7 to day 17, the number of proliferating cells remained constant in the CMC and HA treatment groups but decreased by 67% in the blank treatment group. Thus at day 17, the number of

Ki67$^+$ cells was significantly higher in the scaffold treatment groups than in the blanks. The number of Ki67$^+$ cells decreased slightly from day 17 to day 26, but the level of proliferation in the scaffold treatment groups remained significantly higher than in the blank wounds. From day 26 to day 35, the number of Ki67$^+$ cells decreased by 40% in the scaffold treatment groups and remained constant in the blank treatment group. At day 35, the number of Ki67$^+$ cells in the scaffold treatment groups was comparable to that observed for the blank wounds.

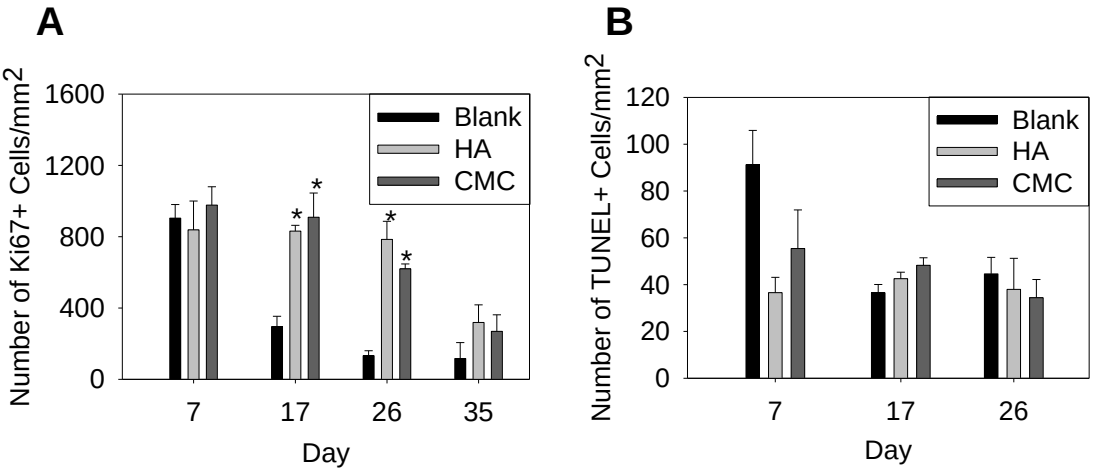

Figure 3.5. Immunohistochemical staining for Ki67 tissue sections from the blank, HA, and CMC treatment groups. (A) Ki67 staining at days 7, 17, 26, and 35. (B) TUNEL staining at days 17, 26, and 35. Asterisks indicate statistically significant differences from the blank treatment group.

TUNEL staining was used to measure cell apoptosis in the wound site (Figure 3.5B). At day 7, the number of cells stained with TUNEL was higher in the blank wounds than in the wounds with scaffolds, but the difference was not statistically significant. From day 7 to day 17, the number of cells stained with TUNEL decreased by 40% in the blank wounds and remained relatively constant in the scaffold treatment groups. The

level of apoptosis did not change in any of the treatment groups from day 17 to day 26. There were no significant differences in the number of cells stained with TUNEL among the three treatment groups at any of the time points.

Analysis of contraction in an excisional wound model

Staining for α-smooth muscle actin (α-SMA) was performed in order to examine the formation of myofibroblasts in the wound site. Representative images of sections stained for α-SMA are displayed in Figure 3.6. In the blank wounds, the number of myofibroblasts was greatest at days 17 and 26 and decreased almost completely by day 35. In contrast, fewer myofibroblasts were present at days 17 and 26 in the HA and CMC treatment groups. Myofibroblast formation in these groups was delayed and remained higher at the day 35 interval than in the blank group. Myofibroblasts were oriented parallel to the epidermis in the blank wounds, forming lines of tension in the skin as is characteristic of wounds undergoing scarring and contraction. In contrast, myofibroblasts were randomly oriented around pieces of PUR in the HA and CMC groups. These results show that myofibroblast formation was delayed in the HA and CMC groups and that fragments of PUR scaffolds disrupted the linear alignment of myofibroblasts.

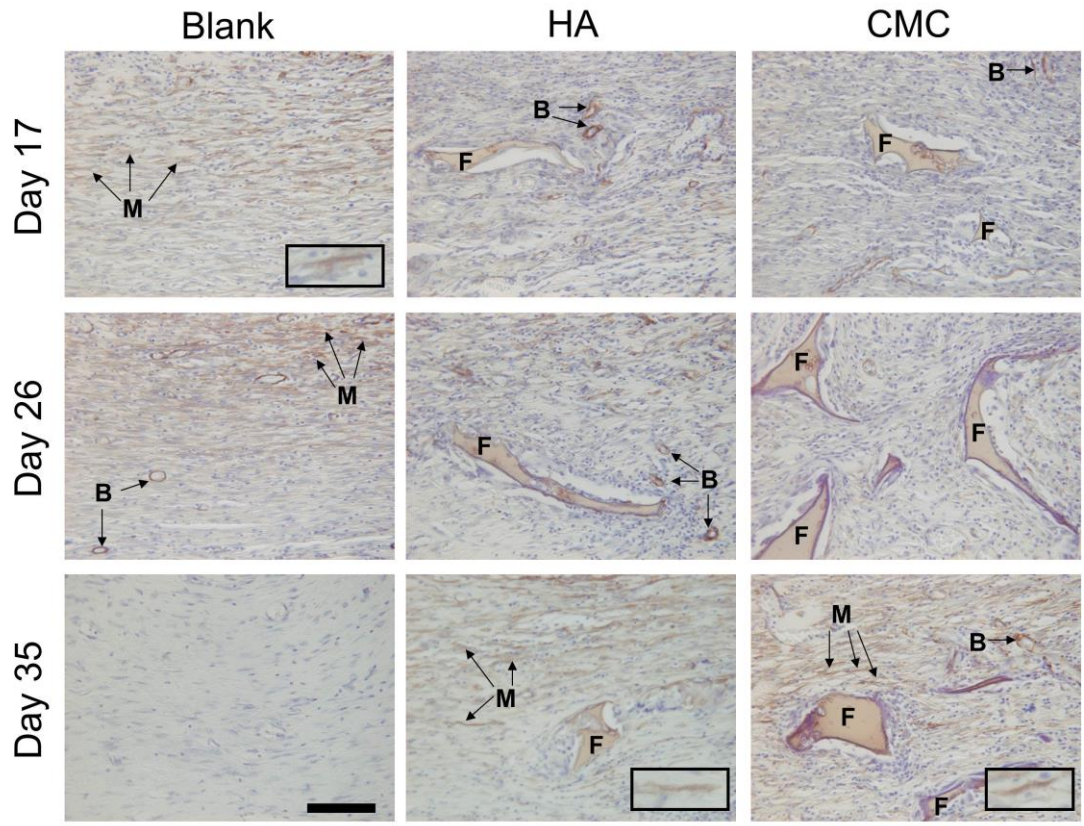

Figure 3.6. Representative images of tissue sections from the blank, HA, and CMC treatment groups at days 17, 26, and 35 stained for α–SMA (scale bar = 100 μm). Remnants of polyurethane foam (F), blood vessels (B), and myofibroblasts (M) are indicated by arrows. Blood vessels, which exhibit immunoreactivity for α–SMA, were ignored in the analysis. Myofibroblast formation in blank wounds was highest at days 17 and 26 and decreased by day 35. In the HA and CMC treatment groups, myofibroblast formation was low at days 17 and 26 and increased at day 35.

During the nascent phases of cutaneous wound repair, the provisional loose connective tissue matrix develops a very robust capillary network, which causes the healing wound to appear red due to the fragile capillaries that bleed easily. If healing progresses through its expected phases, the number of new capillaries peaks and subsequently begins to decline. By days 26 and 35 in the life of the wound, the capillary density is regressing, which is consistent with the histological sections in Figure 3.6. The remodeling phase is underway and is converting the newly formed tissue within the

wound bed into a dense irregular connective tissue that is characterized by a higher density of matrix proteins (predominantly collagens) and a lower number of capillaries. Taken together, the histological sections in Figure 3.6 are consistent with a maturing wound that is progressing past the granulation tissue stage that is typical of chronically impaired wound healing settings.

Analysis of collagen production in the excisional wound model

Picrosirius red staining and procollagen I immunostaining were performed in order to analyze the temporal and spatial production, accumulation, and organization of collagen in the rat excisional wounds. Representative images of sections stained with picrosirius red are shown in Figure 3.7. Picrosirius red staining supports the observation that collagen fiber formation in the HA and CMC treatment groups was more randomly oriented than in the blank wounds. At days 17, 26, and 35, collagen fibers in blank wounds were organized and aligned parallel to the epidermis. In contrast, collagen fibers surrounding polymer remnants in the HA and CMC scaffolds were randomly oriented.

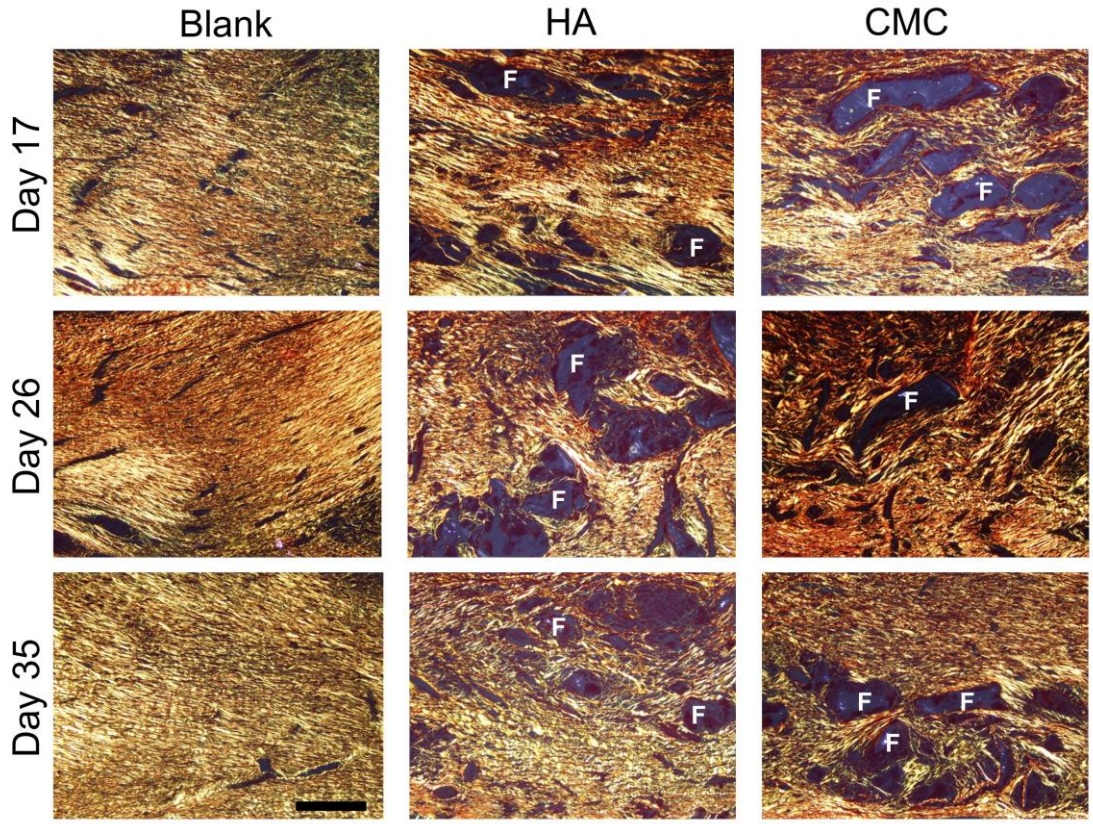

Figure 3.7. Representative images of tissue sections from the blank, HA, and CMC treatment groups at days 17, 26, and 35 stained with picrosirius red and observed with polarized light microscopy (scale bar = 200 μm). Remnants of polyurethane foam are labeled (F). Collagen surrounding pieces of PUR foam in the HA and CMC treatment groups appears less organized and more randomly oriented than collagen in the blank wounds.

Representative images of sections stained for procollagen I are displayed in Figure 3.8A, and the number of procollagen I-producing cells is quantified in Figure 3.8B. At day 17, there were significantly more procollagen I-producing cells in the HA group than in the blanks ($p < 0.02$). At day 26, there were significantly fewer procollagen I-producing cells in the HA group than in the blanks ($p < 0.02$). At day 35, there were significantly fewer procollagen I-producing cells in the CMC group than in the blanks ($p < 0.045$).

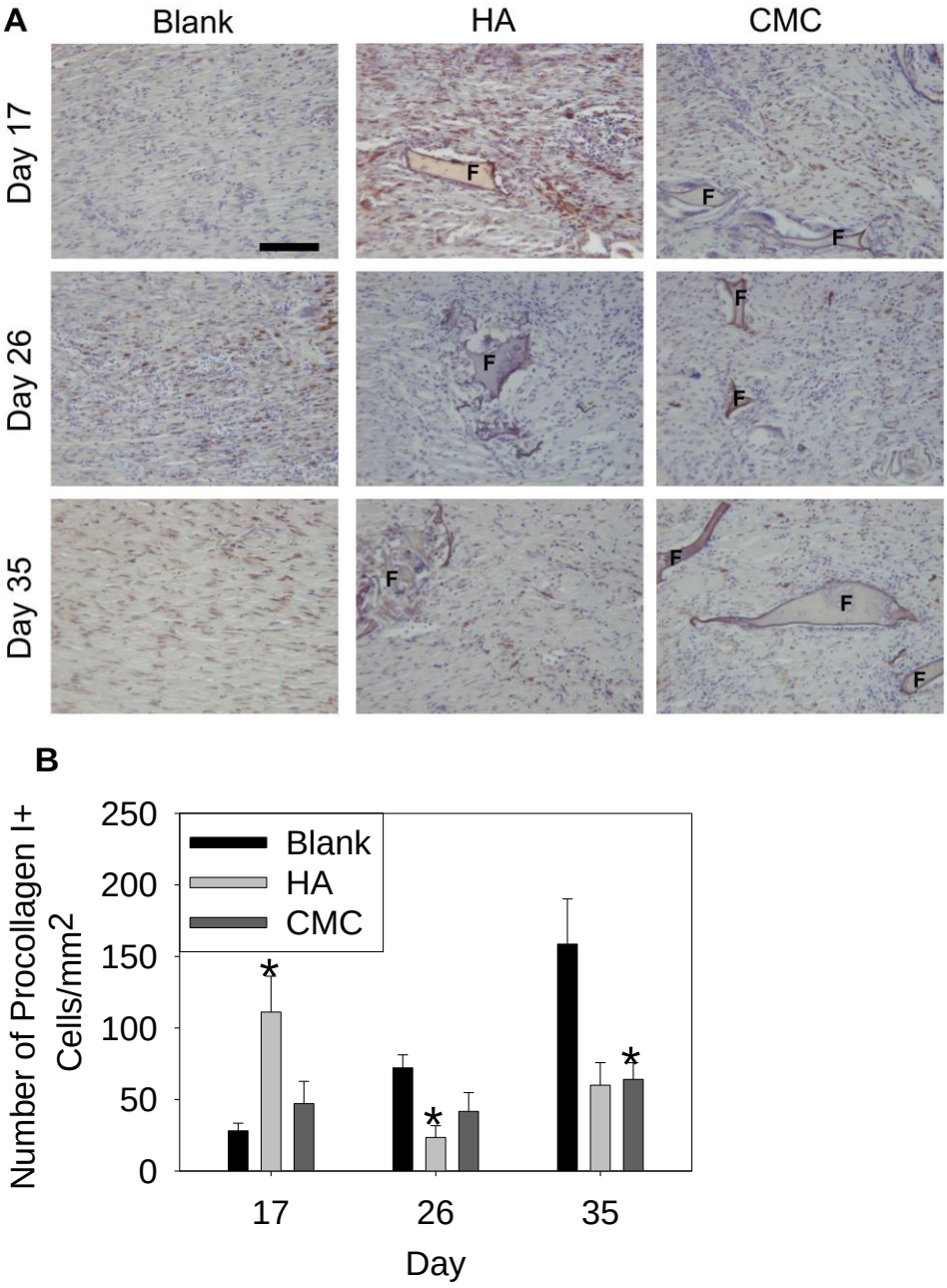

Figure 3.8. (A) Representative images of tissue sections from the blank, HA, and CMC treatment groups at days 17, 26, and 35 stained for procollagen I (scale bar = 100 μm). Remnants of polyurethane foam are labeled (F). (B) Number of procollagen I-producing cells in the three treatment groups. At day 17, HA and CMC treatment groups exhibited modest staining while the blank group had very few procollagen I-producing cells. The staining in the blank group increased at day 26 and day 35. In contrast, minimal immunostaining was seen in the HA and CMC groups at days 26 and 35. Asterisks indicate statistically significant differences from the blank treatment group.

The presence of the scaffold had a modifying impact on collagen I production and deposition. Blank wounds developed a linear pattern of contraction and scarring and were highly cellular. By comparison, scaffold-treated wounds at day 35 revealed reduced cellularity and fewer collagen I-secreting cells. Furthermore, the orientation of the cells and collagen fibers was more random in the presence of scaffolds. These data support the hypothesis that the scaffold hinders or alters the expected scarring and contraction pattern observed in blank wounds.

Discussion

In this study, we have shown that the physical, mechanical, and rheological properties of polyurethane composites render them suitable for use as injectable scaffolds in the setting of cutaneous wound repair. The materials exhibited working and cure times of 5 – 7 and 15 – 19 min, respectively, which are compatible with the temporal practicalities imposed by the clinical setting. Due to their compressive properties, which approach those of intact skin, the scaffolds stented the wounds at early time points and promoted granulation tissue formation while preventing wound contraction. As a result of wound contraction, unstented wounds resurfaced more rapidly. Collagen synthesis and organization, as well as myofibroblast formation, were altered by the presence of the scaffolds with a net positive impact.

Injectable scaffolds are advantageous because they can fill large, irregularly shaped wounds and cavities. Moreover, scaffolds have the added potential to serve as delivery vehicles for additives such as antibacterial and growth factors. Nevertheless, several challenges associated with injectable biomaterials have been described in recent reviews [21]. The reactants and catalyst must not be cytotoxic, and the reaction exotherm

must be minimal to avoid necrosis of surrounding tissues. Achieving interconnected pores while retaining robust mechanical properties presents an additional challenge. In a recent study, injectable poly(propylene fumarate) (PPF) scaffolds with pores ranging from 50 - 500 μm, <61% porosity, and elastic modulus of 20 – 40 MPa were fabricated via a gas-foaming process using an NVP crosslinker and benzoyl peroxide initiator [22]. However, the effects of the solvents and initiator on *in vivo* biocompatibility remain untested to date.

Natural and synthetic polymers including collagen, chitosan, fibrin, and poly(lactic-co-glycolic acid) are currently used in cutaneous wound healing in the form of hydrogels, sheets, sponges, and electrospun scaffolds [4, 23]. These polymers are advantageous due to their biocompatibility and biodegradability, but they present potential drawbacks such as low mechanical properties, small pore size, and low porosity [12]. Low mechanical properties result in undesirable outcomes such as contraction and scarring, and small pores and low porosity lead to slow infiltration and delayed vascularization [23]. Scaffolds with >90% porosity are desirable because they can easily support infiltration of new tissue and transport of nutrients and waste [24]. A previous study has reported optimal pore sizes for fibroblast infiltration and new tissue ingrowth ranging from 90 – 360 μm [25], while another study has shown that the viability of seeded fibroblasts was highest for pore size <160 μm [26, 27]. Another study resulted in low viability of fibroblasts in scaffolds with pores ranging from 50 – 80 μm compared to scaffolds with larger pores [24].

Nanofibrous scaffolds have potential for use in cutaneous wound healing because they mimic the structure and function of natural ECM [23]. Despite their small pores,

their high surface area to volume ratio results in excellent permeability for oxygen and nutrients [23]. Delivery of recombinant human platelet-derived growth factor (rhPDGF) from nanofibrous PLGA scaffolds has been reported to enhance wound healing in rats [28], and another study has examined the use of bioactive poly-N-acetyl-glucosamine nanofibrous membranes in cutaneous wounds in diabetic mice [29]. The nanofibers enhanced keratinocyte migration, cell proliferation, and angiogenesis compared to a cellulose control [29]. However, pre-formed implants such as nanofibrous scaffolds cannot be injected, and thus cannot fill and conform to deep tissue defects.

We have previously reported an injectable polyurethane scaffold for use in bone tissue engineering applications, wherein a matrix comprising allograft bone particles and a two-component reactive polyurethane supported cellular infiltration, extracellular matrix synthesis, and new bone formation in femoral plug defects in rats [13]. In this study, we have applied the findings from our previous work on injectable allograft bone biocomposites to create injectable scaffolds for use in cutaneous wound repair and regeneration. With a working time of <7 min and a setting time of <19 min, the scaffolds can be mixed and injected in a clinically relevant period of time. The pore size ranged from 320 – 370 μm, which is consistent with values reported previously for polyurethane scaffolds [13, 14, 30], and are comparable to those known to facilitate infiltration of cells such as fibroblasts (90 – 360 μm [25]) and osteoblasts [31]. While blank, HA-, and CMC-filled scaffolds showed no significant differences in pore size, the polysaccharide-filled scaffolds exhibited higher density and modulus and lower porosity than the blank scaffolds. However, by day 7 the density, modulus, and porosity of the polysaccharide-filled scaffolds were not significantly different than those properties measured for the

blank scaffolds. These data are consistent with the SEM images in Figure 3.3A and the degradation data in Figure 3.3B suggesting that the polysaccharide had leached from the scaffolds by day 7, resulting in lower modulus and density. They are also in agreement with a previous study showing a reduction in the modulus of PUR scaffolds incorporating 7 – 8% tobramycin after 7 days due to leaching of the tobramycin from the scaffolds [32].

An abundance of fibroblasts was observed in our histological sections. Proliferative assays were performed to demonstrate that the scaffolds supported cellular attachment and proliferation, which provides compelling evidence that the scaffold was non-toxic and biocompatible as it degraded and was replaced by new matrix. In the *in vivo* experiment, there were no significant differences in the level of apoptosis among the three treatment groups, suggesting that the polyurethane scaffolds and their degradation products are noncytotoxic and do not harm the surrounding tissue, which is consistent with previous studies [14, 33-35]. In addition to its role as an initial temporary matrix that provides a surface for cell attachment, the scaffolds also stented the wounds by providing resistance to the contractile forces exerted by the cells. The Young's modulus of the scaffolds measured under compressive deformation approaches that of human skin, which has been reported as 35 kPa for the dermis [36], and rat skin, which we measured to be 400 ± 150 kPa. The injectable polyurethane networks are rubbery elastomers at physiological temperatures with glass transition temperatures (T_g) less than 10°C, and they sustain compressive strains exceeding 50% without mechanical failure [14]. The wound healing (Figure 3.4), cell proliferation (Figure 3.5), and matrix deposition (Figure 3.7) data are consistent with the notion that the scaffold delays contraction and scarring due to the fact that its initial mechanical properties are approaching those of native skin.

Cutaneous wound repair goes through predictable stages, characterized by an initial acute inflammatory phase that leads to ingrowth of granulation tissue followed by a progressive transition to sustained matrix production and remodeling. Rapid wound closure often leads to excessive matrix production and the very undesirable outcomes of scarring and wound contraction, which was not observed with these scaffolds. Matrix production was visibly dampened and the alignment of collagen fibers more random compared to control wounds. Thus, by resisting the contractile forces that are generated in the host tissue, the scaffolds promote cellular infiltration and remodeling rather than excessive matrix deposition and scarring.

Excisional wounds treated with PUR scaffolds were significantly less contracted than blank wounds at day 7 as demonstrated by measures of wound gap (Figure 3.4C). While the cross-sectional area of granulation tissue was similar among all groups, unstented wounds tended to form a thickened eschar, although the differences were not significant (Figure 3.4B). These indicators suggest that the scaffolds stented the wounds at early time points, thus leading to a restorative rather than a scarring/contracting phenotype at later time points. Although wounds treated with injectable scaffolds showed prolongation of the proliferative phase, the effects on myofibroblast accumulation and orientation are potentially advantageous features. Myofibroblasts normally generate unwanted contractile forces that promote wound contraction and fibrosis. The architectural disruption of myofibroblast alignment led to a more reticular arrangement of collagen fibers. Although the upper surface of the scaffolds was approximately flush with the surface of the skin, epidermal resurfacing of the wounds was delayed. While this response was likely due in part to the greater length of the

stented wounds, either the wound covering or the properties of the upper surface of the scaffold may benefit from further modification.

At later time points in the study, the marked difference in the alignment of collagen fibers and cells within the composite scaffolds suggests that the transient presence of the scaffold disrupted the formation of a uniformly aligned extracellular matrix under elevated tension. Ideally the scaffold should degrade at a rate comparable to that of new tissue ingrowth. While Figure 3.3 shows ~20% mass loss of the polyurethane after 24 weeks *in vitro*, we have recently shown that lysine-derived polyurethane scaffolds undergo oxidative degradation to soluble break-down products mediated by macrophages *in vivo* [17]. As a result, the scaffold was almost completely resorbed after 4 weeks post-implantation in rat excisional wounds [17]. Biostable polyurethane foams have been developed as coverings to minimize fibrous encapsulation of breast implants [37, 38]. However, the polyurethane foams slowly degraded *in vivo* into small pieces after periods longer than 18 months post-implantation, thereby inducing fibrous encapsulation of the implant and an intense foreign-body response to the foam fragments. The delayed appearance of myofibroblasts in the injectable scaffolds was also consistent with an altered mechanical environment, particularly in light of the evidence that cell-generated tension in the context of relatively stiff extracellular matrix can lead to the activation of latent TGF-ß, which promotes matrix accumulation and differentiation of the myofibroblast phenotype [39].

Although not tested in the present investigation, the injectable polyurethane scaffolds also have the potential to accelerate wound healing through the local delivery of biologics such as recombinant human platelet-derived growth factor (rhPDGF) [15] or

antibiotics [32, 40]. Delivery of rhPDGF-BB from polyurethane scaffolds implanted in excisional wounds in rats accelerated both ingrowth of new tissue as well as degradation of the scaffolds [15]. In another study, delivery of vancomycin from polyurethane scaffolds implanted in a contaminated femoral segmental defect in rats decreased bacterial counts in both bone and soft tissue [40]. Biologics can be added to the polyester triol component prior to mixing with the prepolymer, thereby facilitating clinical ease of use and customization at the point of care.

Conclusions

In this study, an injectable, biodegradable polyurethane scaffold supported cellular infiltration and ingrowth of new tissue in a rat excisional wound model. The two-component polyurethanes exhibited working times and setting times ranging from 5 – 7 and 15 – 19 minutes, respectively. A micron-sized polysaccharide powder, either hyaluronan or carboxymethylcellulose, added to the liquid polyurethane controlled excessive expansion after injection. The cured scaffolds delayed wound contraction at early time points, with the favorable outcomes of enhanced cellular proliferation and reduced alignment of scar collagen. The biocompatibility, ease of use, clinically relevant working and setting times, support of cellular infiltration, positive impact on matrix remodeling, and potential to deliver biologics at the point of care may present compelling opportunities for injectable polyurethanes as void fillers for healing of cutaneous tissue defects.

References

[1] Praemer A, Furner S, Rice D. Musculoskeletal conditions in the United States. American Academy of Orthopaedic Surgeons. Park Ridge, IL1992. p. 85-124.
[2] Deramond H, Wright NT, Belkoff SM. Temperature elevation caused by bone cement polymerization during vertebroplasty. Bone 1999;25:17S-21S.
[3] Padovani B, Kasriel O, Brunner P, Peretti-Viton P. Pulmonary embolism caused by acrylic cement: a rare complication of percutaneous vertebroplasty. AJNR Am J Neuroradiol 1999;20:375-7.
[4] Khan Y, Yaszemski MJ, Mikos AG, Laurencin CT. Tissue engineering of bone: Material and matrix considerations. Journal of Bone & Joint Surgery: American Edition 2008;90:36-42.
[5] Augst AD, Kong H-J, Mooney DJ. Alginate Hydrogels as Biomaterials. Macromolecular Bioscience 2006;6:623-33.
[6] Chen RR, Mooney DJ. Polymeric growth factor delivery strategies for tissue engineering. Pharmaceutical Research 2003;20:1103-12.
[7] Kipshidze N, Chawla P, Keelan MH. Fibrin Meshwork as a Carrier for Delivery of Angiogenic Growth Factors in Patients With Ischemic Limb. Mayo Clinic Proceedings 1999;74:847-8.
[8] Labhasetwar V, Bonadio J, Goldstein S, Chen W, Levy RJ. A DNA controlled-release coating for gene transfer: Transfection in skeletal and cardiac muscle. Journal of Pharmaceutical Sciences 1998;87:1347-50.
[9] Mizuno K, Yamamura K, Yano K, Osada T, Saeki S, Takimoto N, et al. Effect of chitosan film containing basic fibroblast growth factor on wound healing in genetically diabetic mice. Journal of Biomedical Materials Research Part A 2003;64A:177-81.
[10] Simmons CA, Alsberg E, Hsiong S, Kim WJ, Mooney DJ. Dual growth factor delivery and controlled scaffold degradation enhance in vivo bone formation by transplanted bone marrow stromal cells. Bone 2004;35:562-9.
[11] Zawko SA, Truong Q, Schmidt CE. Drug-binding hydrogels of hyaluronic acid functionalized with β-cyclodextrin. Journal of Biomedical Materials Research Part A 2008;87:1044-52.
[12] Raeber GP, Lutolf MP, Hubbell JA. Molecularly engineered PEG hydrogels: a novel model system for proteolytically mediated cell migration. Biophys J 2005;89:1374-88.
[13] Dumas JE, Zienkiewicz K, Tanner SA, Prieto EM, Bhattacharyya S, Guelcher S. Synthesis and Characterization of an Injectable Allograft Bone/polymer Composite Bone Void Filler with Tunable Mechanical Properties. Tissue Eng Part A 2010;16:2505-18.
[14] Hafeman A, Li B, Yoshii T, Zienkiewicz K, Davidson J, Guelcher S. Injectable biodegradable polyurethane scaffolds with release of platelet-derived growth factor for tissue repair and regeneration. Pharm Res 2008;25:2387-99.
[15] Li B, Davidson JM, Guelcher SA. The effect of the local delivery of platelet-derived growth factor from reactive two-component polyurethane scaffolds on the healing in rat skin excisional wounds. Biomaterials 2009;30:3486-94.
[16] Guelcher SA, Patel V, Gallagher KM, Connolly S, Didier JE, Doctor JS, et al. Synthesis and in vitro biocompatibility of injectable polyurethane foam scaffolds. Tissue Engineering 2006;12:1247-59.

[17] Hafeman AE, Zienkiewicz KJ, Zachman AL, Sung HJ, Nanney LB, Davidson JM, et al. Characterization of the degradation mechanisms of lysine-derived aliphatic poly(ester urethane) scaffolds. Biomaterials 2011;32:419-29.
[18] Hafeman AE LB, Yoshii T, Zienkiewicz K, Davidson JM, Guelcher SA. Injectable biodegradable polyurethane scaffolds with release of platelet-derived growth factor for tissue repair and regeneration. Pharmaceutical Research 2008;25:2387-99.
[19] Szycher M. Szycher's Handbook of Polyurethanes. Boca Raton: CRC Press; 1999.
[20] Guelcher S, Srinivasan A, Hafeman A, Gallagher K, Doctor J, Khetan S, et al. Synthesis, In vitro degradation, and mechanical properties of two-component poly(ester urethane)urea scaffolds: Effects of water and polyol composition. Tissue Engineering 2007;13:2321-33.
[21] Kretlow JD, Klouda L, Mikos AG. Injectable matrices and scaffolds for drug delivery in tissue engineering. Advanced Drug Delivery Reviews 2007;59:263 - 73.
[22] Kim CW, Talac R, Lu L, Moore MJ, Currier BL, Yaszemski MJ. Characterization of porous injectable poly-(propylene fumarate)-based bone graft substitute. J Biomed Mater Res A 2008;85:1114-9.
[23] Lim CT, Zhong SP, Zhang YZ. Tissue scaffolds for skin wound healing and dermal reconstruction. Wiley Interdisciplinary Reviews-Nanomedicine and Nanobiotechnology 2010;2:510-25.
[24] Lawrence BJ, Madihally SV. Cell colonization in degradable 3D porous matrices. Cell Adh Migr 2008;2:9-16.
[25] Wang H, Pieper J, Peters F, van Blitterswijk CA, Lamme EN. Synthetic scaffold morphology controls human dermal connective tissue formation. J Biomed Mater Res A 2005;74:523-32.
[26] Adekogbe I, Ghanem A. Fabrication and characterization of DTBP-crosslinked chitosan scaffolds for skin tissue engineering. Biomaterials 2005;26:7241-50.
[27] Yang J, Shi G, Bei J, Wang S, Cao Y, Shang Q, et al. Fabrication and surface modification of macroporous poly(L-lactic acid) and poly(L-lactic-co-glycolic acid) (70/30) cell scaffolds for human skin fibroblast cell culture. J Biomed Mater Res 2002;62:438-46.
[28] Jin Q, Wei G, Lin Z, Sugai JV, Lynch SE, Ma PX, et al. Nanofibrous Scaffolds Incorporating PDGF-BB Microspheres Induce Chemokine Expression and Tissue Neogenesis In Vivo. PLoS ONE 2008;3:e1729.
[29] Scherer SS, Pietramaggiori G, Matthews J, Perry S, Assmann A, Carothers A, et al. Poly-N-acetyl glucosamine nanofibers: a new bioactive material to enhance diabetic wound healing by cell migration and angiogenesis. Ann Surg 2009;250:322-30.
[30] Kavlock KD, Pechar TW, Hollinger JO, Guelcher SA, Goldstein AS. Synthesis and characterization of segmented poly(esterurethane urea) (PEUUR) elastomers for bone tissue engineering. Acta Biomater 2007;3:475-84.
[31] Murphy CM, Haugh MG, O'Brien FJ. The effect of mean pore size on cell attachment, proliferation and migration in collagen-glycosaminoglycan scaffolds for bone tissue engineering. Biomaterials;31:461-6.
[32] Hafeman AE, Zienkiewicz KJ, Carney E, Litzner B, Stratton C, Wenke JC, et al. Local delivery of tobramycin from injectable biodegradable polyurethane scaffolds. J Biomater Sci Polym Ed 2010;21:95-112.

[33] Guelcher SA, Srinivasan A, Dumas JE, et al. Synthesis, mechanical properties, biocompatibility, and biodegradation of polyurethane networks from lysine polyisocyanates. Biomaterials 2008;29:1762-75.
[34] Zhang J-Y, Beckman EJ, Hu J, Yuang G-G, Agarwal S, Hollinger JO. Synthesis, biodegradability, and biocompatibility of lysine diisocyanate-glucose polymers. Tissue Eng 2002;8:771-85.
[35] Adhikari R, Gunatillake PA, Griffiths I, Tatai L, Wickramaratna M, Houshyar S, et al. Biodegradable injectable polyurethanes: synthesis and evaluation for orthopaedic applications. Biomaterials 2008;29:3762-70.
[36] Pailler-Matteia C, Beca S, Zahouani Z. In vivo measurements of the elastic mechanical properties of human skin by indentation tests Medical Eng and Physics 2007;In Press.
[37] Seare WJ, Jr. Alloplasts and biointegration. J Endourol 2000;14:9-17.
[38] Abramo AC, De Oliveira VR, Ledo-Silva MC, De Oliveira EL. How texture-inducing contraction vectors affect the fibrous capsule shrinkage around breasts implants? Aesthetic Plast Surg;34:555-60.
[39] Hinz B. The myofibroblast: paradigm for a mechanically active cell. J Biomech;43:146-55.
[40] Li B, Brown KV, Wenke JC, Guelcher SA. Sustained release of vancomycin from polyurethane scaffolds inhibits infection of bone wounds in a rat femoral segmental defect model. J Control Release 2010;145:221 - 30.

CHAPTER IV

BIODEGRADABLE LYSINE-DERIVED POLYURETHANE SCAFFOLDS PROMOTE HEALING IN A PORCINE FULL-THICKNESS EXCISIONAL WOUND MODEL

Introduction

Reports estimate that 35 million cases of significant skin loss occur each year in the United States, of which 7 million become infected and chronic with prolonged times to wound closure [1]. Best estimates suggest that over 2 million Americans currently suffer from chronic ulcers, requiring treatment costs of approximately $8 billion per year [1]. Furthermore, in the acute wound category, over one million burns require hospital visits each year [2]. These cutaneous defects create a need for cost-effective wound care products that actually restore skin function. Autografts are the gold standard for treatment of large, acute, non-infected skin deficits, but they are a painful and precious resource to harvest, with high potential for unsightly donor site morbidity [1-3]. Natural and biological-based scaffolds that are currently available, such as Alloderm™, Integra™, Alloskin™ and Oasis™, are thin sheets that provide a temporary wound covering but are not ideal for filling deep tissue defects [4, 5]. Hydrogels have been used to deliver drugs and other biologics to wound sites; however, their small pore size and low porosity can result in delayed cellular infiltration and vascularization, and their low strength and stiffness provide limited mechanical support for tissue infiltration and remodeling [3, 6], hence not reflecting the robust viscoelastic properties that are needed as a protective covering for underlying muscles, nerves and tendons.

Polyurethane (PUR) is a biocompatible synthetic polymer that has been used in medical devices and tissue engineering applications [7]. Lysine-derived PUR scaffolds

(LTI) have been shown to be biocompatible and to degrade into nontoxic decomposition products [8, 9]. Furthermore, PUR scaffolds have potential for injectability and suitability as a delivery platform [10-17]. Chapter III reported that injectable and implantable PUR scaffolds supported cellular infiltration and extracellular matrix synthesis in rat excisional wounds [10]. However, rat skin differs from human skin both physiologically and anatomically. Both the dermis and epidermis are thinner in rats than in humans, the vascularity is much less in rats, and loose-skinned rats heal primarily through contraction rather than production of robust granulation tissue and epithelialization [18]. To achieve greater clinical relevance, the porcine wound model was chosen for the present study since pig and human skin have similar density and distribution of blood vessels, sweat glands, and hair follicles [18]. Furthermore, pigs and humans have similar epidermal thickness and heal primarily through re-epithelialization rather than contraction [18].

Previous studies have investigated the use of void-filling scaffolds in porcine wound models [19-22]. A study by Huang et al. treated full-thickness porcine wounds with a bilayer dressing comprising an internal gelatin sponge layer incorporating basic fibroblast growth factor-loaded microspheres protected by an elastomeric membrane [19]. After 21 days, wounds treated with the dressing had smaller areas, thicker epidermis, and better collagen organization than control wounds treated with Vaseline gauze. Studies by Greenwood and Dearman investigated the use of biodegradable PUR foams as a temporizing matrix prior to skin graft surgery [20, 21]. Porcine excisional wounds treated with a PUR foam sealed with a microporous PUR membrane had no signs of infection and delayed contraction compared to wounds treated with Integra after 28 days.

However, wounds treated with unsealed foams exhibited significant contraction and had thick scar layers above the implants.

The goal of the present study was to define cutaneous wound healing processes in the presence of a biocompatible void filler and to examine the positive or negative impact of two different modifications. We implanted single-layer PUR scaffolds that were synthesized from lysine triisocyanate and a polyester triol and tested for their potential to facilitate dermal wound healing in a full thickness porcine excisional wound model, without the use of protective membranes. Carboxymethylcellulose was added as a porogen to increase scaffold permeability and interconnectivity. Plasma treatment was applied to decrease the hydrophobicity of the scaffold surface. Evaluation of the degradation properties of the scaffolds and their ability to support cellular infiltration and blood vessel formation showed favorable biomaterial performance.

Methods

Materials

Glycolide and D,L-lactide were obtained from Polysciences (Warrington, PA). Glycerol and the sodium salt of carboxymethylcellulose (90 kDa) were purchased from Acros Organics (Morris Plains, NJ). TEGOAMIN33, a tertiary amine catalyst composed of 33 wt % triethylene diamine (TEDA) in dipropylene glycol, was received from Goldschmidt (Hopewell, VA). Lysine triisocyanate was obtained from Kyowa Hakko USA (New York), and stannous octoate catalyst was purchased from Nusil technology (Overland Park, KS). All other reagents were obtained from Sigma–Aldrich (St. Louis,

MO). Glycerol was dried at 10 mm Hg for 3 h at 80°C, and ε-caprolactone was dried over anhydrous magnesium sulfate prior to use. All other materials were used as received.

PUR Scaffold Synthesis

A polyester triol (900 Da) with a backbone comprising 60% caprolactone, 30% glycolide, and 10% lactide was synthesized by reacting a glycerol starter, cyclic ester monomers (ε-caprolactone, glycolide, and D,L-lactide), and stannous octoate catalyst under dry argon for 48 h at 140°C. The resulting polyester triol was vacuum-dried at 80°C for 24 h.

Lysine triisocyanate scaffolds (LTI) were synthesized by reactive liquid molding of the crosslinker with a hardener component comprising the polyester triol, 1.5 parts per hundred parts polyol (pphp) water, 1.5 pphp TEGOAMIN33 catalyst, and 4.0 pphp calcium stearate pore opener. LTI was added to the hardener and mixed for 30 sec in a Hauschild DAC 150 FVZ-K SpeedMixer™ (FlackTek, Inc., Landrum, SC). The resulting mixture then rose freely for 10–20 min and cured. The targeted index (the ratio of NCO to OH equivalents times 100) was 115.

For synthesis of LTI + carboxymethylcellulose scaffolds (CMC), carboxymethylcellulose (15 wt%) was mixed with the hardener component for 30 sec prior to addition of LTI. After curing, the carboxymethylcellulose was leached by incubating for three days in water. For preparation of LTI + carboxymethycellulose + plasma scaffolds (Plasma), leached CMC scaffolds were exposed to oxygen plasma for 60 sec using a Harrick Plasma PDC-001 Plasma Cleaner (Ithaca, NY).

Scaffold Physical and Mechanical Properties

Scaffold densities and porosities were determined from mass and volume measurements of triplicate cylindrical foam cores. The pore size distribution was assessed by scanning electron microscopy (Hitachi S-4200 SEM, Finchampstead, UK) after gold sputter coating with a Cressington Sputter Coater (Vanderbilt Institute for Nanoscale Science and Engineering).

Mechanical testing was performed using a TA Instruments Q800 Dynamic Mechanical Analyzer (DMA) in compression mode (New Castle, DE). Samples were soaked in water for three days prior to mechanical testing. Stress–strain curves were generated by compressing wet cylindrical 12 mm × 8 mm samples at 37°C at a rate of 10% strain per min until they reached 50% strain. The Young's modulus was determined from the slope of the initial linear region of each stress–strain curve.

Air permeability of LTI and CMC scaffolds was determined using the constant pressure gradient method. The air flow rate (Q) necessary to maintain a pressure gradient (ΔP) of 0.12 kPa was measured, and the permeability (k) was calculated by applying Darcy's law:

$$Q = \frac{kA}{m}\frac{\Delta P}{L} \tag{4.1}$$

where L is the scaffold thickness, A is the scaffold cross-sectional area, and μ is the dynamic viscosity of air at room temperature.

Contact Angle Measurements

Polyurethane films were synthesized for contact angle measurement since the porous structure of the scaffolds precludes contact angle measurements on the scaffolds.

PUR films were synthesized by mixing polyester triol, 10 pphp TEGOAMIN33 catalyst, and LTI. The targeted index was 115. The static contact angle of a drop of water on the resulting films was measured using a Rame-Hart goniometer (Succasunna, NJ).

Porcine Excisional Wound Study

All surgical procedures were reviewed and approved by the local Institutional Animal Care and Use Committee. Recommendations from the NIH Guide for the Care and Use of Laboratory Animals (8^{th} Edition, 2011) were observed. The capacity of the scaffolds to facilitate healing in full-thickness cutaneous defects was evaluated in an excisional wound model (6.25 cm^2 square wounds) in female Yorkshire pigs (50 lbs). Treatment groups included untreated wounds (negative control, n = 4) and LTI, CMC, and Plasma PUR scaffolds (n = 6). To reduce production of exudate, excisional wounds were created 24 h prior to scaffold implantation. This delay allowed us to advance beyond the period of hemostasis and thereby reduce the exudative characteristics of the wound bed. Buprenex (an analgesic) and cefazolin (an antibiotic) were given at the time of surgery. For the remainder of the study, the analgesic fentanyl was applied in a 50 mcg/hr transdermal patch that was replaced every three days, and 500 mg of the antibiotic cephalexin was given twice daily.

Before surgery, scaffolds were trimmed into square pieces measuring 2.5 cm x 2.5 cm x 0.3 cm. All scaffolds were sterilized using ethylene oxide. Plasma treatment was applied to Plasma scaffolds immediately prior to implantation. Scaffolds were loosely held in place by an X-shaped configuration of spanning sutures that extended from normal skin to normal skin. After scaffold implantation, each wound was dressed with

TELFA non-adherent dressing (Medline, Mundelein, IL), covered with Opsite adhesive film (Smith & Nephew, St. Petersburg, FL) beneath tube gauze, and secured with Vetwrap bandaging tape (3M, St. Paul, MN). Wounds were cleaned and dressings were changed every 2-3 days. Pigs were sacrificed and wounds were harvested at days 8 and 15 after scaffold implantation.

Tissue Analysis

Wounds were fixed in neutral buffered formalin for 48 h, transferred into 70% ethanol for 48 h, embedded in paraffin, and sectioned at 5 μm and stained with Gomori's trichrome. Reparative responses of tissues were examined and quantified using immunohistochemical markers and procedures that we have previously validated [23]. Actively proliferating cells were immunostained for Ki-67 antigen. After heat-mediated target retrieval in citrate buffer at pH 6.0 (DAKO, Carpenteria, CA), endogenous peroxidase activity was neutralized with 3% H_2O_2 for 40 minutes followed by blocking non-specific reactivity with a casein-based protein block (DAKO, Carpintera, CA) for 20 minutes. Slides were incubated with rabbit anti-human Ki-67 (NovaCastra Laboratories Ltd., Newcastle, UK) diluted at 1:2,000 for 60 min. The rabbit Envision HRP System (DAKO) was used with DAB as substrate and the slides counterstained with hematoxylin. Macrophage infiltration into repairing tissues was assessed using MAC387 antisera (AbD Serotec, Raleigh, NC). After antigen retrieval in 0.01 M Tris/HCL pH 10, quenching for peroxidase activity, and blocking of non-specific immunoreactivity, a monoclonal mouse anti-human antibody to a macrophage epitope (MAC387) was used at 1:10,000 for 60 min. Fragmented DNA of apoptotic cells was visualized with the

DeadEnd Colorimetric TUNEL System (Promega Corporation, Madison, WI). The tissue sections were subjected to a second fixation in 4% paraformaldehyde, rinsed, and permeabilized with proteinase K for 5 minutes. The sections then were treated with equilibration buffer (Promega) followed by biotinylated nucleotide incorporation into apoptotic cells using Terminal Deoxynucleotidyl Transferase (TdT). Endogenous peroxidase was neutralized by applying 0.3% hydrogen peroxide to the sections. Applications of streptavidin/HRP and DAB produced apoptotic-specific visible nuclear staining. Quantitative measurements were performed using Image-Pro Plus scientific image analysis software (Media Cybernetic, Inc., Silver Spring, MD.). Data are expressed as the total number of proliferating cells, immunolabeled macrophages, or apoptotic cells.

Density of new capillaries in the wound bed was determined by immunostaining using antisera for Von Willebrand Factor. Sections underwent antigen retrieval using 5 min of digestion with Proteinase K (DAKO, Carpinteria, CA). Following rinses and endogenous blockade with H_2O_2, sections were incubated at 25^0 C in rabbit polyclonal antisera for Factor VIII-related antigen (Von Willebrand Factor; DAKO) for 30 minutes with a dilution of antibody at 1:900. Following this incubation in primary antisera, the sections were processed through the reagents supplied by rabbit Envision + System, HRP kit (DAKO). Data are expressed as area% of endothelial-lined areas within the wound.

Statistical Analysis

One way analysis of variance (ANOVA) was used to evaluate the statistical significance of results. All p-values less than 0.05 were considered statistically significant. Data are presented as mean ± standard error unless otherwise indicated.

Results

PUR Scaffold Physical and Mechanical Properties

The physical and mechanical properties of PUR scaffolds were characterized *in vitro* (Table 4.1). LTI and CMC scaffolds had similar density, porosity, pore size, and compressive modulus. However, CMC scaffolds had a 2.5-fold higher permeability than LTI scaffolds. Consistent with this analysis, SEM images in Figure 4.1 show that CMC scaffolds had similar pore size but higher interconnectivity than LTI scaffolds.

Table 4.1. Physical and mechanical properties of PUR scaffolds. Data are shown as mean ± standard deviation. Dagger denotes significant difference between LTI and CMC scaffolds ($p < 0.05$).

	LTI	CMC
Density (kg/m^3)	99.9 ± 15.3	109.8 ± 8.5
Porosity (vol %)	91.8 ± 1.3	90.9 ± 0.7
Pore size (mm)	370 ± 110	400 ± 110
Permeability (m^2)	$(1.9 \pm 0.4)*10^{-11}$ †	$(4.9 \pm 0.6)*10^{-11}$ †
Compressive modulus (kPa)	18.2 ± 6.1	16.7 ± 2.9

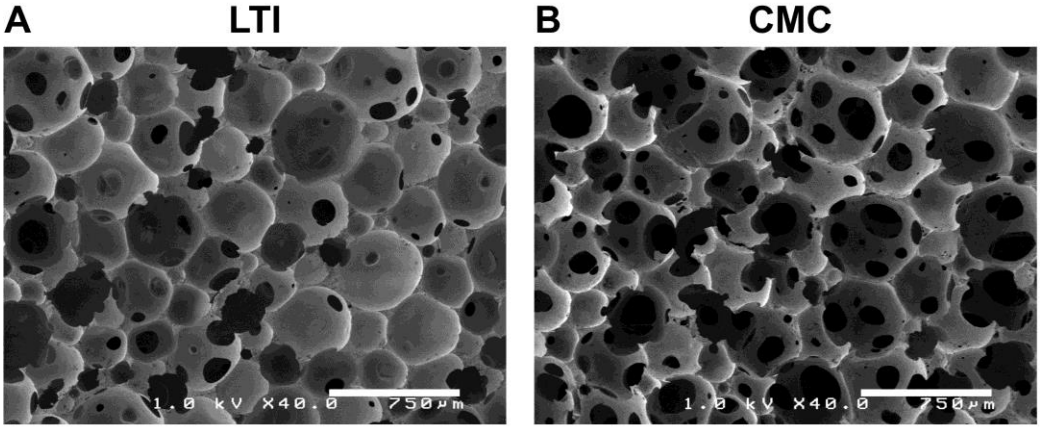

Figure 4.1. SEM images showing pore structure of PUR scaffolds. (A) LTI scaffold. (B) CMC scaffold. LTI and CMC scaffolds exhibit similar pore sizes (300 – 500 μm). CMC scaffolds have more openings in pore walls than LTI scaffolds, resulting in higher permeability. Scale bar = 750 μm.

To confirm that plasma treatment increased the hydrophilicity of the scaffold surface, the contact angle of PUR films was measured before and after plasma treatment. As shown in Figure 4.2, plasma treatment significantly decreased the contact angle from 66° to 46° ($p < 0.005$).

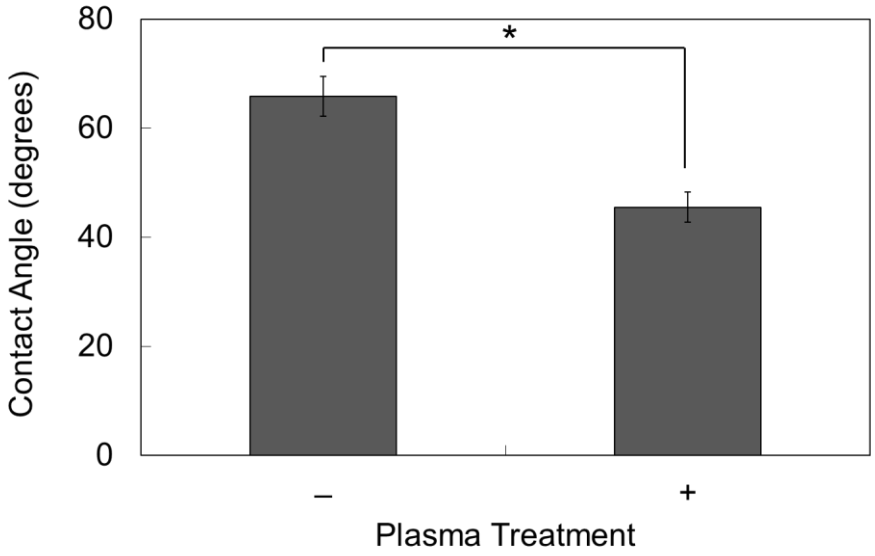

Figure 4.2. Contact angle of LTI films before and after plasma treatment. Contact angle decreased from 65° to 45° after plasma treatment, providing evidence that plasma treatment increases surface hydrophilicity. Asterisk indicates significant difference ($p < 0.005$).

Impact on Wound Dimensions (Wound Contractility)

Measurements of wound dimensions harvested 8 and 15 days after scaffold implantation are shown in Figure 4.3. For all treatment groups, wound area decreased significantly from day 8 to day 15. Untreated wound areas were significantly greater than those of wounds treated with either LTI or Plasma scaffolds at day 8, but there were no significant differences in wound area among treatment groups by day 15 (Fig. 4.3A). There were no differences in epithelialization among the treatment groups at day 8, but untreated wounds were significantly more epithelialized than wounds treated with scaffolds by day 15 (Fig. 4.3B). Representative images of wounds at day 1 and day 15 are shown in Fig. 4.3C, and the degree of wound contraction was quantified in Fig. 4.3D. While wounds from the LTI, CMC, and untreated groups were significantly more

contracted at day 15 than at day 8, wounds treated with scaffolds were significantly less contracted than untreated wounds at day 15.

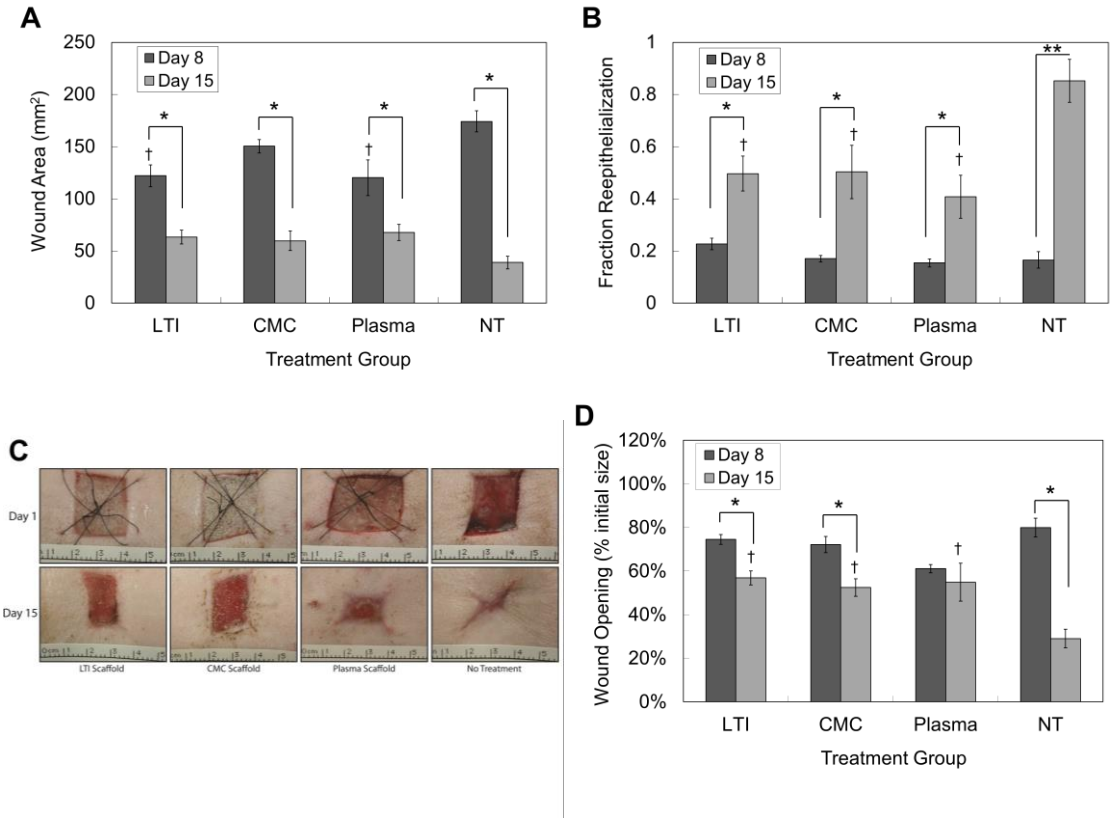

Figure 4.3. Histomorphometry of porcine wounds. (A) Wound cross-sectional area of LTI, CMC, Plasma, and untreated wounds (NT) measured from images of trichrome staining. Asterisks indicate significant difference, and daggers indicate significant difference from no treatment at day 8 ($p < 0.05$). The cross-sectional area of all treatment groups decreased significantly from day 8 to day 15. LTI and Plasma wounds were significantly smaller than untreated wounds at day 8. (B) Fraction reepithelialization measured from images of trichrome staining. Asterisks ($p < 0.05$) and double asterisks ($p < 0.01$) denote significant differences, and daggers indicate significant difference from no treatment at day 15. Epithelialization of all wounds increased from day 8 to day 15, and untreated wounds were more epithelialized than scaffold-treated wounds at day 15. (C) Representative images of wounds at day 1 and day 15. Untreated wounds exhibited greater contraction than scaffold-treated wounds. (D) Wound opening relative to initial size. Asterisks indicate significant difference, and daggers indicate significant difference from no treatment at day 15 ($p < 0.05$). LTI, CMC, and untreated wounds contracted significantly from day 8 to day 15. Untreated wounds had significantly greater contraction than all scaffold-treated wounds at day 15.

Impact on PUR Scaffold Degradation

At day 8, wounds were immature and exhibited little collagen accumulation (Fig. 4.4A), while day 15 wounds that were treated with scaffold showed replacement of the polymer by extracellular matrix (Fig. 4.4B). The progression and extent of PUR degradation, measured by fractional area, decreased significantly from day 8 to day 15 for all scaffold treatment groups (Fig. 4.4C). There were no significant differences in area% PUR among the three PUR treatment groups at both time points, suggesting that the CMC and plasma treatments had an insignificant effect on the rate of PUR degradation. The gradient in trichrome green intensity between the upper (light green) and lower (dark green) regions within the scaffold confirmed that the scaffold-treated wounds have the same polarity of matrix reorganization as untreated wounds.

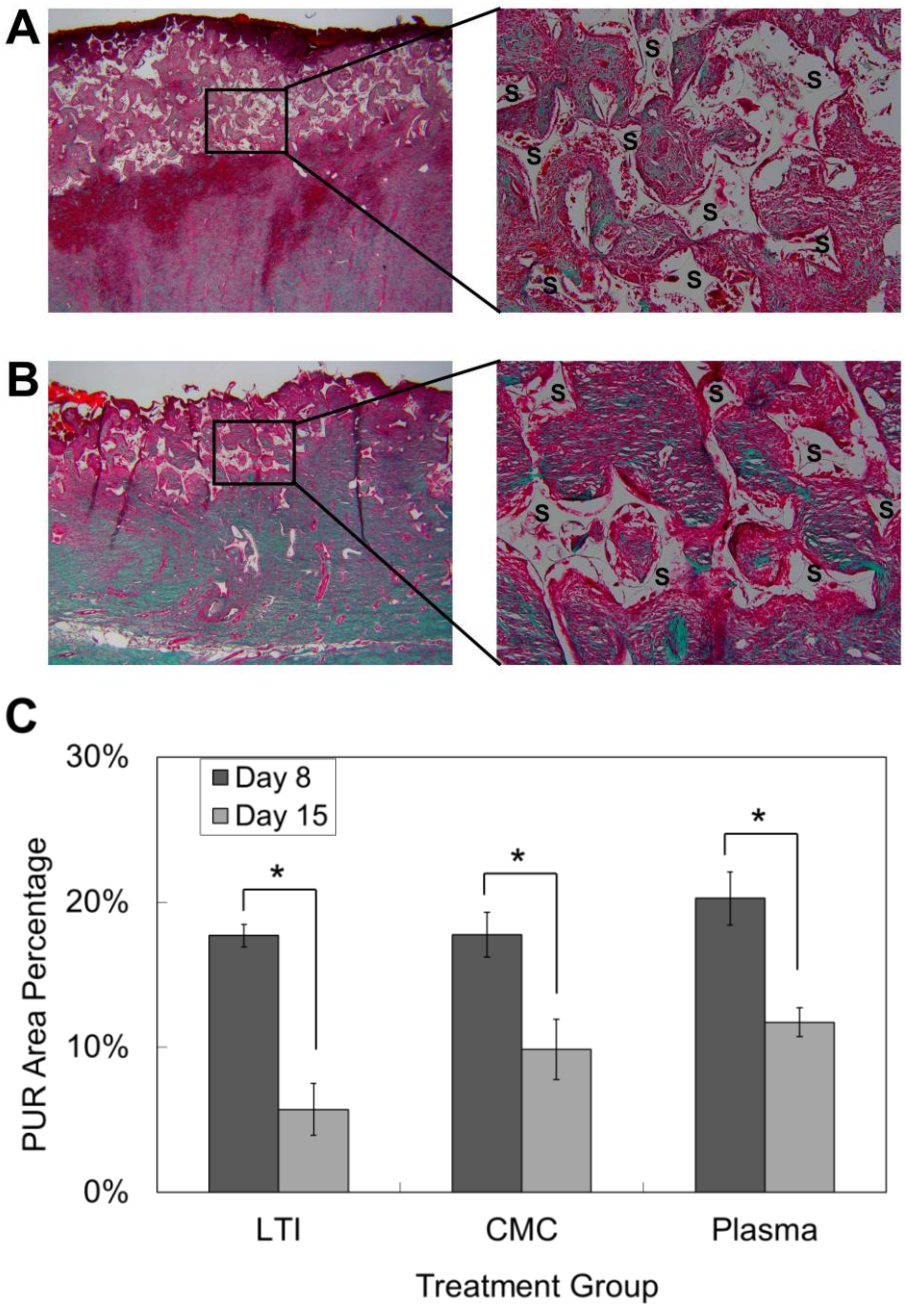

Figure 4.4. PUR scaffold degradation. (A) Representative images of trichrome staining of LTI scaffolds at day 8 at magnifications of 2X (left) and 20X (right). Scaffold fragments are marked by the letter S. (B) Representative images of trichrome staining of CMC scaffolds at day 15 at magnifications of 2x (left) and 20x (right). Fewer scaffold fragments are present at day 15 than at day 8. (C) Percentage of wound cross-sectional area occupied by PUR measured from images of trichrome staining. Asterisks indicate significant difference ($p < 0.05$). All scaffolds-treated wounds had significantly less polyurethane remaining at day 15 than at day 8, providing evidence that PUR scaffolds underwent biodegradation.

Impact on Cell Proliferation and Apoptosis

For all treatment groups, the number of proliferating cells decreased significantly from day 8 to day 15 (Fig. 4.5 A). This result suggests that all wounds were transitioning from the proliferative phase to the maturation phase by day 15. At day 8, untreated wounds had more than three times as many $Ki67^+$ cells as wounds treated with scaffolds ($p < 0.02$), suggesting that the presence of scaffold serves as a signal that dampens the proliferative response. Subtle differences in the proliferative response were detected among the three scaffold treated groups. The LTI treatment group had significantly more $Ki67^+$ cells than the Plasma treatment group, which in turn had significantly more $Ki67^+$ cells than the CMC treatment group. By day 15, untreated wounds had significantly fewer $Ki67^+$ cells than CMC and Plasma treatment groups, suggesting that the formation of granulation tissue develops and resolves more quickly in the absence of scaffolds.

TUNEL staining to assess the effect of scaffolds on apoptosis detected differential responses to treatment (Fig. 4.5B). At day 8, the Plasma treatment group had significantly more $TUNEL^+$ cells than the LTI and CMC groups. The number of $TUNEL^+$ cells increased significantly from day 8 to day 15 in wounds treated with LTI scaffolds. Wounds treated with Plasma scaffolds and untreated wounds had fewer $TUNEL^+$ cells at day 15 than at day 8, which suggests that these wounds were moving more quickly into a resolution/remodeling phase of repair by day 15.

Furthermore, the ratio of proliferation to apoptosis was quantified (Fig. 4.5C). The ratio of $Ki67^+$ cells to $TUNEL^+$ cells was calculated and adjusted assuming that Ki67 is expressed for ~15 h in proliferating cells (the length of a fibroblast cell cycle [24]) and TUNEL is expressed for ~2 h during apoptosis [25]. At day 8, untreated wounds had a

significantly higher ratio than the LTI treatment group, which had a significantly higher ratio than the CMC and Plasma treatment groups. By day 15, there were no significant differences in proliferation/apoptosis ratio, which was slightly greater than one for all treatment groups. These results suggest that all wounds were moving into the remodeling phase by day 15.

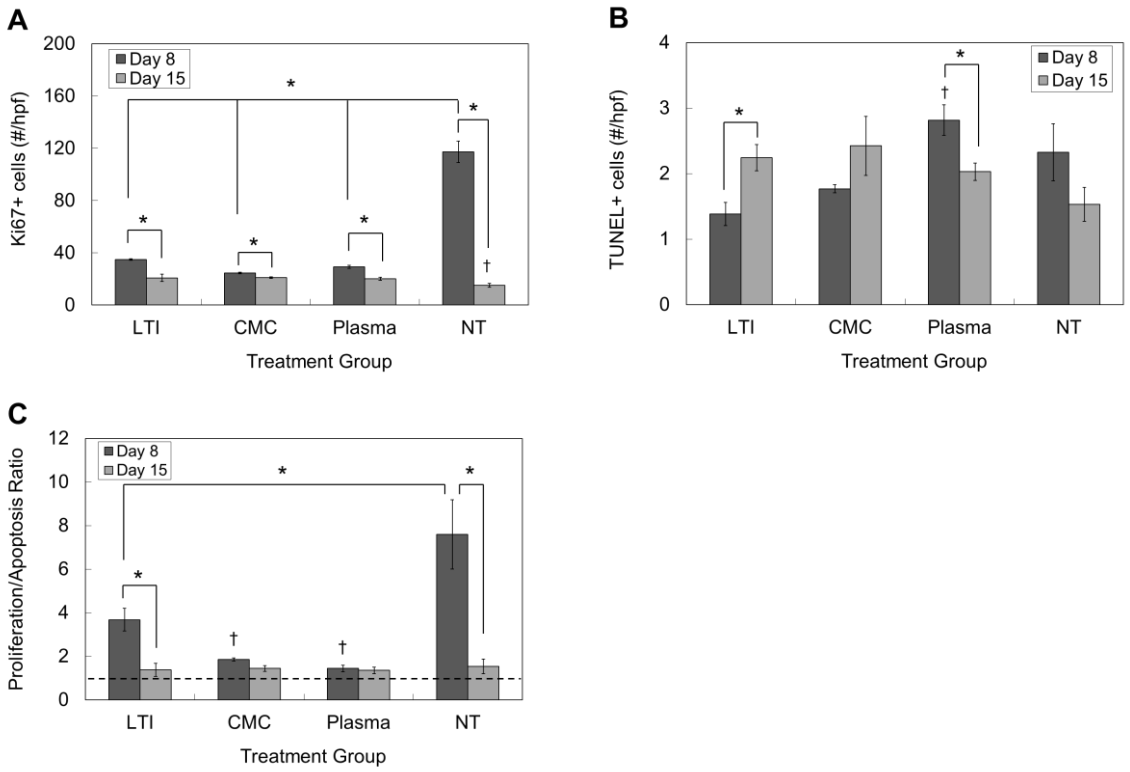

Figure 4.5. Analysis of cell proliferation and apoptosis. (A) Ki67 immunostaining was used to analyze the presence of proliferating cells. Data are presented as number of $Ki67^+$ cells per high power field (hpf). Asterisks indicate significant difference ($p < 0.05$). Dagger indicates significant difference from CMC and Plasma at day 15 ($p < 0.02$). The number of $Ki67^+$ cells decreased significantly from day 8 to day 15 in all treatment groups. At day 8, there were significant differences among all treatment groups. At day 15, CMC and Plasma groups had significantly more proliferating cells than untreated wounds. (B) TUNEL immunostaining was used to analyze the presence of apoptosing cells. Data are presented as number of $TUNEL^+$ cells per hpf. Asterisks indicate significant difference ($p < 0.05$). Dagger indicates significant difference from LTI and CMC at day 8 ($p < 0.01$). The number of $TUNEL^+$ cells increased significantly from day 8 to day 15 in LTI scaffolds and decreased significantly from day 8 to day 15 in Plasma scaffolds. At day 8, wounds treated with Plasma scaffolds had significantly more $TUNEL^+$ cells than wounds treated with LTI and CMC scaffolds. (C) Ratio of proliferation to apoptosis. Dashed line represents a ratio of one. Asterisks indicate significant difference ($p < 0.01$), and dagger denotes significant difference from LTI and untreated wounds at day 8. By day 15, there were no significant differences in proliferation/apoptosis ratio among treatment groups.

Impact on Macrophage Recruitment and Persistence

Macrophage numbers typically peak in the acute wound healing setting at around 4-5 days [26]. Thus, it was anticipated that macrophage numbers would decline in the untreated wounds between day 8 and day 15 in the absence of any scaffold material (foreign body) or inflammatory stimulus. At day 8, there were no significant differences in number of $MAC387^{+}$ macrophages among all treatment groups (Figure 4.6). However, the number of macrophages in wounds treated with CMC or Plasma scaffolds increased significantly from day 8 to day 15 while the number of macrophages decreased for the LTI and untreated groups. The increase in the number of macrophages from day 8 to day 15 in the CMC and Plasma groups reflects the response to the presence of the scaffolds that contained carboxymethylcellulose.

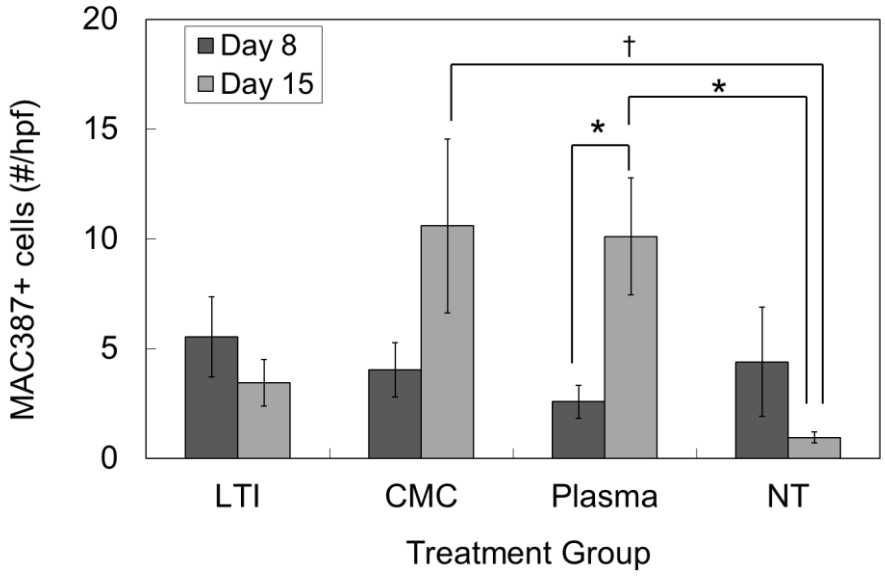

Figure 4.6. Analysis of MAC387$^+$ cells. MAC387 immunostaining was used to analyze the presence of macrophages. Data are presented as number of MAC387$^+$ cells per hpf. Asterisks ($p < 0.02$) and dagger ($p < 0.005$) indicate significant difference. The number of MAC387$^+$ cells increased significantly from day 8 to day 15 in Plasma scaffolds. At day 15, wounds treated with CMC and Plasma scaffolds had significantly more MAC397$^+$ cells than untreated wounds.

Impact on Blood Vessel Formation

Angiogenesis is a major component of granulation tissue progression. As shown in Figure 4.7, the density of factor VIII-positive blood vessels (area% occupied by blood vessels) increased significantly from day 8 to day 15 in LTI, Plasma, and untreated groups. Stated differently, the formation of granulation tissue was robust within all treatment groups and was a prominent feature during the window of time examined in this study. No significant differences in blood vessel percentage among the treatment groups were noted at either time point. These results show that treatment with the three different types of PUR scaffolds did not alter blood vessel formation during the wound healing process.

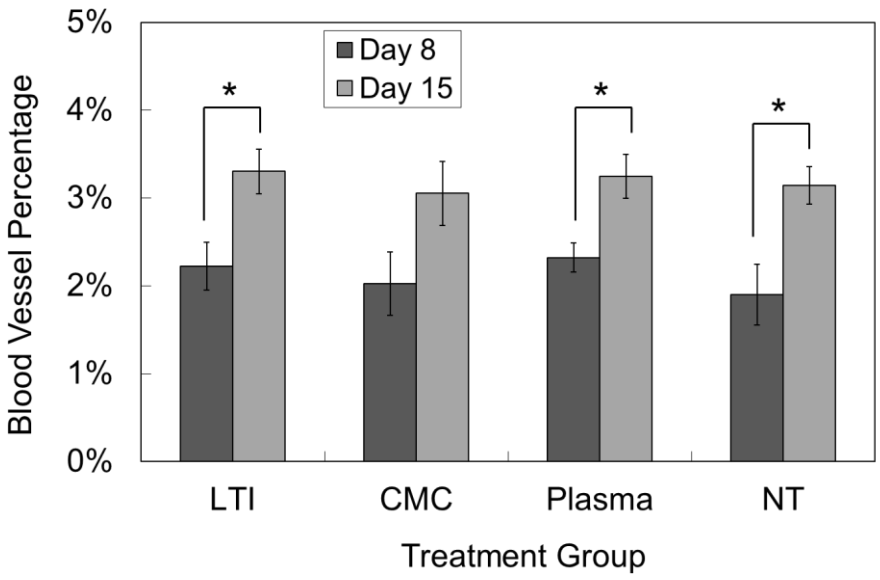

Figure 4.7. Blood vessel formation. Factor VIII immunostaining was used to analyze the presence of blood vessels. Data are presented as area% of blood vessels within the wound. Asterisks indicate significant difference ($p < 0.05$). The blood vessel density increased significantly from day 8 to day 15 in LTI, Plasma, and untreated wounds.

Discussion

PUR scaffolds were tested for their ability to safely and effectively support and modify the healing properties of full-thickness porcine excisional wounds in order to validate their clinical value. Two modifications were applied to the scaffolds to determine if scaffolds could be fine-tuned to increase the degree of cellular infiltration and attachment. Carboxymethylcellulose was added as a porogen to increase pore interconnectivity and thus facilitate cellular infiltration throughout the scaffold. Plasma treatment was applied to decrease the hydrophobicity of the scaffold surface and thereby provide a more hospitable substrate for cell attachment. *In vitro* characterization of the scaffolds showed that addition of carboxymethylcellulose increased the permeability of the scaffolds 2.5-fold, and plasma treatment decreased the contact angle by 20°. The

permeability of the scaffolds is comparable to that of rigid open-cell foams reported by Zhao et al. (10^{-12} – 10^{-10} m^2) [27]. When implanted in porcine excisional wounds, PUR scaffolds stented the wounds, resulting in significantly less wound contraction than untreated wounds at day 15. This result is consistent with our previous study in a loose-skinned, rodent model showing that PUR composite scaffolds stented rat excisional wounds at early time points, thereby diminishing the degree of undesirable contraction and scarring [10]. All three versions of the scaffolds showed a statistically significant rate of biodegradation between the day 8 and day 15 that reduced — but did not prevent — wound contraction. Further optimization of the degradation rate of the PUR scaffold may help to achieve the long sought after aesthetic and functional goal: a lessening of undesirable wound contraction.

In untreated wounds, the number of macrophages decreased from day 8 to day 15, consistent with wounds moving into resolution in the absence of scaffold material that — while transiently present — promotes a typical foreign body response [26]. As the scaffolds underwent infiltration, degradation and fragmentation between day 8 and day 15, the number of macrophages only increased in the CMC and Plasma groups, suggesting that carboxymethylcellulose treatment influenced the innate immune response. Macrophage presence in the wounds that were treated with carboxymethylcellulose-containing scaffolds was significantly greater than in untreated wounds at day 15. We have previously shown that PUR scaffolds undergo oxidative degradation mediated by macrophages [9]. The increase in macrophages in CMC and Plasma groups provides evidence that the scaffolds were being degraded by macrophages. It is possible that LTI scaffolds were slower to attract macrophages due to

their lower permeability and hydrophilicity than the other scaffold groups, leading to a slower rate of oxidative degradation at these relatively early time points.

All treatment groups had significantly fewer $Ki67^+$ cells at day 15 than at day 8, an indication that all wounds were moving from the proliferative phase to the remodeling phase by day 15 [26]. At day 15, the proliferation/apoptosis ratio was slightly greater than one for all treatment groups. Furthermore, the number of $TUNEL^+$ cells and the blood vessel area% in untreated wounds were not significantly different from scaffold-treated groups at either time point. These data suggest that the PUR scaffolds do not adversely affect the wound healing process in porcine excisional wounds.

There were few significant differences in wound healing among LTI, CMC, and Plasma scaffolds. By day 8, all three scaffolds exhibited good tissue infiltration, which suggests that the changes in interconnectivity and hydrophilicity of the scaffolds by addition of carboxymethylcellulose or plasma treatment did not significantly improve scaffold performance. We have reported that injectable, lysine-derived PUR scaffolds reduced wound contraction in rat excisional wounds. However, porcine skin has an elastic modulus of 5.9 ± 1.5 MPa [28], which is 15 times greater than that of rat skin (0.40 ± 0.15 MPa) [10]. Another study has reported that a biodegradable PUR foam with a sealing membrane resulted in less contraction than Integra in a porcine excisional wound model while PUR foams without a sealing membrane did not reduce contraction [21], but the relative contributions of the foam and the membrane to space maintenance are not known. In the present study, single-layer PUR scaffolds prevented contraction without the use of protective membranes. In summary, PUR scaffolds implanted in porcine excisional wounds were biocompatible and supported tissue infiltration and

wound healing. Future work will involve testing injectable PUR scaffolds in porcine excisional wounds.

Conclusions

In conclusion, PUR scaffolds were biocompatible, biodegradable, and supported tissue infiltration in porcine excisional wounds. PUR scaffolds stented the wounds, lessening unwanted contraction at day 15. Consistent with previous studies showing macrophage-mediated degradation of PUR scaffolds, higher numbers of macrophages were present in scaffold-treated wounds compared to untreated wounds. Analysis of proliferating cells, apoptosing cells, and blood vessels suggests that the presence of scaffolds did not otherwise interfere with the wound healing process.

References

[1] Clark RAF, Ghosh K, Tonnesen MG. Tissue engineering for cutaneous wounds. Journal of Investigative Dermatology 2007;127:1018-29.
[2] Supp DM, Boyce ST. Engineered skin substitutes: practices and potentials. Clinics in Dermatology 2005;23:403-12.
[3] Lim CT, Zhong SP, Zhang YZ. Tissue scaffolds for skin wound healing and dermal reconstruction. Wiley Interdisciplinary Reviews-Nanomedicine and Nanobiotechnology 2010;2:510-25.
[4] Eccleston GM, Boateng JS, Matthews KH, Stevens HNE. Wound healing dressings and drug delivery systems: A review. Journal of Pharmaceutical Sciences 2008;97:2892-923.
[5] Mostow EN, Haraway GD, Dalsing M, Hodde JP, King D, Grp OVUS, et al. Effectiveness of an extracellular matrix graft (OASIS Wound Matrix) in the treatment of chronic leg ulcers: A randomized clinical trial. Journal of Vascular Surgery 2005;41:837-43.
[6] Raeber GP, Lutolf MP, Hubbell JA. Molecularly engineered PEG hydrogels: a novel model system for proteolytically mediated cell migration. Biophysical journal 2005;89:1374-88.
[7] Guelcher SA. Biodegradable polyurethanes: Synthesis and applications in regenerative medicine. Tissue Engineering Part B-Reviews 2008;14:3-17.
[8] Guelcher SA, Srinivasan A, Dumas JE, Didier JE, McBride S, Hollinger JO. Synthesis, mechanical properties, biocompatibility, and biodegradation of polyurethane networks from lysine polyisocyanates. Biomaterials 2008;29:1762-75.
[9] Guelcher SA, Hafeman AE, Zienkiewicz KJ, Zachman AL, Sung HJ, Nanney LB, et al. Characterization of the degradation mechanisms of lysine-derived aliphatic poly(ester urethane) scaffolds. Biomaterials 2011;32:419-29.
[10] Adolph EJ, Hafeman AE, Davidson JM, Nanney LB, Guelcher SA. Injectable Polyurethane Composite Scaffolds Delay Wound Contraction and Support Cellular Infiltration and Remodeling in Rat Excisional Wounds. Wound Repair and Regeneration 2011;19:A9-A.
[11] Guelcher SA, Dumas JE, Zienkiewicz K, Tanner SA, Prieto EM, Bhattacharyya S. Synthesis and Characterization of an Injectable Allograft Bone/Polymer Composite Bone Void Filler with Tunable Mechanical Properties. Tissue Engineering Part A 2010;16:2505-18.
[12] Guelcher SA, Patel V, Gallagher KM, Connolly S, Didier JE, Doctor JS, et al. Synthesis and in vitro biocompatibility of injectable polyurethane foam scaffolds. Tissue Engineering 2006;12:1247-59.
[13] Hafeman AE, Zienkiewicz KJ, Li B, Davidson JM, Guelcher SA. Synthesis and in vivo characterization of injectable and biodegradable polyurethane scaffolds in a wound healing model. Tissue Engineering Part A 2008;14:910-1.
[14] Nelson CE, Kim AJ, Adolph EJ, Gupta MK, Yu F, Hocking KM, et al. Tunable delivery of siRNA from a biodegradable scaffold to promote angiogenesis in vivo. Advanced materials (Deerfield Beach, Fla) 2014;26:607-14, 506.

[15] Dumas JE, BrownBaer PB, Prieto EM, Guda T, Hale RG, Wenke JC, et al. Injectable reactive biocomposites for bone healing in critical-size rabbit calvarial defects. Biomedical materials (Bristol, England) 2012;7:024112.
[16] Guelcher SA, Li B, Davidson JM. The effect of the local delivery of platelet-derived growth factor from reactive two-component polyurethane scaffolds on the healing in rat skin excisional wounds. Biomaterials 2009;30:3486-94.
[17] Guelcher SA, Hafeman AE, Li B, Yoshii T, Zienkiewicz K, Davidson JM. Injectable biodegradable polyurethane scaffolds with release of platelet-derived growth factor for tissue repair and regeneration. Pharmaceutical research 2008;25:2387-99.
[18] Sullivan TP, Eaglstein WH, Davis SC, Mertz P. The pig as a model for human wound healing. Wound repair and regeneration : official publication of the Wound Healing Society [and] the European Tissue Repair Society 2001;9:66-76.
[19] Huang S, Deng T, Wu H, Chen F, Jin Y. Wound dressings containing bFGF-impregnated microspheres. Journal of Microencapsulation 2006;23:277-90.
[20] Greenwood JE, Dearman BL. Split skin graft application over an integrating, biodegradable temporizing polymer matrix: immediate and delayed. Journal of burn care & research : official publication of the American Burn Association 2012;33:7-19.
[21] Greenwood JE, Dearman BL. Comparison of a sealed, polymer foam biodegradable temporizing matrix against Integra(R) dermal regeneration template in a porcine wound model. Journal of burn care & research : official publication of the American Burn Association 2012;33:163-73.
[22] van der Veen VC, van der Wal MBA, van Leeuwen MCE, Ulrich MMW, Middelkoop E. Biological background of dermal substitutes. Burns 2010;36:305-21.
[23] Nanney LB, Woodrell CD, Greives MR, Cardwell NL, Pollins AC, Bancroft TA, et al. Calreticulin enhances porcine wound repair by diverse biological effects. The American journal of pathology 2008;173:610-30.
[24] Kasinathan P, Knott JG, Moreira PN, Burnside AS, Jerry DJ, Robl JM. Effect of fibroblast donor cell age and cell cycle on development of bovine nuclear transfer embryos in vitro. Biology of reproduction 2001;64:1487-93.
[25] Gavrieli Y, Sherman Y, Ben-Sasson SA. Identification of programmed cell death in situ via specific labeling of nuclear DNA fragmentation. The Journal of cell biology 1992;119:493-501.
[26] Braiman-Wiksman L, Solomonik I, Spira R, Tennenbaum T. Novel insights into wound healing sequence of events. Toxicologic pathology 2007;35:767-79.
[27] Zhao W, Pizzi A, Fierro V, Du G, Celzard A. Effect of composition and processing parameters on the characteristics of tannin-based rigid foams. Part I: Cell structure. Materials Chemistry and Physics 2010;122:175-82.
[28] Zak M, Kuropka P, Kobielarz M, Dudek A, Kaleta-Kuratewicz K, Szotek S. Determination of the mechanical properties of the skin of pig foetuses with respect to its structure. Acta of bioengineering and biomechanics / Wroclaw University of Technology 2011;13:37-43.

CHAPTER V

INJECTABLE BIODEGRADABLE POLYURETHANE SCAFFOLDS SUPPORT TISSUE INFILTRATION AND DELAY WOUND CONTRACTION IN A PORCINE EXCISIONAL MODEL

Introduction

The number of people affected by chronic wounds is growing rapidly due to the aging of the population and a rising incidence of diseases such as diabetes and obesity [1-4]. Reports estimate that $25 billion is spent annually on treatment for chronic wounds in the United States [1-3]. Furthermore, patients with acute wounds or scarring resulting from surgical or traumatic injuries require healthcare that costs $12 billion annually [1]. The morbidity, incidence, and cost of these cutaneous defects create a need for cost-effective wound care products that restore tissue function. Injectable biomaterials that can conform to fill deep tissue defects, incorporate and deliver biologics at the point of care, offer patient-specific customization, and be applied with minimally invasive surgical techniques are a promising approach to skin wound healing [5]. However, successful injectable scaffolds must meet several requirements. The reactants and intermediates must be noncytotoxic, and the reaction exotherm must be minimal [5, 6]. The injectable biomaterial must be flowable for a sufficient time (the working time) so that it can be applied as a liquid, and it must cure within minutes (the setting time) to avoid long surgical procedures. In addition, porous scaffolds must have reproducible porosity, permeability, and pore size that are sufficient for cell migration, nutrient exchange, and tissue ingrowth [7].

Injectable hydrogels and smart biomaterials have been used as drug delivery systems in a variety of applications. A fluorocarbon-functionalized poly(ethylene glycol)

phase separation system was shown to deliver therapeutic proteins with diffusion-controlled release kinetics [8], and a copolymer of N-isopropylacrylamide and propylacrylic acid has been developed for use as a delivery vehicle for angiogenic factors to sites of ischemia [9]. However, these biomaterials are not well-suited for tissue engineering applications due to their weak mechanical properties (low modulus and strength and high fragility). In contrast, *in situ* polymerizable scaffolds can achieve robust mechanical properties due to polymerization and crosslinking. Our group has used lysine-derived polyurethane (PUR) scaffolds for skin wound healing and bone regeneration applications [10-15]. These scaffolds have been shown to be biocompatible and biodegradable, and they have tunable mechanical and degradation properties [16]. Moreover, they have potential for injectability and delivery of biologics [10, 11, 17]. In one study, injectable allograft bone/PUR composite scaffolds were shown to support tissue infiltration and new bone formation in femoral plug defects in rats [12]. In the rat excisional wound study described in Chapter III, injectable PUR scaffolds stented wounds, delayed wound contraction, and supported cellular infiltration and matrix remodeling [13].

In the present study, injectable PUR scaffolds were applied in a porcine full-thickness excisional wound model. Due to the promising results from the small animal models, PUR scaffolds were tested in a large animal model with greater clinical relevance. The porcine wound model was used because pigs and humans have many anatomical and physiological similarities. Pigs and humans have comparable dermal and epidermal thickness and similar density and distribution of blood vessels, sweat glands, and hair follicles [18]. Pigs and humans heal primarily through epithelialization and

granulation tissue formation; in contrast, loose-skinned rodents heal mainly through wound contraction [18]. Previous studies on the use of scaffolds in porcine full-thickness wounds have involved pre-formed implants with multiple layers. A study by Huang et al. found that full-thickness porcine wounds treated with a bilayer dressing comprising an internal gelatin sponge layer incorporating basic fibroblast growth factor-loaded microspheres protected by an elastomeric membrane had smaller area, thicker epidermis, and better collagen organization than control wounds treated with Vaseline gauze [19]. Furthermore, Greenwood and Dearman showed that wounds treated with biodegradable PUR foams sealed with a microporous PUR membrane had no signs of infection and delayed contraction compared to wounds treated with Integra after 28 days [20, 21]. In Chapter IV, single-layer implantable polyurethane scaffolds were shown to delay contraction and facilitate healing in porcine excisional wounds. To our knowledge, injectable scaffolds have not been tested previously in a porcine cutaneous wound model. In this study, injectable PUR scaffolds were compared to pre-formed PUR implants in their ability to support cellular infiltration and facilitate wound healing. The physical, mechanical, and rheological properties of the scaffolds were characterized *in vitro*. In the porcine excisional wound study, PUR scaffold impact on wound contraction, epithelialization, cell proliferation and apoptosis, macrophage presence, and blood vessel formation was analyzed.

Methods

Materials

Glycolide and D,L-lactide were obtained from Polysciences (Warrington, PA). Glycerol was purchased from Acros Organics (Morris Plains, NJ). Lysine triisocyanate-poly(ethylene glycol) (LTIPEG) prepolymer was obtained from Ricerca (Concord, OH). TEGOAMIN33, a tertiary amine catalyst composed of 33 wt % triethylene diamine (TEDA) in dipropylene glycol, was received from Goldschmidt (Hopewell, VA). Sucrose was obtained from Spectrum® (New Brunswick, NJ), and stannous octoate catalyst was purchased from Nusil technology (Overland Park, KS). All other reagents were obtained from Sigma–Aldrich (St. Louis, MO). Glycerol was dried at 10 mm Hg for 3 h at 80°C, and ε-caprolactone was dried over anhydrous magnesium sulfate prior to use. All other materials were used as received.

PUR Scaffold Synthesis

A polyester triol (900 Da) with a backbone comprising 60% caprolactone, 30% glycolide, and 10% lactide was synthesized by reacting a glycerol starter with the cyclic ester monomers (ε-caprolactone, glycolide, and D,L-lactide) in the presence of stannous octoate catalyst. After carrying out the reaction under dry argon for 48 h at 140°C, the resulting polyester triol was vacuum-dried at 80°C for 24 h.

40% sucrose implants were synthesized by reactive liquid molding of the LTIPEG prepolymer with a hardener component and sucrose (300 – 500 μm). The hardener comprised 100 parts polyester triol, 5 parts per hundred parts polyol (pphp) water, and 5.5 pphp 30% TEGOAMIN catalyst in dipropylene glycol. The hardener was combined

with sucrose and mixed with a spatula for 30 sec. The prepolymer was then added and mixed with a spatula for 30 sec. The resulting mixture rose freely and cured. The targeted index (the ratio of NCO to OH equivalents times 100) was 115. After curing, the scaffold was cut into pieces of various sizes for the pig study or *in vitro* characterization.

Physical and Mechanical Properties

Scaffold densities and porosities were determined from mass and volume measurements of triplicate cylindrical foam cores. To determine physical properties after leaching, scaffolds were incubated in DPBS on a shaker for 72 h. Scaffolds were then blotted dry and vacuum-dried for 24 – 48 h. The pore size distribution was assessed by scanning electron microscopy (Hitachi S-4200 SEM, Finchampstead, UK) after gold sputter coating with a Cressington Sputter Coater (Vanderbilt Institute for Nanoscale Science and Engineering).

Mechanical testing was performed using a TA Instruments Q800 Dynamic Mechanical Analyzer (DMA) in compression mode (New Castle, DE). Samples were leached in DPBS for three days prior to mechanical testing. Stress–strain curves were generated by compressing wet cylindrical 12 × 8 mm samples at 37°C at a rate of 10% strain per min until they reached 50% strain. The Young's modulus was determined from the slope of the initial linear region of each stress–strain curve.

Permeability

The permeability of PUR scaffolds foamed in different environments was investigated. The PUR reaction mixture was injected into empty Teflon containers (dry environment) or Teflon containers filled with water (wet environment to mimic surgery

conditions) and allowed to cure. Scaffolds were cut into 2 x 2 x 0.5 cm pieces. During scaffold formation, a film with lower porosity than the bulk material formed on the surface. Permeability was measured before and after removal of the surface film. To determine permeability after leaching, scaffolds were incubated in DPBS on a shaker for 72 h. Scaffolds were then dried under vacuum for 24 – 48 h. Air permeability of PUR scaffolds was determined using the constant pressure gradient method. The air flow rate (Q) necessary to maintain a pressure gradient (ΔP) of 0.12 kPa was measured, and the permeability (k) was calculated by applying Darcy's law.

$$Q = \frac{kA}{m}\frac{\Delta P}{L} \tag{5.1}$$

where L is the scaffold thickness, A is the scaffold cross-sectional area, and μ is the dynamic viscosity of air at room temperature.

Rheological Properties

The cure profile of 40% sucrose scaffolds was measured using a TA Instruments parallel plate AR 2000ex rheometer operating in dynamic mode with 25 mm disposable aluminum plates (New Castle, DE). After mixing the LTIPEG with the hardener and sucrose for 30 sec, the reaction mixture was loaded onto the bottom plate of the rheometer. An oscillation time sweep was run with a controlled strain of 1% and a frequency of 6.28 rad/s in order to obtain the cure profile. The storage modulus (G') and loss modulus (G") were determined as a function of time. The working time was determined to be the G-crossover point. To measure the tack-free time, the surface of the

foam was contacted with a spatula at regular intervals of one minute. The tack-free time was determined to be the time at which the foam did not stick to the spatula.

Pig Study Surgery

All surgical procedures were reviewed and approved by the local Institutional Animal Care and Use Committee. NIH Guide for the Care and Use of Laboratory Animals (8^{th} Edition, 2011) were observed. The capacity of the scaffolds to facilitate healing in full-thickness cutaneous defects was evaluated in an excisional wound model (9 cm^2 square wounds) in female Yorkshire pigs (50 lbs). Treatment groups included untreated wounds (negative control) and 70% sucrose injectable, 40% sucrose injectable, and 40% sucrose implant scaffolds. The study design is displayed in Table 5.1. Due to the poor performance of 70% injectable scaffolds in the first study with two pigs sacrificed at days 9 and 13, this treatment group was removed from the second study with three pigs sacrificed at days 9, 13, and 30. Excisional wounds were created 24 h prior to scaffold implantation. This delay allowed us to advance beyond the period of hemostasis and thereby reduce the exudative characteristics of the wound bed. Buprenex (an analgesic) and cefazolin (an antibiotic) were given at the time of surgery. For the remainder of the study, the analgesic fentanyl was applied in a 50 mcg/hr transdermal patch that was replaced every three days, and 500 mg of the antibiotic cephalexin was given twice daily.

Table 5.1. Experimental design for porcine excisional wound study.

Time Point	Number of Pigs	70% Injectable	40% Injectable	40% Implant	No Treatment
Day 9	2	n = 4	n = 9	n = 9	n = 9
Day 13	2	n = 4	n = 9	n = 9	n = 9
Day 30	1	n = 0	n = 5	n = 5	n = 5

40% sucrose implants as well as reactants for 40% and 70% sucrose injectables were prepared prior to surgery. 40% sucrose scaffolds were cut into 3.5 x 3.5 x 0.2 cm implants, sterilized using ethylene oxide, and then leached in sterile DPBS for 72 h. For 40% and 70% sucrose injectable scaffolds, reactants were sterilized prior to scaffold formation. Polyester triol, LTIPEG prepolymer, and TEGOAMIN catalyst were sterilized using gamma irradiation. Sucrose was sterilized with ethylene oxide exposure. Water was sterilized by filtration (0.2 μm pore size). Immediately prior to surgery, the hardener component was added to sucrose and mixed for 30 sec with a spatula. The prepolymer was added and mixed for 30 sec. The resulting mixture (1 g) was then spread in a wound bed with a spatula and allowed to cure. Scaffolds were loosely held in place by an X-shaped configuration of spanning sutures that extended from normal skin to normal skin. Each wound was dressed with TELFA non-adherent dressing (Medline, Mundelein, IL), covered with Opsite adhesive film (Smith & Nephew, St. Petersburg, FL) beneath tube gauze, and secured with Vetwrap bandaging tape (3M, St. Paul, MN). Wounds were cleaned and dressings were changed every 2-3 days. Pigs were sacrificed and wounds were harvested at days 9, 13, and 30 after scaffold implantation.

Tissue Analysis

Wounds were fixed in neutral buffered formalin for 48 h, transferred into 70% ethanol for 48 h, embedded in paraffin, and sectioned at 5 μm and stained with Gomori's trichrome. Reparative responses of tissues were examined and quantified using immunohistochemical markers and procedures that we have previously validated [22]. Actively proliferating cells were immunostained for Ki-67 antigen. After heat-mediated target retrieval in citrate buffer at pH 6.0 (DAKO, Carpenteria, CA), endogenous peroxidase activity was neutralized with 3% H_2O_2 for 40 minutes followed by blocking non-specific reactivity with a casein-based protein block (DAKO, Carpintera, CA) for 20 minutes. Slides were incubated with rabbit anti-human Ki-67 (NovaCastra Laboratories Ltd., Newcastle, UK) diluted at 1:2,000 for 60 min. The rabbit Envision HRP System (DAKO) was used with DAB as substrate and the slides counterstained with hematoxylin. Macrophage infiltration into repairing tissues was assessed using MAC387 antisera (AbD Serotec, Raleigh, NC). After antigen retrieval in 0.01 M Tris/HCL pH 10, quenching for peroxidase activity, and blocking of non-specific immunoreactivity, a monoclonal mouse anti-human antibody to a macrophage epitope (MAC387) was used at 1:10,000 for 60 min. Fragmented DNA of apoptotic cells was visualized with the DeadEnd Colorimetric TUNEL System (Promega Corporation, Madison, WI). The tissue sections were subjected to a second fixation in 4% paraformaldehyde, rinsed, and permeabilized with proteinase K for 5 minutes. The sections then were treated with equilibration buffer (Promega) followed by biotinylated nucleotide incorporation into apoptotic cells using Terminal Deoxynucleotidyl Transferase (TdT). Endogenous peroxidase was neutralized by applying 0.3% hydrogen peroxide to the sections.

Applications of streptavidin/HRP and DAB produced apoptotic-specific visible nuclear staining. Quantitative measurements were performed using Image-Pro Plus scientific image analysis software (Media Cybernetic, Inc., Silver Spring, MD.). Data are expressed as the total number of proliferating cells, immunolabeled macrophages, or apoptotic cells.

Density of new capillaries in the wound bed was determined by immunostaining using antisera for Von Willebrand Factor. Sections underwent antigen retrieval using 5 min of digestion with Proteinase K (DAKO, Carpinteria, CA). Following rinses and endogenous blockade with H_2O_2, sections were incubated at 25˚C in rabbit polyclonal antisera for Factor VIII-related antigen (Von Willebrand Factor; DAKO) for 30 minutes with a dilution of antibody at 1:900. Following this incubation in primary antisera, the sections were processed through the reagents supplied by rabbit Envision + System, HRP kit (DAKO). Data are expressed as area% of endothelial-lined areas within the wound.

Statistical Analysis

One way analysis of variance (ANOVA) was used to evaluate the statistical significance of results. All p-values less than 0.05 were considered statistically significant. Data are expressed as mean ± standard error unless otherwise indicated.

Results

Physical, Mechanical, and Rheological Properties of PUR Scaffolds

Scaffold density, porosity, and pore size were measured before and after sucrose leaching (Table 5.2). As expected, leaching significantly decreased the density and increased the porosity of 40% and 70% sucrose scaffolds. The compressive modulus

decreased after leaching, but this difference was only significant for the 70% sucrose scaffolds. SEM imaging was performed to analyze pore morphology and sucrose bead distribution (Figure 5.1). SEM images show sucrose beads embedded in the walls of 40% (Fig. 5.1A) and 70% sucrose scaffolds (Fig. 5.1B). After leaching, sucrose was no longer visible (panels C and D). The rheological properties of 40% sucrose scaffolds are shown in Figure 5.2. The working time was considered to be the gel point, which was determined from the G-crossover point. The working time of the scaffolds was 4.8 ± 1.2 min, and the tack-free time was 16 ± 3 min.

Table 5.2. Physical and mechanical properties of 40% and 70% scaffolds before and after leaching. Data are expressed as mean ± standard deviation. Asterisks indicate significant difference before and after leaching ($p < 0.01$).

	40% Sucrose		**70% Sucrose**	
Leaching	**–**	**+**	**–**	**+**
Density (kg m^{-3})	490 ± 30	280 ± 20 *	660 ± 60	190 ± 10 *
Porosity (%)	59 ± 3	77 ± 2 *	45 ± 5	84 ± 1 *
Pore Size (μm)	280 ± 80	290 ± 110	300 ± 140	250 ± 80
Compressive Modulus (kPa)	70 ± 40	50 ± 20	150 ± 30	50 ± 10 *

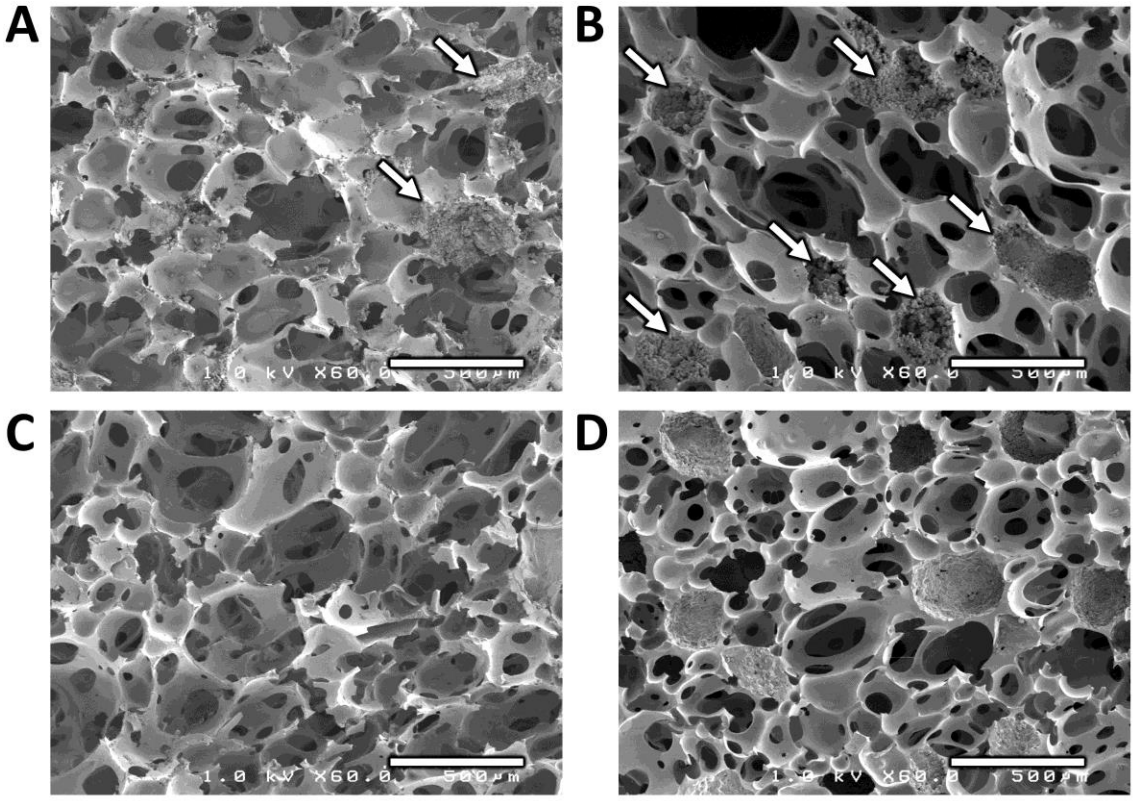

Figure 5.1. SEM images of PUR scaffolds. Panels A and C show 40% sucrose scaffolds before (A) and after (C) leaching. Panels B and D show 70% sucrose scaffolds before (B) and after (D) leaching. Arrows indicate sucrose beads embedded in pore walls. Scale bar = 500 μm.

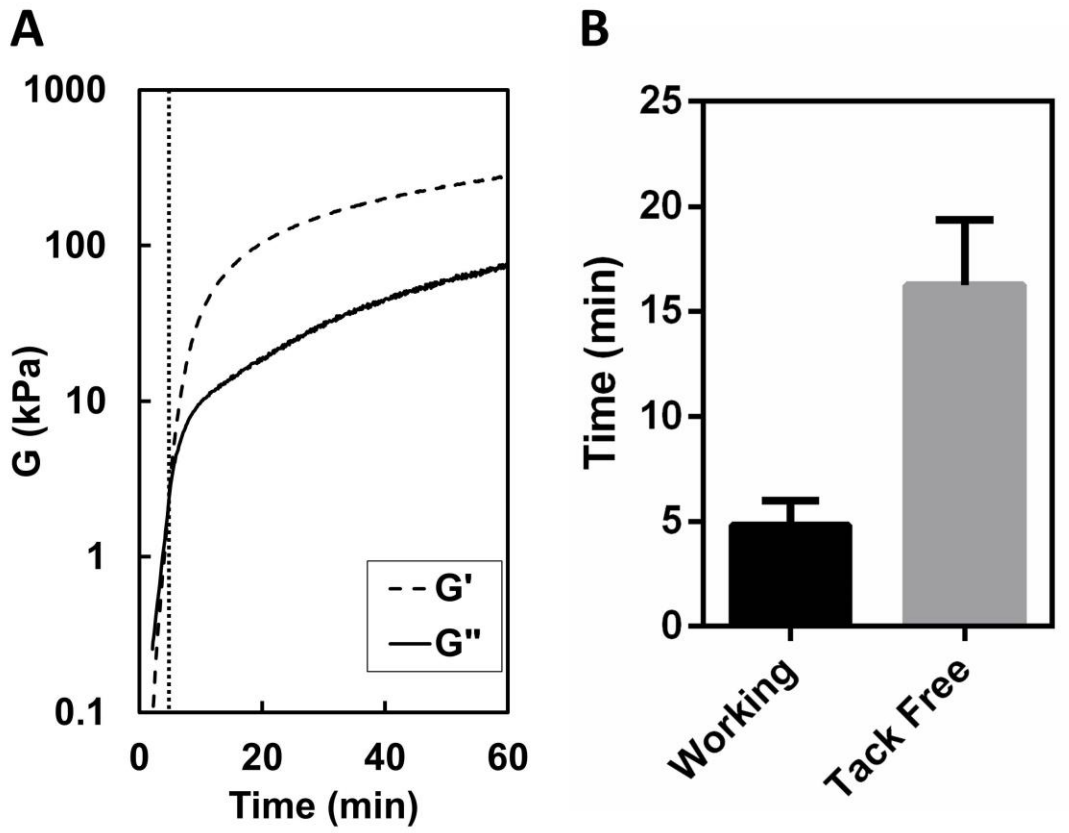

Figure 5.2. Rheological properties of PUR scaffolds. A) Representative cure profile of 40% scaffold. Vertical dashed line indicates G-crossover point, which was used to determine the working time. B) Average working and tack-free times of 40% scaffolds.

Permeability of PUR Scaffolds

The permeability of PUR scaffolds with a variety of treatments was evaluated using the constant pressure gradient method (Table 5.3). Some scaffolds were foamed in a wet environment to mimic the conditions of injection in the porcine excisional wound study. Since the surface of PUR scaffolds has lower porosity than the bulk material, the surface of some scaffolds was removed. Increasing the sucrose from 40% to 70%, leaching the scaffolds, foaming the scaffolds in a wet environment, and removing the surface film all increased the permeability of the scaffolds. All samples investigated had

permeability > 10^{-10} m^2, which is comparable to the permeability of rigid open-cell foams reported elsewhere [23].

Table 5.3. Permeability of 40% and 70% sucrose scaffolds foamed in dry or wet environments with or without surface film. Leaching the scaffolds significantly increased their permeability ($p < 0.01$). Asterisks indicate significant difference from samples D, K, and L ($p < 0.05$). Daggers indicate significant difference from samples D and L ($p < 0.05$). Double dagger indicates significant difference from sample L ($p < 0.05$).

Sample	Sucrose	Leaching	Environment	Film	Permeability (10^{-10} m^2)	Significance
A	70%	–	Dry	+	4.1 ± 1.8	†
B	70%	+	Dry	+	7.3 ± 1.6	‡
C	70%	–	Wet	+	9.4 ± 1.9	‡
D	70%	+	Wet	+	19.6 ± 3.2	
E	40%	–	Dry	+	1.5 ± 0.2	*
F	40%	+	Dry	+	1.7 ± 0.1	*
G	40%	–	Wet	+	4.4 ± 0.5	†
H	40%	+	Wet	+	14.2 ± 0.6	
I	40%	–	Dry	–	3.3 ± 1.5	*
J	40%	+	Dry	–	7.7 ± 2.2	‡
K	40%	–	Wet	–	19.0 ± 6.2	
L	40%	+	Wet	–	28.9 ± 6.1	

Wound Dimensions

Representative trichrome green images of porcine excisional wounds are shown in Figure 5.3. Collagen is stained green, cytoplasm is stained pink or red, and PUR scaffolds appear white because they do not take up the stain. At day 9, images with low (2x) and high (20x) magnification show cellular infiltration into the pores of PUR scaffolds in all scaffold treatment groups (Fig. 5.3A). All wounds appeared immature with little collagen accumulation. There were larger polyurethane fragments and less polyurethane present in

wound treated with 70% injectable scaffolds, indicating that these scaffolds did not infiltrate with tissue as well as the 40% scaffolds. At day 13, collagen production increased in all treatment groups (Fig. 5.3B). There was less polyurethane visible in wounds treated with 70% injectables than in wounds treated with 40% injectables or implants, providing further evidence that the 70% scaffolds did not infiltrate as well as the 40% scaffolds. All scaffold treatment groups had less PUR remaining at day 13 than at day 9. By day 30, only a few fragments of PUR remained in the scaffold treatment groups (Fig. 5.3C). Furthermore, collagen production increased and cellularity decreased in all treatment groups.

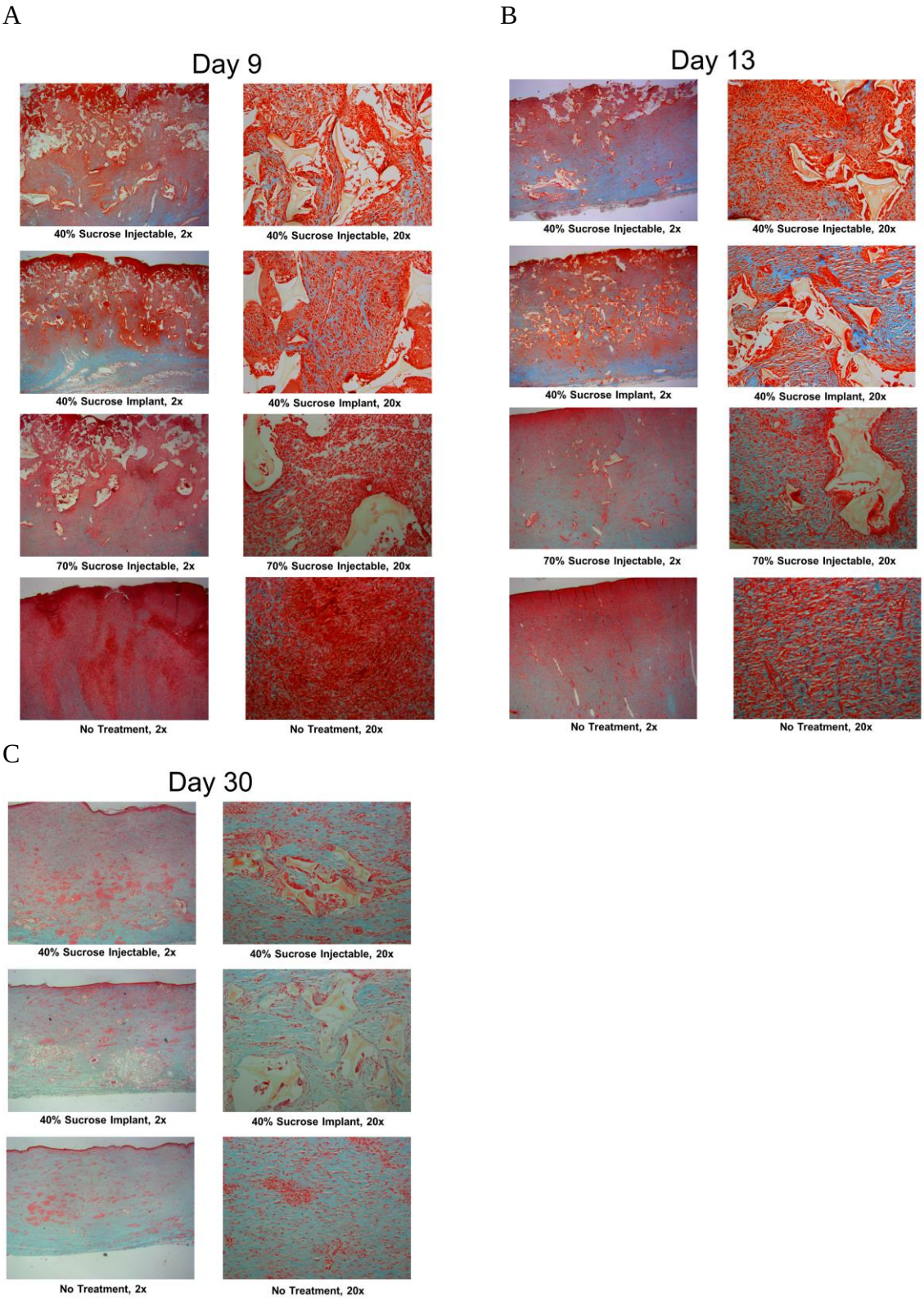

Figure 5.3. Representative images of trichrome green staining at days 9 (A), 13 (B), and 30 (C) at magnifications of 2x (left) and 20x (right). Collagen is green or blue, cytoplasm is red or pink, and PUR scaffolds are unstained and appear white.

Wound measurements were obtained from images of trichrome staining and gross images (Figure 5.4). 40% implant scaffolds had significantly less contraction than untreated wounds at days 9, 13, and 30 (Fig. 5.4A). 40% injectable scaffolds had significantly less contraction than untreated wounds at day 9. Furthermore, the cross-sectional area of untreated scaffolds decreased significantly from day 9 to day 13 while the cross-sectional area of wounds treated with 40% implant and injectable scaffolds did not decrease significantly until day 30 (Fig. 5.4B). These results provide evidence that PUR scaffolds prevented unwanted wound contraction at early time points. There were no significant differences in wound contraction or cross-sectional area between 40% implants and injectables at any of the time points, suggesting that injectable scaffolds are able to stent the wounds and delay contraction as well as implants.

In addition, epithelialization and PUR scaffold degradation were evaluated using trichrome images. Wounds treated with scaffolds had slightly lower epithelialization than untreated wounds at day 13, but these differences were not significant (Fig. 5.4C). By day 30, there were no differences in epithelialization among treatment groups. The progression of PUR degradation was evaluated by measuring fractional area of PUR within the wound (Fig. 5.4D). The fractional area of PUR decreased significantly from day 9 to day 13 in 40% injectable groups and from day 13 to day 30 in 40% implant groups. There were no significant differences among treatment groups at any of the time points, providing evidence that applying PUR scaffolds by injection instead of implantation did not adversely affect scaffold biodegradation and persistence.

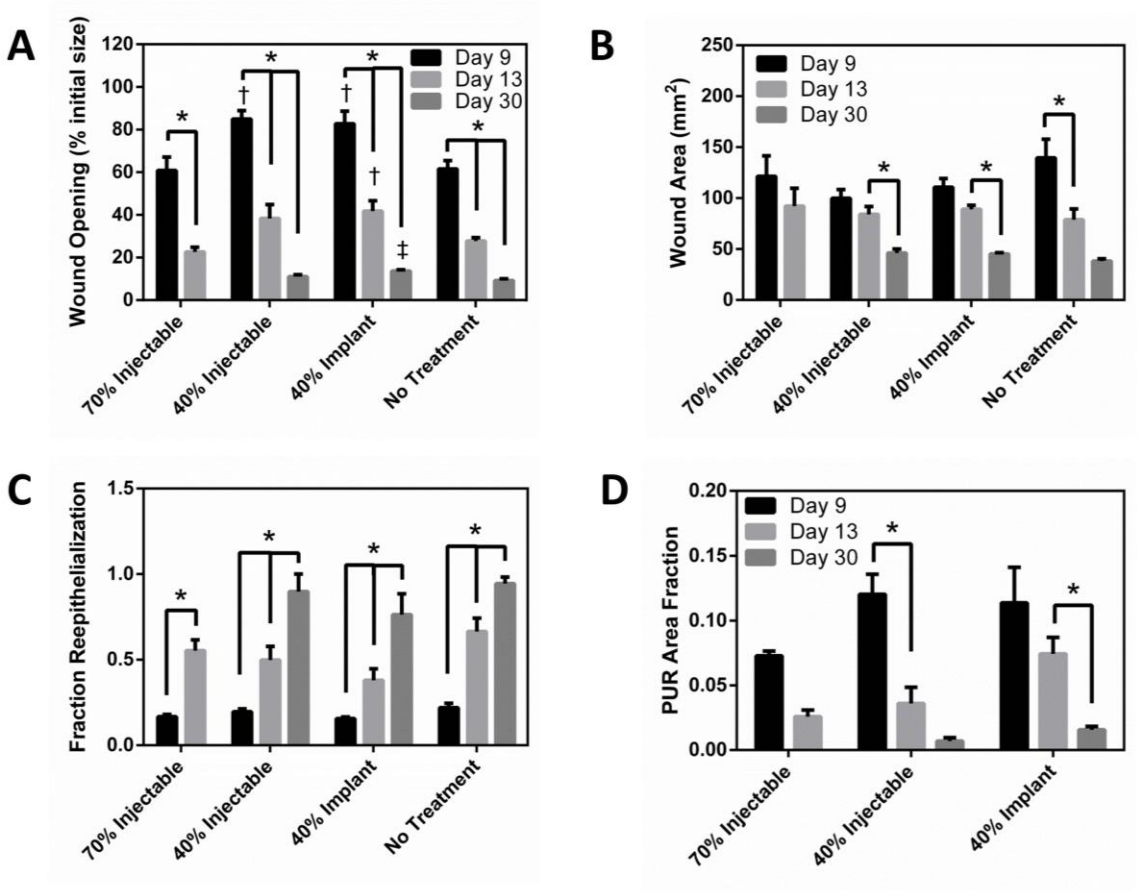

Figure 5.4. Wound measurements from porcine full-thickness excisional wound study. (A) Wound opening measured from gross images. Asterisks indicate significant difference ($p < 0.01$). Daggers indicate significant difference from 70% injectable and no treatment at days 9 and 13 ($p < 0.05$). Double dagger indicates significant difference from no treatment at day 30 ($p < 0.01$). (B) Cross-sectional area of wounds measured from images of trichrome staining. Asterisks denote significant difference ($p < 0.05$). (C) Fraction reepithelialization. Asterisks indicate significant difference ($p < 0.01$). (D) Area fraction of PUR in the wound measured from images of trichrome staining. Asterisks indicate significant difference ($p < 0.05$).

Scaffold Impact on Cell Proliferation and Apoptosis

The effects of PUR scaffold treatment on cell proliferation and apoptosis was investigated (Figure 5.5). Ki67 immunostaining was used to assess the level of cell proliferation at days 9 and 13 (Fig. 5.5A). At day 9, wounds treated with 70% and 40%

injectable scaffolds had significantly more $Ki67^+$ cells than untreated wounds. The number of $Ki67^+$ cells decreased significantly from day 9 to day 13 in all treatment groups, and there were no differences in proliferating cells by day 13. Furthermore, apoptosis was evaluated using TUNEL immunostaining (Fig. 5.5B). All scaffold groups had slightly higher levels of apoptosis than untreated wounds, but this difference was only significant in wounds treated with 40% implants at day 9. There were no significant differences among scaffold treatment groups at either time point. In addition, the ratio of proliferation to apoptosis was quantified (Fig. 5.5C). The ratio of $Ki67^+$ cells to $TUNEL^+$ cells was calculated and adjusted assuming that Ki67 is expressed for ~15 h in proliferating cells (the length of a fibroblast cell cycle [24]) and TUNEL is expressed for ~2 h during apoptosis [25]. The proliferation/apoptosis ratio ranged from 5 – 15 for all treatment groups at day 9. By day 13, the ratio decreased to two for all treatment groups. These results indicate that the wounds were moving from the proliferating phase to the remodeling phase by day 13. There were no significant differences in proliferation/apoptosis ratio among treatment groups at either time point.

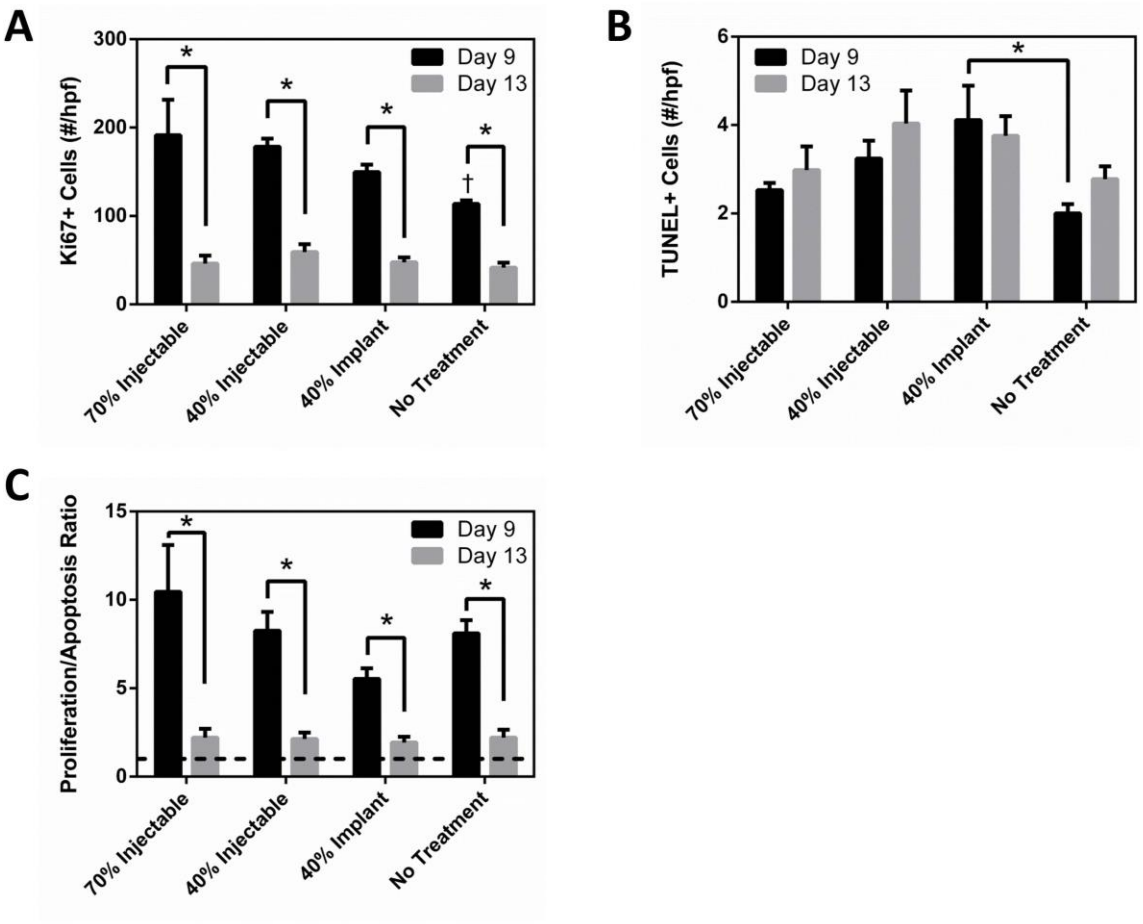

Figure 5.5. Cell proliferation and apoptosis. (A) Quantification of Ki67 immunostaining at days 9 and 13. Asterisks denote significant difference ($p < 0.0001$). Dagger indicates significant difference from 70% injectable and 40% injectable at day 9 ($p < 0.005$). (B) Quantification of TUNEL immunostaining at days 9 and 13. Asterisk indicates significant difference ($p < 0.005$). (C) Ratio of proliferation to apoptosis. Dashed line represents ratio of one. Asterisks denote significant difference ($p < 0.05$).

Scaffold Impact on Macrophage Presence

Macrophage presence was evaluated using MAC387 immunostaining (Figure 5.6). Wounds treated with 70% injectables or 40% implants had more than thrice as many $MAC387^{+}$ macrophages as wounds treated with 40% injectables or untreated wounds, but this difference was only significant in wounds treated with 70% injectables. Our group

has previously shown that PUR scaffolds undergo macrophage-mediated oxidative degradation [16], and the elevated macrophage presence in scaffold-treated wounds provides evidence that the scaffolds were being degraded by macrophages. Since macrophages numbers usually peak 4-5 days after wounding, it was expected that macrophage numbers would decrease between day 9 and day 13 [26]. Macrophage presence declined from day 9 to day 13 in all treatment groups, and there were no significant differences among treatment groups by day 13.

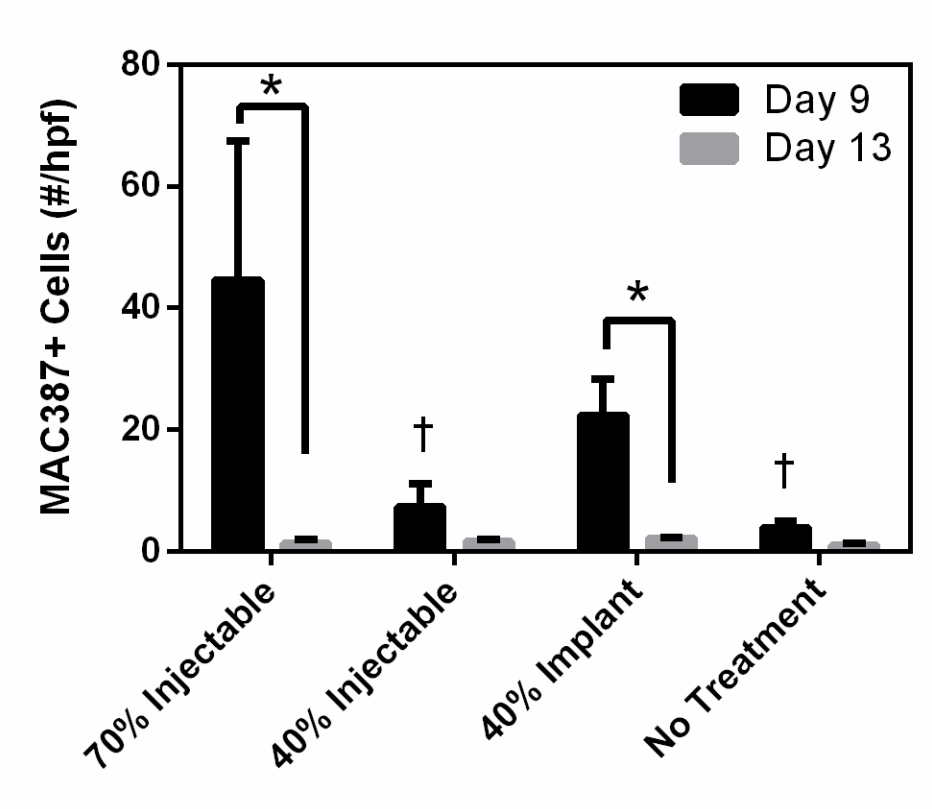

Figure 5.6. Analysis of macrophage presence at days 9 and 13. Asterisks denote significant difference ($p < 0.005$). Daggers indicate significant difference from 70% injectable at day 9 ($p < 0.005$).

Scaffold Impact on Blood Vessel Formation

Factor VIII immunostaining was used to assess blood vessel abundance at days 9 and 13 (Figure 5.7). At day 9, all scaffold treatment groups had slightly higher blood vessel density (area% occupied by blood vessels) than untreated wounds, but these differences were not significant. At day 13, blood vessel density was significantly higher in wounds treated with 40% injectables than in wounds treated with 40% implants and untreated wounds. Blood vessel density decreased from day 9 to day 13 in all treatment groups, but this difference was only significant in wounds treated with 40% implants. These results suggest that the wounds were moving into the remodeling phase of healing by day 13.

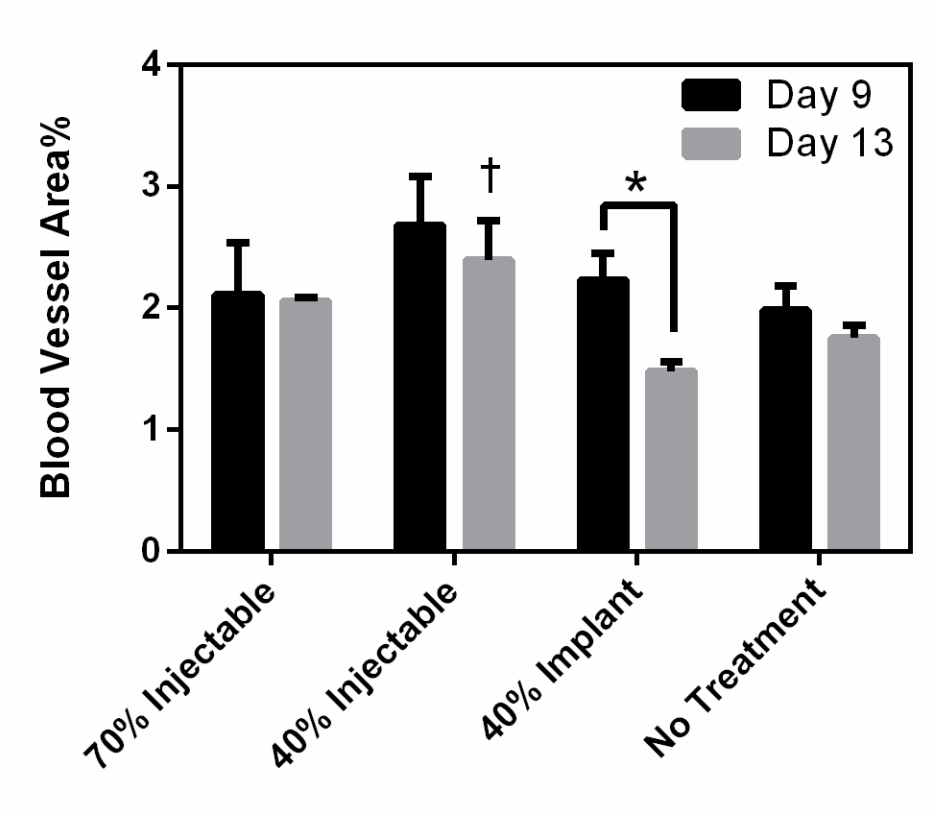

Figure 5.7. Analysis of blood vessel density at days 9 and 13. Asterisk indicates significant difference ($p < 0.05$). Dagger indicates significant difference from 40% implant and no treatment at day 13 ($p < 0.05$).

Discussion

In this study, the capacity of injectable and implantable PUR scaffolds to facilitate wound healing in a porcine excisional model was investigated. The scaffolds were characterized *in vitro* to ensure that they met the requirements for injectable scaffolds. PUR scaffolds had working and setting times of 4.8 ± 1.2 min and 16 ± 3 min, respectively, which are appropriate for the clinical setting. After leaching sucrose from the scaffolds, they had similar density, porosity, and pore size to injectable PUR scaffolds used for skin wound healing in a previous study [13]. The permeability of the scaffolds was measured before and after leaching, with foaming in dry or wet environments, and before and after removal of the surface film. All scaffolds investigated had permeability > 10^{-10} m^2, which is greater than the permeability of rigid open-cell foams reported by Zhao et al. (10^{-12} – 10^{-10} m^2) [23]. The high permeability and porosity, robust mechanical properties, and clinically relevant working and setting times of the scaffolds provided evidence that they would support cellular infiltration and stent wounds when injected in a porcine excisional model.

In the porcine excisional wound study, implantable and injectable 40% sucrose scaffolds stented the wounds at early time points, delaying unwanted wound contraction. Injectable and implantable scaffolds had significantly less wound contraction than untreated wounds at day 9. Furthermore, wounds treated with 40% sucrose implants or injectables did not significantly decrease in size until day 30 while untreated wound area decreased significantly from day 9 to day 13. Optimization of scaffold mechanical properties and degradation rate could further improve the stenting effect of the PUR

scaffolds. Although wounds treated with scaffolds were slightly less epithelialized than untreated wounds at day 9 and 13, this difference was not significant.

In all scaffold treatment groups, polyurethane presence decreased over time with few fragments remaining by day 30. The number of $MAC387^{+}$ macrophages was elevated in scaffold-treated wounds compared to untreated wounds at days 9 and 13, but this difference was only significant for 70% sucrose injectables and 40% sucrose implants at day 9. These results are consistent with oxidative degradation of PUR scaffolds mediated by macrophages [16]. The number of proliferating cells, ratio of proliferation to apoptosis, macrophage presence, and blood vessel density decreased from day 9 to day 13 in all treatment groups. Moreover, images of trichrome staining provide evidence that collagen accumulation increased from day 9 to day 13 in all treatment groups. These results suggest that the wounds were moving from the proliferative phase of healing to the remodeling phase by day 13.

Overall, there were few statistically significant differences between wounds treated with 40% implants and 40% injectables. Implants and injectables had similar rates of wound contraction, polyurethane biodegradation, and epithelialization. Implants had significantly higher macrophage presence at day 9 and lower blood vessel density at day 13 than injectables. Otherwise, cell proliferation, apoptosis, macrophage presence, and blood vessel formation were comparable in the 40% implant and 40% injectable treatment groups. The histological analysis indicates that injectable PUR scaffolds do not adversely affect the wound healing process or scaffold persistence compared to implantable PUR scaffolds.

Other research on the use of void-filling scaffolds in porcine excisional wounds has involved implants with multiple layers. In one study, a wound dressing comprising an outer elastomeric membrane and an inner gelatin sponge layer incorporating basic fibroblast growth factor-loaded microspheres resulted in faster wound closure and better extracellular matrix organization than Vaseline gauze [19]. An investigation on the use of biodegradable PUR foams sealed with a microporous PUR membrane found that these bilayer scaffolds had no signs of infection and reduced contraction compared to Integra after 28 days [21]. To our knowledge, the use of injectable void-filling scaffolds in porcine cutaneous wounds has not been investigated prior to the present study. Previous research by our group on the use of injectable PUR scaffolds in rat excisional wounds (Chapter III) [13] and implantable PUR scaffolds in porcine excisional wounds (Chapter IV) has shown that PUR scaffolds are biocompatible, stent wounds to reduce wound contraction, and support cellular infiltration. The present study provides further evidence that implantable and injectable PUR scaffolds facilitate wound healing, support tissue infiltration and matrix production, and delay wound contraction in a clinically relevant animal model.

Conclusions

In summary, injectable PUR scaffolds with high permeability, robust mechanical properties, and working and setting times appropriate for the clinical setting were developed. Injectable and implantable PUR scaffolds had a stenting effect in porcine excisional wounds, resulting in the favorable outcome of delayed wound contraction. The patterns of cell proliferation, macrophage presence, and blood vessel formation from day

9 to day 13 were similar in all treatment groups. Macrophage numbers were slightly elevated in scaffold-treated wounds since the polyurethane scaffolds are degraded by a macrophage-mediated oxidative mechanism. These findings suggest that PUR scaffolds support tissue infiltration and wound healing in a porcine excisional wound model, and applying PUR scaffolds by injection rather than implantation does not adversely affect the wound healing process or scaffold biodegradation. This study focused on testing the biocompatibility of injectable PUR scaffolds in a porcine excisional model with high clinical relevance to human skin wounds. Injectable PUR scaffolds also have potential to incorporate and deliver biologics at the point of care, which is the focus of ongoing work.

References

[1] Sen CK, Gordillo GM, Roy S, Kirsner R, Lambert L, Hunt TK, et al. Human skin wounds: a major and snowballing threat to public health and the economy. Wound repair and regeneration : official publication of the Wound Healing Society [and] the European Tissue Repair Society 2009;17:763-71.
[2] Zhao G, Usui ML, Lippman SI, James GA, Stewart PS, Fleckman P, et al. Biofilms and Inflammation in Chronic Wounds. Advances in wound care 2013;2:389-99.
[3] Volk SW, Iqbal SA, Bayat A. Interactions of the Extracellular Matrix and Progenitor Cells in Cutaneous Wound Healing. Advances in wound care 2013;2:261-72.
[4] Clark RAF, Ghosh K, Tonnesen MG. Tissue engineering for cutaneous wounds. Journal of Investigative Dermatology 2007;127:1018-29.
[5] Mikos AG, Kretlow JD, Klouda L. Injectable matrices and scaffolds for drug delivery in tissue engineering. Advanced drug delivery reviews 2007;59:263-73.
[6] Belkoff SM, Deramond H, Wright NT. Temperature elevation caused by bone cement polymerization during vertebroplasty. Bone 1999;25:17s-21s.
[7] Laurencin CT, Khan Y, Yaszemski MJ, Mikos AG. Tissue engineering of bone: Material and matrix considerations. Journal of Bone and Joint Surgery-American Volume 2008;90A:36-42.
[8] Tae G, Kornfield JA, Hubbell JA. Sustained release of human growth hormone from in situ forming hydrogels using self-assembly of fluoroalkyl-ended poly(ethylene glycol). Biomaterials 2005;26:5259-66.
[9] Garbern JC, Hoffman AS, Stayton PS. Injectable pH- and temperature-responsive poly(N-isopropylacrylamide-co-propylacrylic acid) copolymers for delivery of angiogenic growth factors. Biomacromolecules 2010;11:1833-9.
[10] Guelcher SA, Li B, Davidson JM. The effect of the local delivery of platelet-derived growth factor from reactive two-component polyurethane scaffolds on the healing in rat skin excisional wounds. Biomaterials 2009;30:3486-94.
[11] Guelcher SA, Li B, Brown KV, Wenke JC. Sustained release of vancomycin from polyurethane scaffolds inhibits infection of bone wounds in a rat femoral segmental defect model. Journal of Controlled Release 2010;145:221-30.
[12] Guelcher SA, Dumas JE, Zienkiewicz K, Tanner SA, Prieto EM, Bhattacharyya S. Synthesis and Characterization of an Injectable Allograft Bone/Polymer Composite Bone Void Filler with Tunable Mechanical Properties. Tissue Engineering Part A 2010;16:2505-18.
[13] Adolph EJ, Hafeman AE, Davidson JM, Nanney LB, Guelcher SA. Injectable Polyurethane Composite Scaffolds Delay Wound Contraction and Support Cellular Infiltration and Remodeling in Rat Excisional Wounds. Wound Repair and Regeneration 2011;19:A9-A.
[14] Dumas JE, BrownBaer PB, Prieto EM, Guda T, Hale RG, Wenke JC, et al. Injectable reactive biocomposites for bone healing in critical-size rabbit calvarial defects. Biomedical materials (Bristol, England) 2012;7:024112.
[15] Guelcher SA, Dumas JE, Davis T, Holt GE, Yoshii T, Perrien DS, et al. Synthesis, characterization, and remodeling of weight-bearing allograft bone/polyurethane composites in the rabbit. Acta Biomaterialia 2010;6:2394-406.

[16] Guelcher SA, Hafeman AE, Zienkiewicz KJ, Zachman AL, Sung HJ, Nanney LB, et al. Characterization of the degradation mechanisms of lysine-derived aliphatic poly(ester urethane) scaffolds. Biomaterials 2011;32:419-29.
[17] Nelson CE, Kim AJ, Adolph EJ, Gupta MK, Yu F, Hocking KM, et al. Tunable delivery of siRNA from a biodegradable scaffold to promote angiogenesis in vivo. Advanced materials (Deerfield Beach, Fla) 2014;26:607-14, 506.
[18] Sullivan TP, Eaglstein WH, Davis SC, Mertz P. The pig as a model for human wound healing. Wound repair and regeneration : official publication of the Wound Healing Society [and] the European Tissue Repair Society 2001;9:66-76.
[19] Huang S, Deng T, Wu H, Chen F, Jin Y. Wound dressings containing bFGF-impregnated microspheres. Journal of Microencapsulation 2006;23:277-90.
[20] Greenwood JE, Dearman BL. Split skin graft application over an integrating, biodegradable temporizing polymer matrix: immediate and delayed. Journal of burn care & research : official publication of the American Burn Association 2012;33:7-19.
[21] Greenwood JE, Dearman BL. Comparison of a sealed, polymer foam biodegradable temporizing matrix against Integra(R) dermal regeneration template in a porcine wound model. Journal of burn care & research : official publication of the American Burn Association 2012;33:163-73.
[22] Nanney LB, Woodrell CD, Greives MR, Cardwell NL, Pollins AC, Bancroft TA, et al. Calreticulin enhances porcine wound repair by diverse biological effects. The American journal of pathology 2008;173:610-30.
[23] Zhao W, Pizzi A, Fierro V, Du G, Celzard A. Effect of composition and processing parameters on the characteristics of tannin-based rigid foams. Part I: Cell structure. Materials Chemistry and Physics 2010;122:175-82.
[24] Kasinathan P, Knott JG, Moreira PN, Burnside AS, Jerry DJ, Robl JM. Effect of fibroblast donor cell age and cell cycle on development of bovine nuclear transfer embryos in vitro. Biology of reproduction 2001;64:1487-93.
[25] Gavrieli Y, Sherman Y, Ben-Sasson SA. Identification of programmed cell death in situ via specific labeling of nuclear DNA fragmentation. The Journal of cell biology 1992;119:493-501.
[26] Braiman-Wiksman L, Solomonik I, Spira R, Tennenbaum T. Novel insights into wound healing sequence of events. Toxicologic pathology 2007;35:767-79.

CHAPTER VI

ENHANCED PERFORMANCE OF PLASMID DNA POLYPLEXES STABILIZED BY A COMBINATION OF CORE HYDROPHOBICITY AND SURFACE PEGYLATION

Introduction

Chapters III – V focused on the development of injectable and implantable polyurethane (PUR) scaffolds and their use in skin wound healing applications. The scaffolds were shown to be biocompatible and biodegradable in rat and porcine excisional wound models. The scaffolds also reduced contraction and supported tissue infiltration and matrix production in those wound models. However, PUR scaffolds alone are not enough to accelerate wound healing. PUR scaffolds have potential to deliver therapeutic proteins, drugs, and nucleic acids to enhance wound healing. This chapter discusses the development of a PUR delivery system for plasmid DNA (pDNA).

Nonviral gene therapy is a promising approach for promoting tissue restoration and treating various genetic diseases. Plasmids can be produced efficiently and lacks the immunogenic risk associated with viral vectors. The endocytotic entry of pDNA is aided by condensation into stable nanoparticles. Ideally, the pDNA nanocarriers should be stable in physiological conditions (i.e., presence of proteins and salts) and should protect the plasmid cargo from nuclease degradation in the extracellular environment. After endocytosis, the vectors must escape the endo-lysosomal pathway into the cytoplasm, and the plasmid must be unpackaged and trafficked to the nucleus. A variety of synthetic polymer- and lipid-based carriers have been developed, but these transfection reagents have been optimized for *in vitro* use and face several challenges for *in vivo* transfection.

In order to be delivered from PUR scaffolds, pDNA must be stabilized during lyophilization and the PUR reaction.

One strategy for nonviral gene delivery is electrostatic condensation of plasmids into nanoparticles using cationic polymers or lipids. Electrostatic interactions between positively charged amine groups on polymers such as polyethylenimine (PEI) or poly(2-(dimethylamino)ethyl methacrylate) (PDMAEMA) and negatively charged phosphates on DNA result in the condensation of the pDNA into polyplexes (50 – 200 nm nanoparticles) [1, 2]. After entering cells through endocytosis, polyplexes made from amine-containing polymers with pK_a in the range 5.0 – 7.4 buffer the acidification of endosomes. Proton and counterion influx increases, causing osmotic swelling and rupture of endosomes. This "proton sponge" effect enables release of pDNA into the cytoplasm [3, 4]. Although electrostatic condensation of pDNA has been effective for *in vitro* transfection, delivery of polyplexes from tissue-engineered scaffolds has been challenging due to polyplex aggregation [8, 9]. Studies by Segura et al. have shown that lyophilization of PEI-pDNA polyplexes with excipients such as sucrose decreased polyplex aggregation and improved transfection efficiency [10, 11]. However, approaches to improve the inherent stability of polyplexes and studies on the contribution of colloidal stability to transfection efficiency have not been extensively investigated.

Block copolymers have been developed to improve colloidal stability, increase transfection efficiency, and decrease cytotoxicity of nonviral carriers. Complexation of pDNA with block copolymers comprising polycations and polyethylene glycol (PEG) enhanced steric stability of polyplexes by formation of a PEG corona [12-14]. Titration of hydrophobic content into the cationic, pDNA-condensing polymer block has also been

investigated as a strategy for reducing charge density, increasing stability, decreasing toxicity, and enhancing endosomal escape of polycations. For example, delivery of the pro-apoptotic TRAIL gene using terpolymers synthesized by enzyme-catalyzed copolymerization of lactone with dialkyl diester and amino diol significantly inhibited tumor growth in a xenograft model [15]. The high molecular weight and increased hydrophobicity were conjectured to compensate for the low charge density of the nanoparticles, resulting in low cytotoxicity and high transfection efficiency. Recently, we were the first to investigate a PEG-stabilized polyplex system in which siRNA cargo was loaded into the particle core, which contained a balance of BMA and DMAEMA, and yielded enhanced performance following intravenous injection *in vivo* [21]. Here, we extend this work and apply simple, controlled polymerization methods to synthesize polymers in a single step that can be used to form pDNA carriers that provide steric stabilization by incorporating a PEG corona as well as an optimal balance of cationic and hydrophobic content to allow improved stability, reduced toxicity, and endosomal escape. The current study also explores structure-property relationships governing the effects of poly(DMAEMA-*co*-BMA) composition and molecular weight on polyplex stabilization and performance.

In this study, a library of poly(ethylene glycol-*b*-(dimethylaminoethyl methacrylate-*co*-butyl methacrylate)) [poly(EG-*b*-(DMAEMA-*co*-BMA))] polymers was synthesized using a one-step reversible-addition fragmentation chain transfer (RAFT) polymerization from a PEG-based macro-chain transfer agent (macro-CTA). These polymers were designed such that DMAEMA initiates nucleic acid electrostatic interactions and triggers formation of polyplexes that are further stabilized by the

hydrophobic interactions of the BMA in the polyplex core. The PEG corona was designed to shield the polyplex charge in the core and to provide enhanced steric stabilization while the poly(DMAEMA-*co*-BMA) block was designed to enhance colloidal stability and to achieve pH-dependent membrane disruption tuned to promote endosomal escape. The controlled nature of RAFT [22] was leveraged to synthesize a well-defined library of polymers containing a range of compositions with varied mol% BMA titrated into the cationic DMAEMA block. We also used controlled synthesis to make monodispersed polymers with varied molecular weights to enable study of the effect of molecular weight of the cationic block on performance of polymers with optimal [DMAEMA]/[BMA] ratios. The block copolymers were characterized for pDNA packaging efficiency, physicochemical properties of the polyplexes, colloidal stability, and *in vitro* transfection bioactivity before and after lyophilization. The lead candidate was used to create pDNA polyplexes that were incorporated into PUR scaffolds and delivered to cells *in vitro*.

Methods

Materials

Luciferase reporter plasmid (pPK-CMV-R3) and PromoFluor-500 fluorescent labeling kit were purchased from Promokine (Heidelberg, Germany). Live/dead viability/cytotoxicity kit, Opti-MEM reduced serum media, Dulbecco's phosphate buffered saline (DPBS), Dulbecco's Modified Eagle Medium (DMEM), fetal bovine serum (FBS), penicillin streptomycin, and 0.4% trypan blue stain were purchased from Invitrogen (Grand Island, NY). Pierce™ BCA Protein Assay Kit was obtained from

Thermo Fisher Scientific (Waltham, MA). NAP-5 desalting columns were purchased from GE. Lysine triisocyanate-poly(ethylene glycol) (LTIPEG) prepolymer was obtained from Ricerca (Concord, OH). TEGOAMIN33, a tertiary amine catalyst composed of 33 wt% triethylene diamine (TEDA) in dipropylene glycol, was received from Goldschmidt (Hopewell, VA). MDA-MB-231 breast cancer cell line was obtained from ATCC (Manassas, VA). All other reagents were purchased from Sigma Aldrich (St. Louis, MO).

Poly(EG-b-(DMAEMA-co-BMA)) Synthesis and Characterization

RAFT polymerization was used to synthesize a library of diblock copolymers. The chain transfer agent (CTA) 4-Cyano-4-(ethylsulfanylthiocarbonyl) sulfanylvpentanoic acid was synthesized following standard procedures and was subsequently conjugated to 5 kDa mono-methoxy-PEG using DCC and DMAP, resulting in 91% substitution of the PEG [21, 23]. The polymerization reaction was carried out at 70°C for 24 h using azobisisobutyronitrile as the initiator with a 5:1 [CTA]:[Initiator] molar ratio. A series of polymerizations were carried out with monomer feed ratios of 0, 25, 40, 50, or 60 mol% BMA and 100, 75, 60, 50, or 40 mol% DMAEMA. For polymers with short block length, the degree of polymerization was 150, and the polymerization time was 6 h. For 0, 25, 40, and 60% BMA with long block length and 50% BMA with medium block length, the degree of polymerization was 150, and the polymerization time was 24 h. For 50% BMA with long block length, the degree of polymerization was 200, and the polymerization time was 24 h. All polymerizations were carried out with 40% wt/vol of monomer + CTA in dioxane. The reaction was stopped by exposing the polymerization solution to air, and the resulting diblock polymers were precipitated into

an excess of pentane. The isolated polymers were vacuum-dried, re-dissolved in water, further purified using PD10 columns, and lyophilized. Polymers were characterized for composition and molecular weight by ^{1}H nuclear magnetic resonance spectroscopy (NMR, Bruker 400Mhz Spectrometer equipped with 9.4 Tesla Oxford magnet). Absolute molecular weight of the polymers was determined using DMF mobile phase gel permeation chromatography (GPC, Agilent Technologies, Santa Clara, CA, USA) with inline Agilent refractive index and Wyatt miniDAWN TREOS light scattering detectors (Wyatt Technology Corp., Santa Barabara, CA).

Polymer-pDNA Polyplex Formation

Prior to mixing, both pDNA and poly(EG-*b*-(DMAEMA-*co*-BMA)) polymers were diluted in 100 mM citric acid/sodium citrate buffer solution (pH 4). Polyplexes were formed by mixing equal volumes of pDNA and polymer solutions by pipetting. After incubating the polyplexes 15 min at room temperature, sodium carbonate/bicarbonate buffer (pH 10.8) was added to bring the pH to 7.4. The concentration of pDNA in the final solution was 25 μg/ml, and the concentration of the polymer solution was dependent on the desired amine/phosphate (N/P) ratio (1, 2, 5, 10, 20, or 30). The N/P ratio was defined as the ratio of the total amines in the polymer to the total phosphates in pDNA. Some polyplexes were desalted by filtering through a GE NAP-5 column according to the manufacturer's instructions (Fairfield, CT). Polyplexes were not desalted unless indicated.

To make control polyplexes, PEI (25,000 Da, branched) and pDNA were separately diluted in equal volumes of phosphate buffer (pH 7.4). Polyplexes were

formed by mixing the PEI and pDNA solutions by pipetting. The mixture was incubated 15 min before adding to cells. The concentration of pDNA in the final solution was 25 μg/ml, and the concentration of the polymer solution was dependent on the desired amine/phosphate (N/P) ratio (1, 2, 5, 10, 20, or 30).

Polymer-pDNA Polyplex Lyophilization

Polymer-pDNA polyplexes were formed as described above. Prior to lyophilization, trehalose or hydroxyprolyl β-cyclodextrin (HPBCD) was added as a cryprotectant and excipient. The mass ratio of trehalose:polymer was 200, and the ratio of HPBCD:polymer ranged from 10 – 80. Polyplexes were frozen at a rate of -1˚C/min until the temperature reached -45˚C. Polyplexes were lyophilized overnight with a vacuum of 0.045 mbar and a collector temperature of -45˚C. For transfection and uptake experiments, polyplexes were reconstituted in water and incubated for 15 min before adding to cells.

Agarose Gel Electrophoresis

To determine the ability of the polymers to efficiently package pDNA, agarose gel electrophoresis was performed. Polymer-pDNA polyplexes were formed as described above. Samples containing 300 ng pDNA were loaded onto a 0.8% agarose gel and subjected to electrophoresis at 100 V for 45 min. Ethidium bromide was then added to the gel to visualize pDNA.

Dynamic Light Scattering (DLS)

Polyplexes were formed as described above and diluted to a concentration of 1.5 μg/ml pDNA in DPBS or KCl solutions. Polyplex size was measured using a Zetasizer Nano ZS (Malvern Instruments, Worchestershire, UK). DLS was performed with a wavelength of 633 nm using a 4.0 mW Helium-Neon laser at a backscattering angle of 173˚. Polyplex size was determined from the average of at least 10 runs of 10 seconds each. For the aggregation study, polyplexes were incubated at room temperature, and size was measured using DLS at various time points up to 72 h. For ζ-potential measurements, polyplexes were diluted in 1 mM KCl at pH 7 and the ζ-potential determined from the average of at least 10 runs using a universal dip cell. Data were fitted to diffusion-limited or reaction-limited models of colloidal aggregation.

In Vitro *Transfection*

MDA-MB-231 human breast cancer cells or immortalized murine dermal fibroblasts (IMDF) were plated in complete DMEM (10% FBS, 100 U/ml penicillin, and 100 μg/ml streptomycin) at a density of 20,000 cells/well in 96-well plates 24 hours prior to transfection. Immediately before transfection, media were aspirated and replaced with 100 μl Opti-MEM + 2% FBS or Opti-MEM without FBS. Polyplex solution containing 150 ng pDNA was then added to each well. At 24 h after transfection, transfection media were aspirated and replaced with 100 μl of 1 mg/ml luciferin in complete DMEM. Luminescence was measured using a Xenogen IVIS 200 bioluminescence imaging system (Perkin Elmer, Waltham, MA) after luciferin was added. Relative luminescence in each well was quantified using Living Image™ software. Cells were lysed using RIPA

buffer and total protein measured using the Pierce™ BCA Protein Assay Kit according to the manufacturer's instructions.

Cell Viability

The cytotoxicity of polyplexes was determined using calcein AM staining to detect live cells. *In vitro* transfection experiments were carried out as described above. 24 h after transfection, media were aspirated and replaced with 200 μl of a solution of 1 μg/ml calcein AM in DPBS. After incubating 30 min at 37 ˚C, fluorescence intensity was measured using an FL600 microplate reader with an excitation wavelength of 485 nm and an emission wavelength of 530 nm (Bio-Tek Instruments, Winooski, Vermont).

pH-dependent Red Blood Cell Hemolysis Assay

To screen for endosomolytic activity, a red blood cell hemolysis assay was used to measure the pH-dependent membrane disruptive activity of the polyplexes [24]. Polyplexes with N/P ratio of 10 were prepared as described above. Human red blood cells were incubated with polyplexes for one hour in buffers with pH 7.4, 6.8, 6.2, or 5.6 to mimic different stages in the endo-lysosomal pathway. After centrifugation to remove intact cells, the absorbance of the supernatant was measured at 405 nm to determine the amount of hemoglobin released. The absorbance of supernatant from untreated cells was subtracted, and the percent red blood cell disruption was normalized to positive control samples lysed with Triton X-100.

Confocal Microscopy

Colocalization of plasmid and endosomes was analyzed using confocal microscopy. Plasmid DNA was fluorescently labeled using a PromoFluor-500 labeling kit according to the manufacturer's instructions (PromoKine). MDA-MB-231 cells were plated in complete DMEM at a density of 10,000 cells/well in 8-well chamber slides 24 h prior to transfection. Immediately before transfection, media were aspirated and replaced with Opti-MEM + 2% FBS. Polyplex solution containing 150 ng pDNA was then added to each well. At 24 h after transfection, media were aspirated and replaced with complete DMEM + 75 nM LysoTracker Red probe + 1 μg/ml Hoechst stain. After 30 min incubation, cells were imaged with a Zeiss LSM 710 fluorescent confocal microscope (Oberkochen, Germany) to determine distribution of plasmid and endosomes within the cells. ImageJ software was used to analyze colocalization of plasmid and endosomes.

In Vitro *Transfection on PUR Scaffolds*

Desalted 40L polyplexes were prepared as described above and lyophilized with HPBCD (10:1 HPBCD:40L). PUR scaffolds were synthesized by reacting a polyester triol (900 Da) with a backbone comprising 60% caprolactone, 30% glycolide, and 10% lactide, 2.7 parts per hundred parts polyol (pphp) TEGOAMIN33 catalyst, 10 pphp water, 2 pphp calcium stearate, lyophilized polyplexes (2.5 or 5 wt% relative to scaffold mass), and LTIPEG prepolymer (index = 115). All reactants were sterilized prior to scaffold formation. After curing, scaffolds were cut into 8x2 mm pieces and placed in untreated 24-well plates. 200,000 IMDF cells were seeded on each scaffold and incubated in 1 ml

Opti-MEM + 2% FBS. Every 24 h, media were replaced with Opti-MEM + 2% FBS + 1 mg/ml luciferin, and luminescence was read on the IVIS imager as previously described.

Statistical analysis

One way analysis of variance (ANOVA) was used to evaluate the statistical significance of results. All p-values less than 0.05 were considered statistically significant.

Results

Poly(EG-b-(DMAEMA-co-BMA)) Characterization

A library of diblock copolymers with varying compositions and molecular weights were synthesized. Results of polymer characterization using GPC and ^{1}H-NMR are shown in Table 6.1. The abbreviated names of the polymers indicate the mol% BMA in the DMAEMA-*co*-BMA block and the relative length of the DMAEMA-*co*-BMA block (short [S], medium [M], or long [L]). PEG block molecular weight was held constant at 5000 Da.

Table 6.1. Block lengths and composition of poly(EG-*b*-(DMAEMA-*co*-BMA)) polymers.

Polymer Name	PEG (Da)	DMAEMA-co-BMA (Da)	% BMA in DMAEMA-*co*-BMA block	PDI
0S	5000	13,743	0.00%	1.045
0L	5000	17,035	0.00%	1.092
25S	5000	13,128	24.50%	1.045
25L	5000	18,747	23.80%	1.075
40S	5000	12,428	39.3%	1.079
40L	5000	20,765	39.6%	1.117
50S	5000	13,683	48.5%	1.045
50M	5000	18,041	48.3%	1.040
50L	5000	22,857	49.7%	1.161
60S	5000	8550	58.6%	1.127
60L	5000	19,939	58.6%	1.081

Fresh Polyplex Transfection

The effects of BMA content (0 – 60% BMA) and poly(DMAEMA-*co*-BMA) block length (short or long) on transfection efficiency were assessed by delivering a luciferase reporter plasmid to MDA-MB-231 cells. As shown in Figure 6.1, transfection efficiency was maximized at 40% BMA, and polymers with 40 or 50 mol% BMA had significantly higher transfection than all other diblock copolymers. Furthermore, increasing the DMAEMA-*co*-BMA block length increased the transfection efficiency at each mol% BMA. 40L polyplexes had significantly higher transfection than PEI

polyplexes. Due to their superior transfection efficiency, polymers with 40 and 50 mol% BMA were the focus of subsequent experiments.

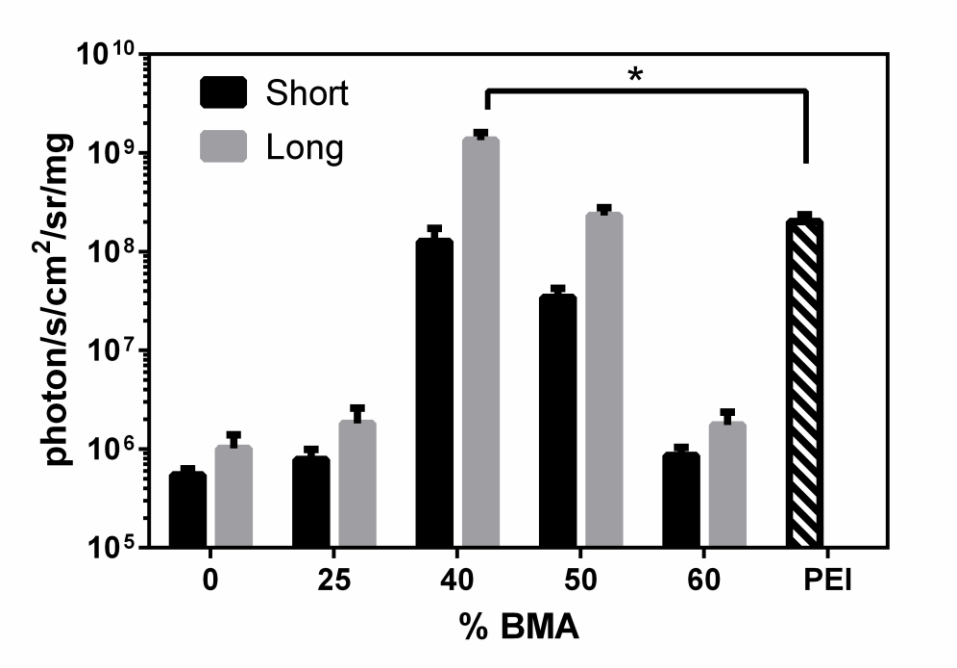

Figure 6.1. Transfection efficiency of polymer-pDNA polyplexes. Luminescence produced by MDA-MB-231 cells transfected with fresh polyplexes containing luciferase pDNA (normalized to total protein). Asterisk indicates significant difference ($p < 0.05$). Data are plotted as mean ± standard deviation.

Agarose Gel Electrophoresis

Agarose gel electrophoresis was performed to assess the ability of the transfection reagents to package pDNA, as shown in Figure 6.2. Poly(EG-*b*-(DMAEMA-*co*-BMA))-pDNA polyplexes with N/P ratios of 5, 10, and 20 did not migrate out of the loading wells, and no free pDNA was detected at any of the N/P ratios investigated (Figure 6.2A). 40L polyplex formation was further investigated at lower N/P ratios (Figure 6.2B). Some free pDNA was detected at N/P ratios of 1 and 2 for 40L polyplexes and N/P ratio of 1 or PEI polyplexes. No free pDNA was visible at N/P ratios of 5 or above for 40L polyplexes

and 2 or above for PEI polyplexes. These results indicate that poly(EG-*b*-(DMAEMA-*co*-BMA)) polymers efficiently encapsulate pDNA at N/P ratios of 5 or above.

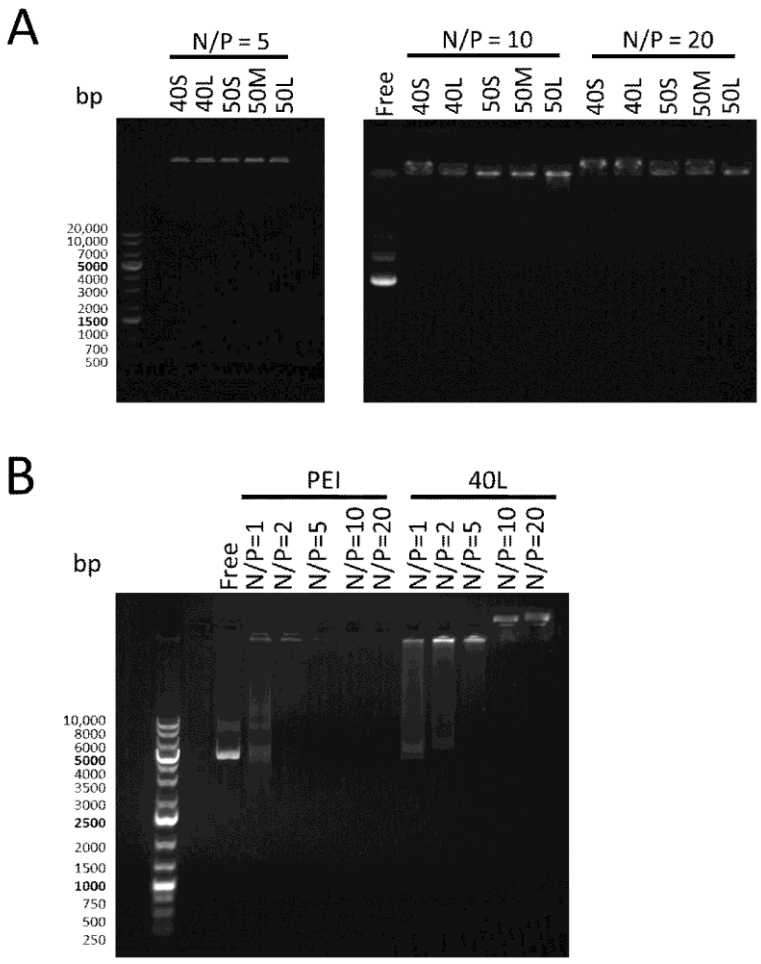

Figure 6.2. Agarose gel electrophoresis of polymer-pDNA polyplexes. Polyplexes were loaded onto a 0.8% agarose gel. Free pDNA and a DNA ladder were also included on the gel. (A) Poly(EG-b-(DMAEMA-co-BMA)) polyplexes with N/P ratios of 5, 10, or 20. pDNA is visible in the loading wells in the lanes containing polyplexes, and no free pDNA is visible in these lanes. (B) 40L and PEI polyplexes with varying N/P ratios. Free pDNA is visible lanes containing 40L polyplexes with N/P ratios of 1 and 2 and PEI polyplexes with N/P ratio of 1.

Polyplex Size and ζ-potential

The size of polyplexes with N/P ratio of 10 was measured in DPBS before and after lyophilization (Figure 6.3A). Before lyophilization, the diameter of poly(EG-*b*-(DMAEMA-*co*-BMA)) polyplexes ranged from 130 – 180 nm. BMA content and block length did not significantly affect initial polyplex size. After lyophilization, the size of PEI polyplexes and 50% BMA polyplexes increased significantly ($p < 0.05$), while the size of 40% BMA polyplexes did not significantly increase. In addition, the effect of N/P ratio on stability after lyophilization was investigated (data not shown). N/P ratio had no effect on polyplex size prior to lyophilization, but increasing the N/P ratio increased the stability of lyophilized polyplexes, leading to smaller increases in diameter after lyophilization. This trend was only significant for 50M polyplexes.

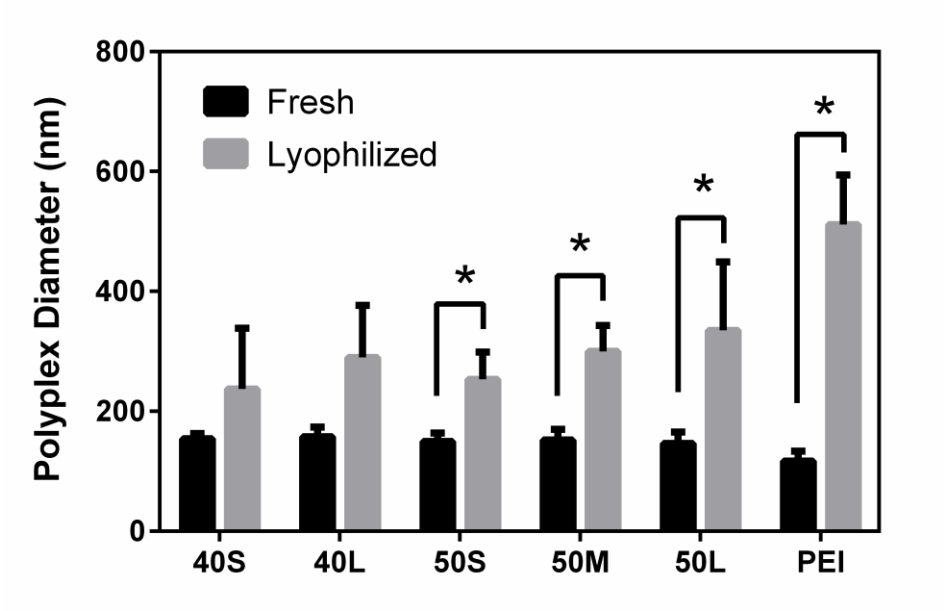

Figure 6.3. Effect of lyophilization on the size of polymer-pDNA polyplexes measured by DLS. Polyplexes were diluted to a concentration of 1.5 μg/ml pDNA in DPBS. Hydrodynamic diameter of polyplexes with N/P ratio of 10 before and after lyophilization and subsequent reconstitution. Asterisks indicate significant difference ($p < 0.05$). Data are plotted as means ± standard deviation.

Since 40L was identified as the lead candidate for *in vitro* transfection and showed no significant change in polyplex size pre- versus post-lyophilization, it was the focus of subsequent investigations. As shown in Figure 6.4, the ζ-potential of 40L and PEI polyplexes measured in 1 mM KCl at pH 7 increased with N/P ratio. At N/P ratios ≥ 5, the ζ-potential of 40L polyplexes approached 0 mV. Even at higher N/P of 20 and 30, the ζ-potential of 40L polyplexes was neutral due to shielding of the excess cationic charge in the polyplex core by the PEG corona. In contrast, the ζ-potential of PEI polyplexes increased up to an N/P ratio of 20, at which point it asymptotically approached +20 mV.

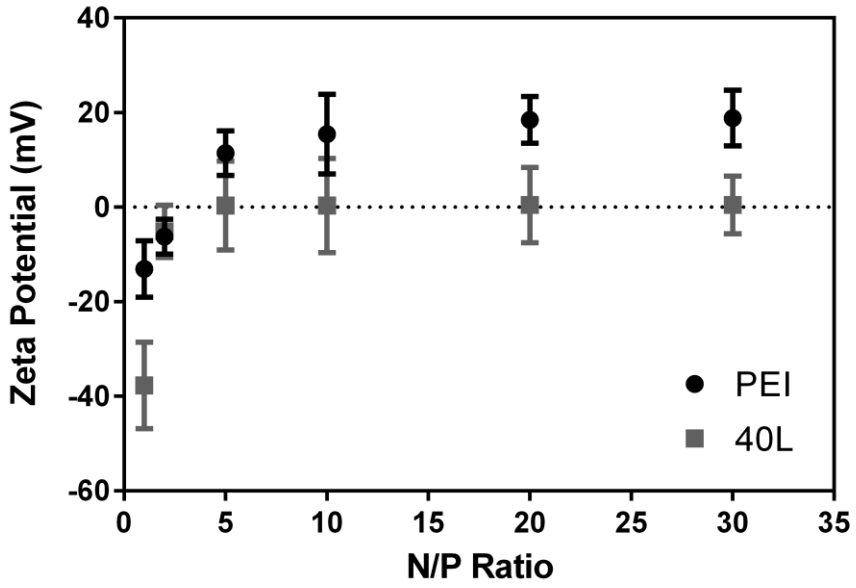

Figure 6.4. ζ-potential of polymer-pDNA complexes measured by DLS. ζ-potential was measured in 1 mM KCl pH 7.0. ζ-potential of 40L and PEI polyplexes increased with N/P ratio. ζ-potential of 40L-pDNA polyplexes approached ~0 mV for N/P of 5 or greater while ζ-potential of PEI-pDNA polyplexes approached ~20 mV for N/P of 20 or greater. Data are plotted as mean ± standard deviation.

Aggregation Studies and Modeling Analysis

Due to the presence of the PEG corona and a combination of electrostatic and hydrophobic interactions to stabilize the core, the poly(EG-*b*-(DMAEMA-*co*-BMA)) polyplexes were expected to show increased colloidal stability compared to PEI polyplexes. The interaction potential between PEI polyplexes was calculated using DLVO theory by summing the short-range van der Waals attraction and the long-range electrostatic repulsion forces. In these calculations, no potential maximum was observed, thereby suggesting the absence of an energy barrier and consequent rapid (i.e., diffusion-controlled) flocculation (stability ratio $W \approx 1$). In contrast, poly(EG-*b*-(DMAEMA-*co*-BMA)) polyplexes were stabilized by the terminally attached PEG corona, resulting in an

interfacial layer ~6 nm thick. Thus, the relatively short-range van der Waals forces are screened by the long-range steric repulsion, resulting in a high stability ratio ($W >> 1$) and consequent slow (i.e., reaction-limited) flocculation.

To quantify poly(EG-*b*-(DMAEMA-*co*-BMA)) polyplex stability, the aggregation kinetics were assessed in pH 7.4 DPBS at N/P ratios of 5 (Figure 6.5A) and 10 (Figure 6.5B). The aggregation kinetics of PEI polyplexes are shown in Figure 6.5C. PEI polyplexes exhibited faster aggregation than poly(EG-*b*-(DMAEMA-*co*-BMA)) polyplexes, forming aggregates 1000 nm in diameter in less than 5 hours. For all polymers, polyplexes with N/P ratio of 5 were less stable than those with N/P ratio of 10. 40L polyplexes with N/P ratio of 10 exhibited the greatest stability, remaining <200 nm in diameter after more than 60 hours in DPBS.

Previous studies have shown that for slow flocculation, the floc diameter grows exponentially with time. Weitz described a reaction-limited colloidal aggregation model for systems with $W >> 1$ [25]:

$$\overline{R}_h \sim e^{t_a/t_0} \tag{6.1}$$

where R_h is a scaling parameter approximating the average hydrodynamic radius, t_a is aggregation time, and t_0 is an aggregation time constant that varies with initial particle concentration and single particle sticking probability. For systems with $W \approx 1$, a power law model describing diffusion-limited aggregation can be applied:

$$\overline{R}_h \sim t^{1/d_f} \tag{6.2}$$

where d_f is the fractal dimension of the aggregates. As anticipated from the colloidal stability predictions, the reaction-limited model fit the data for poly(EG-*b*-(DMAEMA-*co*-BMA)) polyplexes (Figures 6.5A and 6.5B; R^2 = 0.85 – 0.98), while the diffusion-

limited model fit the data for PEI polyplexes (Figure 6.5C; R^2 = 0.95 – 0.98). Increasing the N/P ratio from 5 to 10 approximately doubled the aggregation time constants for 40L polyplexes.

Polymer 40L (Figure 6.5D) and PEI (Figure 6.5E) polyplex stability was also investigated as a function of ionic strength by varying KCl concentration. As [KCl] increased, PEI polyplexes aggregated more rapidly, a behavior that was consistent with the notion that PEI polyplexes are stabilized by electrostatic repulsion. In contrast, [KCl] had no effect on aggregation rate of 40L polyplexes. 40L polyplexes did not aggregate substantially, remaining <200 nm in diameter after 72 h at all KCl concentrations investigated. These observations suggested that 40L polyplexes are stabilized by steric interactions and not by electrostatic repulsion; hence, ionic strength does not affect their aggregation rate. In contrast, the diffusion-limited aggregation model fit the data for PEI polyplexes well (Figure 6.5F; R^2 = 0.95 – 0.99), and PEI polyplex stability decreased with increasing [KCl].

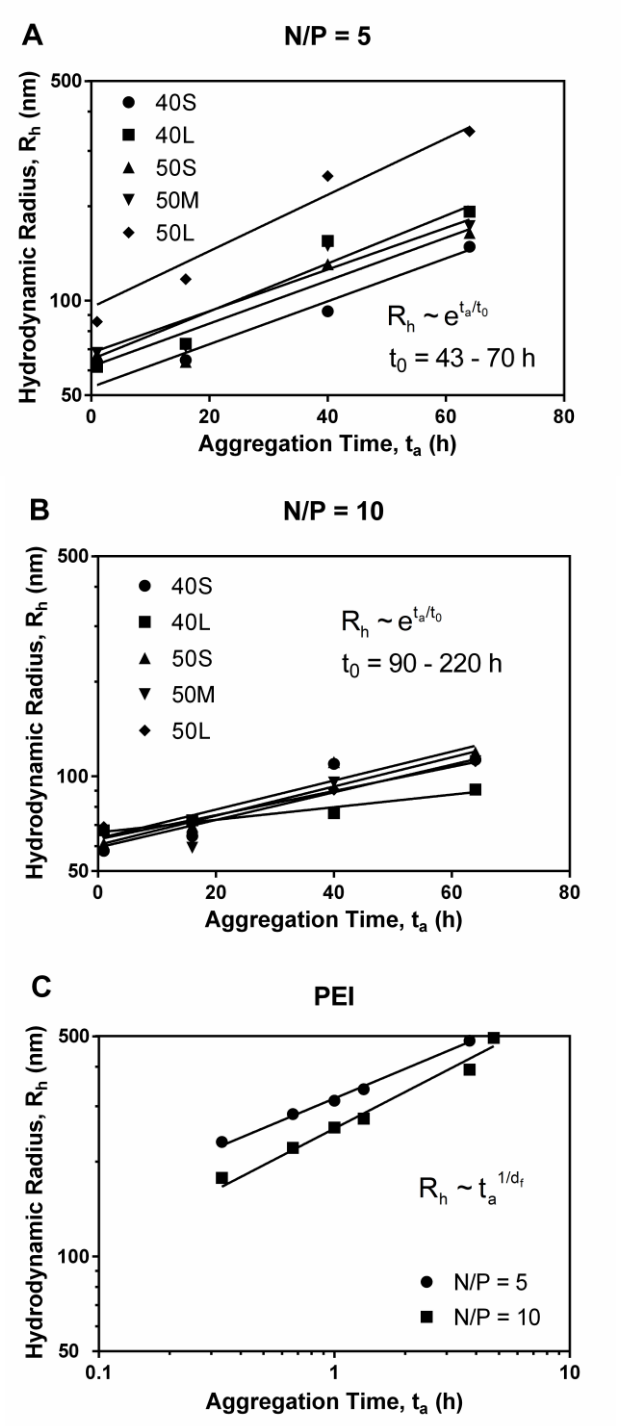
A
N/P = 5
Hydrodynamic Radius, R_h (nm)
500
100
50
0
20
40
60
80
Aggregation Time, t_a (h)
40S
40L
50S
50M
50L
$R_h \sim e^{t_a/t_0}$
t_0 = 43 - 70 h
B
N/P = 10
Hydrodynamic Radius, R_h (nm)
500
100
50
0
20
40
60
80
Aggregation Time, t_a (h)
40S
40L
50S
50M
50L
$R_h \sim e^{t_a/t_0}$
t_0 = 90 - 220 h
C
PEI
Hydrodynamic Radius, R_h (nm)
500
100
50
0.1
1
10
Aggregation Time, t_a (h)
$R_h \sim t_a^{1/d_f}$
N/P = 5
N/P = 10

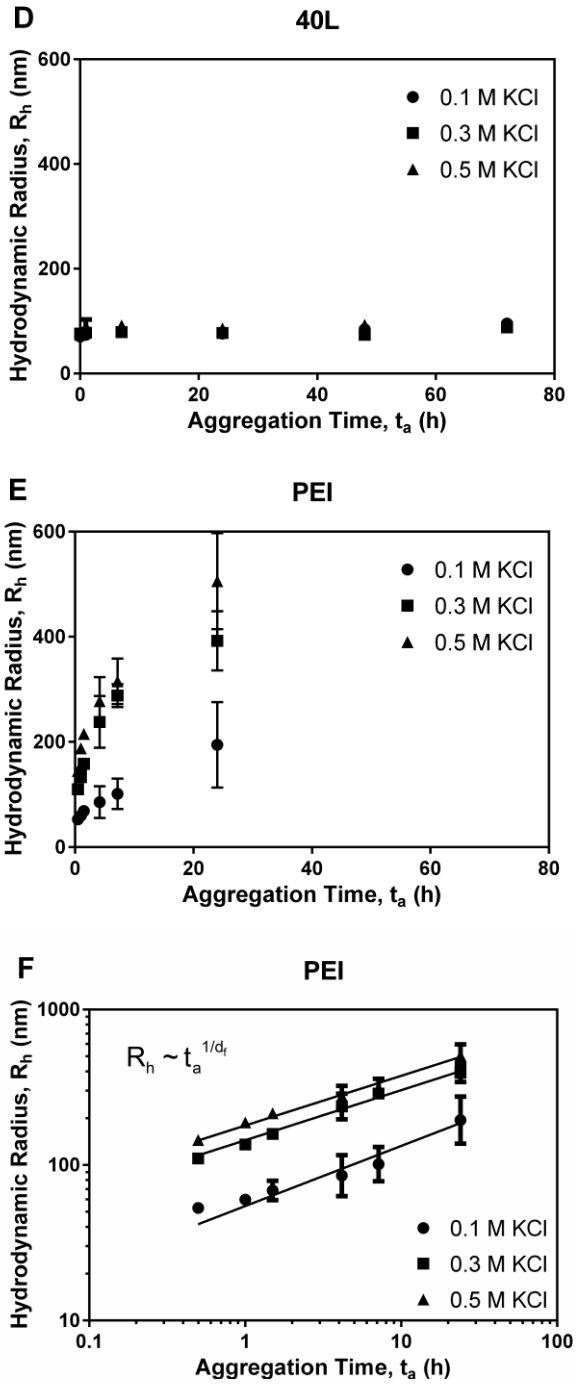

Figure 6.5. Aggregation kinetics of polyplexes in the presence of buffer salts. Panels A and B illustrate aggregation of polyplexes with N/P ratio of 5 (A) and 10 (B) in DPBS over time. Data for diblock copolymers were fit to the reaction-limited colloidal aggregation model. (C) Data for PEI in DPBS were fit to the diffusion-limited colloidal aggregation model. Panels D and E show effects of ionic strength of KCl on aggregation of 40L (D) and PEI (E) polyplexes. (F) Data for PEI in KCl were fit to the diffusion-limited colloidal aggregation model. Data are plotted as mean ± standard deviation.

In Vitro *Transfection and Cytotoxicity of Lyophilized Polyplexes*

The ability of the lyophilized polyplexes to transfect MDA-MB-231 cells *in vitro* was assessed by delivering a luciferase reporter plasmid (Figure 6.6A). At N/P ratio of 5, 40L polyplexes had significantly higher transfection than PEI. At N/P ratio of 10, all poly(EG-*b*-(DMAEMA-*co*-BMA)) polyplexes investigated had significantly higher transfection efficiency than PEI. At N/P ratio of 20, 40S, 40L, 50S, and 50M polyplexes produced significantly higher transfection than PEI. To determine cytotoxicity of fresh and lyophilized polyplexes, calcein AM staining was used to quantify number of live cells after transfection (Figure 6.6B). All wells treated with poly(EG-*b*-(DMAEMA-*co*-BMA)) polyplexes had >70% viability relative to untreated wells. The viability of cells treated with poly(EG-*b*-(DMAEMA-*co*-BMA)) polyplexes was comparable to or higher than cells treated with PEI polyplexes.

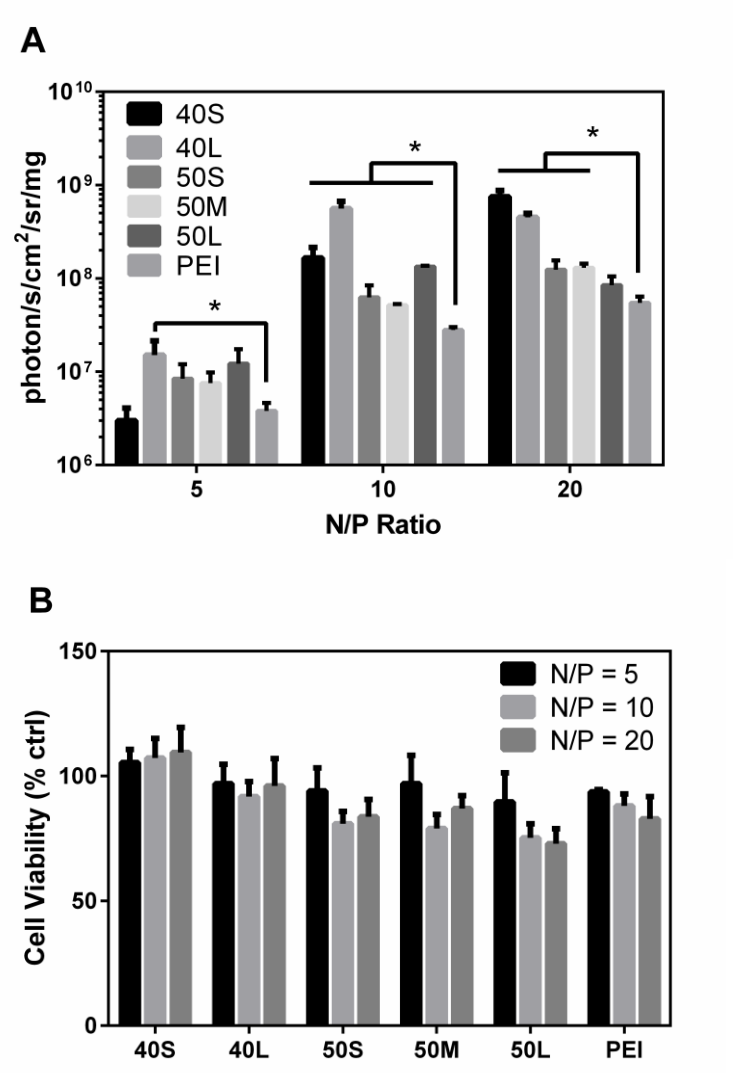

Figure 6.6. Transfection efficiency and cytotoxicity of lyophilized polymer-pDNA polyplexes. MDA-MB-231 cells were transfected with polymer-pDNA polyplexes lyophilized using trehalose as an excipient (200:1 trehalose:polymer). (A) Luminescence produced by cells transfected with lyophilized polyplexes normalized to total protein. Asterisks indicate significant increase in transfection compared to PEI ($p < 0.05$). (B) Cell viability after transfection with lyophilized polyplexes relative to untreated cells was assessed using calcein AM staining. Data are plotted as mean ± standard deviation.

pH-dependent Membrane Disruption and Endosomal Escape

A red blood cell hemolysis assay was performed to determine pH-dependent membrane disruption by polyplexes with N/P ratio of 10. As shown in Figure 6.7A, all

polyplexes had <5% hemolysis at pH 7.4 (mimicking extracellular and cytosolic pH), which is important for minimizing polyplex cytotoxicity. As pH decreased, hemolytic behavior of the polyplexes increased significantly. All polyplexes produced 100% hemolysis (statistically equivalent to Triton X detergent) at pH 5.6 (mimicking late endosomes), suggesting that the polyplexes can achieve efficient endosomal escape.

The ability of the diblock copolymers to aid in endosomal escape was further investigated using confocal microscopy. Images of cells transfected with 40L polyplexes (Figure 6.7B) were analyzed to quantify the colocalization of green (plasmid) and red (endosomes) fluorescent probes (Figure 6.7C). As the N/P ratio of 40L increased from 5 to 20, the fraction of green colocalized with red decreased significantly ($p < 0.05$). These results provide evidence that in this setting, the active, pH-dependent membrane disruptive mechanism of 40L is concentration dependent and is similar in efficacy to the pure proton sponge mechanism of PEI.

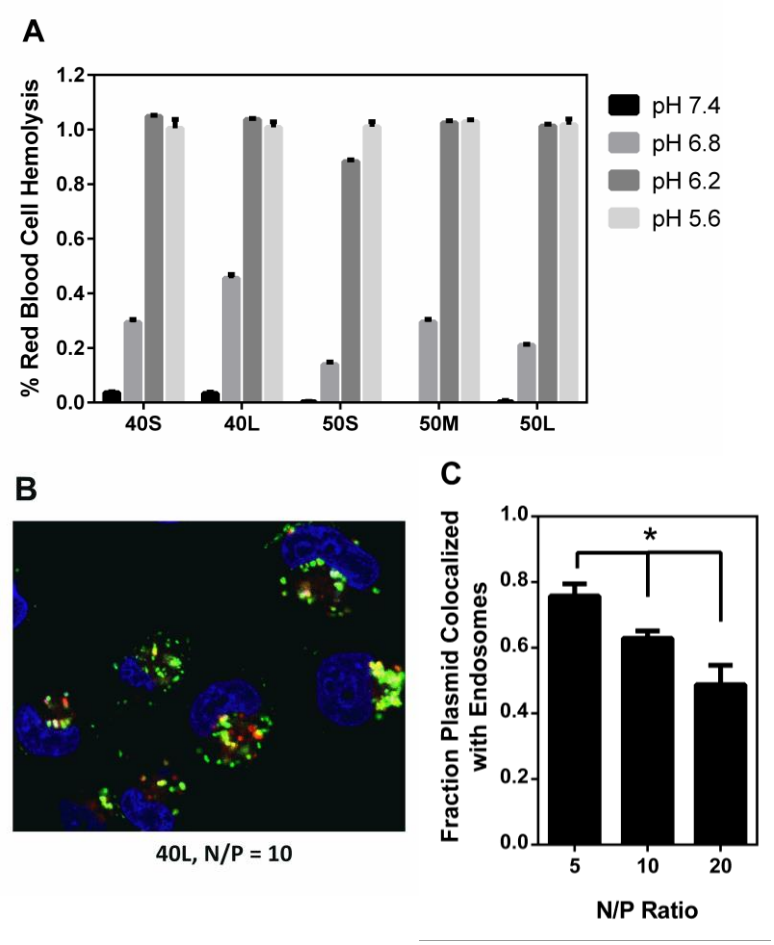

Figure 6.7. Endosomal escape and pH-dependent membrane disruption. (A) pH-dependent red blood cell hemolysis assay. All polyplexes investigated exhibited pH-dependent membrane disruption, displaying minimal hemolysis at physiologic pH and switch-like transition into a membrane disruptive confirmation at endo-lysosomal pHs. Data are plotted as mean ± standard error. (B) Confocal microscopy images of MDA-MB-231 cells transfected with 40L-pDNA polyplexes with N/P ratio of 10 showing distribution of plasmid (green), endosomes (red), and nuclei (blue). (C) Percentage of plasmid colocalized with Lysotracker dye. Data are plotted as mean ± standard error, and asterisk indicates statistically significant difference ($p < 0.05$).

In Vitro *Transfection on PUR Scaffolds*

Although 40L-pDNA polyplexes achieved efficient transfection after lyophilization, a large amount of excipient was needed to stabilize the polyplexes (200:1 trehalose:polymer). The excipient must be decreased in order to incorporate lyophilized

polyplexes into tissue-engineered scaffolds with a high enough dose of pDNA to be effective. In this study, two strategies were applied to decrease the amount of excipient. First, polyplexes were desalted prior to lyophilization. Second, the excipient was changed to HPBCD, a β-cyclodextrin derivative that has been shown to be effective in stabilizing PEGylated nanoparticles [26]. As shown in Figure 6.8A, desalting the polyplexes resulted in higher transfection both before and after lyophilization. Furthermore, efficient transfection was achieved with a ratio of HPBCD:40L as low as 10, which is 20-fold lower than the amount of trehalose required to stabilize the polyplexes.

Desalted polyplexes were lyophilized with HPBCD with an excipient to polymer ratio of 10 and incorporated into PUR scaffolds with 2.5 or 5 wt% HPBCD relative to scaffold mass. As controls, polyplexes were injected into premade scaffolds immediately before cell seeding, adsorbed onto the scaffold surface at room temperature, or lyophilized onto the scaffold surface. Cells seeded on the scaffolds with 2.5% HPBCD had significantly higher transfection than cells seeded on scaffolds containing polyplexes that were injected into the scaffold pores or adsorbed or lyophilized on the scaffold surface for three days. This result provides evidence that incorporation of 40L-pDNA polyplexes in PUR scaffolds is a promising approach for stabilization and delivery of genes for therapeutic factors in local gene therapy applications.

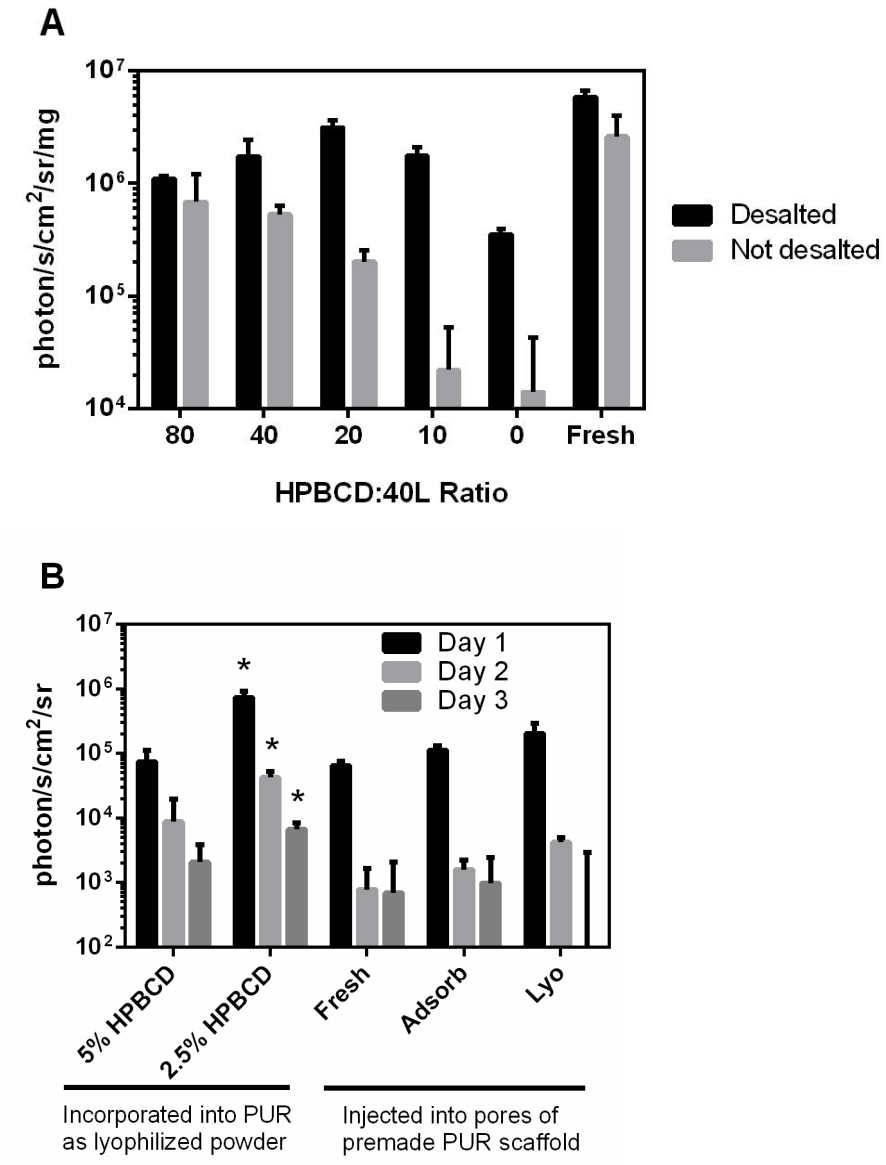

Figure 6.8. Transfection of polyplexes delivered from PUR scaffolds. (A) IMDF cells were transfected with desalted polyplexes that were lyophilized using HPBCD as an excipient. Transfection was achieved with a ratio of HPBCD:40L as low as 10. Data are plotted as mean ± standard deviation. (B) Transfection of IMDF cells seeded on PUR scaffolds containing 5 μg pDNA. Data are plotted as mean ± standard error. Asterisks indicate significant difference from all other treatments ($p < 0.05$). Scaffolds incorporating polyplexes as a lyophilized powder with 2.5% HPBCD resulted in significantly higher transfection than scaffolds containing polyplexes that were injected into the scaffold pores (Fresh) or adsorbed (Adsorb) or lyophilized (Lyo) on the scaffold surface.

Discussion

Local gene therapy has applications for tissue restoration, wound healing, and treatment of disease. Previous research on delivery of naked or nanoparticulate pDNA incorporated into hydrogels and biomaterial scaffolds has produced transgene expression and tissue responses *in vivo*. However, these systems often suffer from low transfection efficiency, burst release of pDNA, or nanoparticle aggregation in physiologic conditions, necessitating delivery of high doses of pDNA. In this study, we designed pDNA polyplexes with high colloidal stability and enhanced cellular uptake and transfection efficiency compared to conventional PEI-pDNA polyplexes. The new polyplexes were composed of diblock polymers containing DMAEMA to electrostatically bind DNA, BMA to provide hydrophobic interactions and enhance polyplex core stability, and a PEG corona to shield charge and enhance steric stability. These polyplexes exhibited significantly less aggregation than PEI polyplexes after lyophilization or in the presence of high salt concentrations. In addition to being optimized to overcome extracellular barriers to polyplex stability, the poly(EG-*b*-(DMAEMA-*co*-BMA)) polyplexes were also designed to overcome intracellular endo-lysosomal delivery barriers through finely-tuned pH-dependent membrane disruptive activity. Several polyplex formulations had higher transfection efficiency than PEI complexes both before and after lyophilization. Furthermore, cells seeded on PUR scaffolds incorporating lyophilized polyplexes were efficiently transfected. These results point to the potential broad utility of diblock copolymer-pDNA polyplexes for tissue, intravenous, or local gene delivery when incorporated into tissue engineering scaffolds.

Despite being considered a gold standard for nonviral gene delivery, PEI has several disadvantageous properties. PEI polyplexes have been shown to have poor stability at high concentrations, in the presence of salt and serum, and during lyophilization [10, 11, 27]. Excipients can reduce aggregation through increased viscosity [10], but sucrose and agarose excipients add to the overall complexity of the formulation and may have adverse biological effects or alter the curing or mechanical properties of the delivery vehicle. It has been reported that plasma proteins adsorb to PEI-pDNA polyplexes, resulting in rapid aggregation that can be reduced by polyplex PEGylation [28]. In the present study, DLS measurements revealed that PEI polyplexes aggregated rapidly during lyophilization. Consistent with the notion that PEI polyplexes are electrostatically stabilized, their aggregation rate increased with increasing salt concentration due to screening of the electrostatic repulsion forces. While PEI polyplexes aggregated slowly in 0.1 M KCl, PEI polyplexes aggregated rapidly in 0.3 M and 0.5 M KCl and also in DPBS, a buffer that mimics physiologic conditions.

In contrast to PEI, the best performing diblock copolymer-pDNA polyplexes (40L with N/P = 10) was stable after lyophilization and at high salt concentrations. Consistent with the notion that the polyplexes were sterically stabilized, the electrolyte concentration did not affect the polyplex aggregation rate. To more quantitatively assess the kinetics of aggregation of nanoparticles in DPBS, the particle size time-course data (Figure 6.4) were fit to colloidal aggregation models [25]. Diblock copolymer polyplex aggregation was reaction-limited while PEI polyplex aggregation was diffusion-controlled, providing evidence that diblock copolymers have greater stability than PEI. The diblock copolymer polyplexes are stabilized sterically by the PEG corona as well as by DMAEMA-pDNA

electrostatic interactions and BMA hydrophobicity in the core. Thus, they can be readily tuned by varying the BMA content to optimize polyplex stability. Due to their high colloidal stability, poly(EG-*b*-(DMAEMA-*co*-BMA))-pDNA required a small amount of excipient during lyophilization. Polyplexes lyophilized with an excipient:polymer ratio of 10 achieved efficient transfection when delivered from PUR scaffolds *in vitro*.

Previous studies suggest that PEGylation increases stability but decreases transfection efficiency. In the present study, several poly(EG-*b*-(DMAEMA-*co*-BMA)) polyplexes had better transfection efficiency in serum than PEI before and after lyophilization despite having neutral ζ-potential. The best performing diblock copolymer-pDNA polyplex, 40L with N/P = 10, had greater luminescence production than PEI both before and after lyophilization. This observation is consistent with a previous study reporting that dextran-PEI complexes had moderately lower transfection efficiency than PEI in serum-free medium at 4 h, but in the presence of serum at longer time points (48 h), significantly higher transfection efficiencies were observed for dextran-PEI complexes compared to PEI [29]. Another study has reported that PEI transfection decreases 2-20 fold in the presence of 10% serum compared to serum-free media [30]. Taken together with these previous studies, our data suggest that sterically stabilized polyplexes (i.e., 40L and dextran-PEI) have a slower initial rate of uptake *in vitro* due to lower ζ-potential, but their increased steric stability in the presence of salts and serum provides them with superior long-term performance under physiologically relevant conditions.

Polymer-pDNA nanoparticles used for local gene delivery from tissue engineering scaffolds must not only be effectively stabilized against colloidal aggregation

but also support efficient endosomal escape in order to achieve high levels of transfection. PEGylation and titration of hydrophobic content into polycations are known to have several beneficial effects on nonviral gene therapy [17]. Triblock copolymers composed of PEG, hydrophobic poly(n-butyl acrylate) (PnBA), and cationic DMAEMA have been reported to form polyplexes with DNA that exhibit improved stability against aggregation and reduced interactions with negatively charged serum components [31]. While NMR spectroscopy measurements revealed that the PEG corona shielded the charged DMAEMA-DNA polyplex, incorporation of the hydrophobic PnBA homopolymer block decreased transfection efficiency, which was conjectured to occur due to decreased intracellular release of pDNA from the polyplexes.

Poly(EG-*b*-(DMAEMA-*co*-BMA)) polymers have been shown to be effective for packaging of siRNA for intravenous delivery [21] but had not been tested yet for formation and stabilization of pDNA polyplexes that mediate endosomal escape through an active, pH-dependent membrane disruption mechanism. Previous studies have reported that active membrane disruption mechanisms can be used to enhance endosome escape and transfection efficiency relative to relying solely on proton sponge osmotic disruption of endosomes (i.e., as achieved using PEI or homopolymers of DMAEMA). For example, the membrane-porating peptide melittin has been shown to aid in endosome escape and increase transfection efficiency of PEI- and lysine-based polyplexes [32, 33]. In the present study, the composition and molecular weight of the DMAEMA-*co*-BMA block were tuned to achieve an optimal balance of pH-responsiveness and hydrophobic interactions in order to form colloidally stable nanoparticles that increase endosomal escape and transfection efficiency.

Conclusions

Poly(EG-*b*-(DMAEMA-*co*-BMA) diblock copolymers were synthesized and tested for stability, endosomal escape, and transfection efficiency of pDNA. The polymers formed pDNA polyplexes that exhibited increased colloidal stability after lyophilization and in the presence of salt relative to PEI-pDNA polyplexes, with polymer 40L exhibiting optimal performance. Poly(EG-*b*-(DMAEMA-*co*-BMA))-pDNA polyplexes had greater transfection efficiency than PEI-pDNA polyplexes and achieved pH-dependent membrane disruption leading to improved endosomal escape. Polyplexes incorporated into and delivered from PUR scaffolds transfected cells *in vitro*. The enhanced colloidal stability and transfection efficiency of the lyophilized diblock copolymer-pDNA polyplexes underscores their potential utility for numerous applications including local nonviral gene delivery from 3D scaffolds, which is the focus of ongoing studies.

References

[1] Boussif O, Lezoualc'h F, Zanta MA, Mergny MD, Scherman D, Demeneix B, et al. A versatile vector for gene and oligonucleotide transfer into cells in culture and in vivo: polyethylenimine. Proc Natl Acad Sci U S A 1995;92:7297-301.
[2] Cherng J-Y, van de Wetering P, Talsma H, Crommelin DA, Hennink W. Effect of Size and Serum Proteins on Transfection Efficiency of Poly ((2-dimethylamino)ethyl Methacrylate)-Plasmid Nanoparticles. Pharmaceutical Research 1996;13:1038-42.
[3] Behr JP. The proton sponge, a means to enter cells viruses never thought of. M S-Med Sci 1996;12:56-8.
[4] Behr JP. The proton sponge: A trick to enter cells the viruses did not exploit. Chimia 1997;51:34-6.
[5] Wang S, Ma N, Gao SJ, Yu H, Leong KW. Transgene expression in the brain stem effected by intramuscular injection of polyethylenimine/DNA complexes. Molecular therapy : the journal of the American Society of Gene Therapy 2001;3:658-64.
[6] Kichler A, Chillon M, Leborgne C, Danos O, Frisch B. Intranasal gene delivery with a polyethylenimine-PEG conjugate. Journal of controlled release : official journal of the Controlled Release Society 2002;81:379-88.
[7] Aoki K, Furuhata S, Hatanaka K, Maeda M, Remy JS, Behr JP, et al. Polyethylenimine-mediated gene transfer into pancreatic tumor dissemination in the murine peritoneal cavity. Gene therapy 2001;8:508-14.
[8] Lei P, Padmashali RM, Andreadis ST. Cell-controlled and spatially arrayed gene delivery from fibrin hydrogels. Biomaterials 2009;30:3790-9.
[9] Trentin D, Hubbell J, Hall H. Non-viral gene delivery for local and controlled DNA release. Journal of controlled release : official journal of the Controlled Release Society 2005;102:263-75.
[10] Lei Y, Huang S, Sharif-Kashani P, Chen Y, Kavehpour P, Segura T. Incorporation of active DNA/cationic polymer polyplexes into hydrogel scaffolds. Biomaterials 2010;31:9106-16.
[11] Lei Y, Rahim M, Ng Q, Segura T. Hyaluronic acid and fibrin hydrogels with concentrated DNA/PEI polyplexes for local gene delivery. Journal of controlled release : official journal of the Controlled Release Society 2011;153:255-61.
[12] Itaka K, Yamauchi K, Harada A, Nakamura K, Kawaguchi H, Kataoka K. Polyion complex micelles from plasmid DNA and poly(ethylene glycol)â€“poly(l-lysine) block copolymer as serum-tolerable polyplex system: physicochemical properties of micelles relevant to gene transfection efficiency. Biomaterials 2003;24:4495-506.
[13] Verbaan FJ, Oussoren C, Snel CJ, Crommelin DJ, Hennink WE, Storm G. Steric stabilization of poly(2-(dimethylamino)ethyl methacrylate)-based polyplexes mediates prolonged circulation and tumor targeting in mice. The journal of gene medicine 2004;6:64-75.
[14] Vader P, van der Aa LJ, Engbersen JF, Storm G, Schiffelers RM. Physicochemical and biological evaluation of siRNA polyplexes based on PEGylated Poly(amido amine)s. Pharmaceutical research 2012;29:352-61.
[15] Zhou J, Liu J, Cheng CJ, Patel TR, Weller CE, Piepmeier JM, et al. Biodegradable poly(amine-co-ester) terpolymers for targeted gene delivery. Nature materials 2012;11:82-90.

[16] Piest M, Engbersen JFJ. Effects of charge density and hydrophobicity of poly(amido amine)s for non-viral gene delivery. Journal of Controlled Release 2010;148:83-90.
[17] Liu Z, Zhang Z, Zhou C, Jiao Y. Hydrophobic modifications of cationic polymers for gene delivery. Progress in Polymer Science 2010;35:1144-62.
[18] Manganiello MJ, Cheng C, Convertine AJ, Bryers JD, Stayton PS. Diblock copolymers with tunable pH transitions for gene delivery. Biomaterials 2012;33:2301-9.
[19] Convertine AJ, Benoit DSW, Duvall CL, Hoffman AS, Stayton PS. Development of a novel endosomolytic diblock copolymer for siRNA delivery. Journal of Controlled Release 2009;133:221-9.
[20] Duvall CL, Convertine AJ, Benoit DSW, Hoffman AS, Stayton PS. Intracellular Delivery of a Proapoptotic Peptide via Conjugation to a RAFT Synthesized Endosomolytic Polymer. Molecular Pharmaceutics 2009;7:468-76.
[21] Nelson CE, Kintzing JR, Hanna A, Shannon JM, Gupta MK, Duvall CL. Balancing cationic and hydrophobic content of PEGylated siRNA polyplexes enhances endosome escape, stability, blood circulation time, and bioactivity in vivo. ACS nano 2013;7:8870-80.
[22] Chiefari J, Chong YK, Ercole F, Krstina J, Jeffery J, Le TPT, et al. Living Free-Radical Polymerization by Reversible Addition−Fragmentation Chain Transfer: The RAFT Process. Macromolecules 1998;31:5559-62.
[23] Convertine AJ, Benoit DS, Duvall CL, Hoffman AS, Stayton PS. Development of a novel endosomolytic diblock copolymer for siRNA delivery. Journal of controlled release : official journal of the Controlled Release Society 2009;133:221-9.
[24] Evans BC, Nelson CE, Yu SS, Beavers KR, Kim AJ, Li H, et al. Ex vivo red blood cell hemolysis assay for the evaluation of pH-responsive endosomolytic agents for cytosolic delivery of biomacromolecular drugs. Journal of visualized experiments : JoVE 2013:e50166.
[25] Lin MY, Lindsay HM, Weitz DA, Ball RC, Klein R, Meakin P. Universal reaction-limited colloid aggregation. Phys Rev A 1990;41:41.
[26] van den Hoven JM, Metselaar JM, Storm G, Beijnen JH, Nuijen B. Cyclodextrin as membrane protectant in spray-drying and freeze-drying of PEGylated liposomes. International Journal of Pharmaceutics 2012;438:209-16.
[27] Oster CG, Wittmar M, Unger F, Barbu-Tudoran L, Schaper AK, Kissel T. Design of amine-modified graft polyesters for effective gene delivery using DNA-loaded nanoparticles. Pharm Res 2004;21:927-31.
[28] Ogris M, Brunner S, Schuller S, Kircheis R, Wagner E. PEGylated DNA/transferrin-PEI complexes: reduced interaction with blood components, extended circulation in blood and potential for systemic gene delivery. Gene Ther 1999;6:595-605.
[29] Jiang D, Salem AK. Optimized dextran-polyethylenimine conjugates are efficient non-viral vectors with reduced cytotoxicity when used in serum containing environments. Int J Pharm 2012;427:71-9.
[30] Dong X, Lin L, Chen J, Guo Z, Tian H, Li Y, et al. A serum-tolerant hydroxyl-modified polyethylenimine as versatile carriers of pDNA/siRNA. Macromol Biosci 2013;13:512-22.
[31] Sharma R, Lee JS, Bettencourt RC, Xiao C, Konieczny SF, Won YY. Effects of the incorporation of a hydrophobic middle block into a PEG-polycation diblock copolymer

on the physicochemical and cell interaction properties of the polymer-DNA complexes. Biomacromolecules 2008;9:3294-307.
[32] Boeckle S, Fahrmeir J, Roedl W, Ogris M, Wagner E. Melittin analogs with high lytic activity at endosomal pH enhance transfection with purified targeted PEI polyplexes. Journal of Controlled Release 2006;112:240-8.
[33] Schellinger JG, Pahang JA, Johnson RN, Chu DSH, Sellers DL, Maris DO, et al. Melittin-grafted HPMA-oligolysine based copolymers for gene delivery. Biomaterials 2013;34:2318-26.

CHAPTER VII

CONCLUSIONS

In conclusion, research on the development of injectable polyurethane (PUR) scaffolds with delivery of biologics was described in this dissertation. The main results of this work provide evidence that injectable PUR scaffolds support wound healing in animal models and can be used to deliver plasmid DNA encoding genes for regenerative factors. Overall, this research suggests that an injectable PUR delivery system for plasmid DNA has high potential for use in wound healing applications.

Previous research on PUR scaffolds has demonstrated that they are biocompatible and support healing in skin and bone defects in several small animal models [1-5]. In Chapter III, injectable PUR biocomposite scaffolds were developed for use in skin wound healing applications [6]. These scaffolds were shown to support cellular infiltration and extracellular matrix remodeling in a rat excisional wound model. Injectable scaffolds can conform to irregular wounds, are easy to use at the point of care, and offer options for patient-specific customization [7]. However, injectable biomaterials must have noncytotoxic reactants and intermediates, low reaction exotherms, and working and settting times on the order of minutes to be useful in a clinical setting [8]. In this study, injectable PUR scaffolds exhibited a minimal reaction exotherm and clinically relevant working and setting times. A polysaccharide filler, either carboxymethylcellulose or hyaluronic acid, was added to the reactive polyurethane mixture to control excessive expansion after injection. Due to their compressive mechanical properties, which approach those of native skin, the PUR scaffolds stented the wounds at early time points and delayed wound contraction. The stenting effect of the scaffolds resulted in the

positive outcomes of enhanced cellular proliferation and reduced collagen alignment and the negative outcome of delayed epithelialization. The scaffolds did not have significant effects on the level of apoptosis at any time point, suggesting that the polyurethane was biocompatible and non-cytotoxic. These results present compelling opportunities for the use of injectable polyurethanes as void fillers for healing of cutaneous tissue defects.

Due to the promising results from the use of injectable scaffolds in a small animal model, PUR scaffolds were investigated in a large animal model to more closely approximate human wounds. Chapter IV discussed the testing of implantable PUR scaffolds in a porcine excisional model. The porcine model was chosen because pig skin is anatomically and physiologically similar to human skin [9]. Two modifications were applied to implantable lysine-derived PUR scaffolds (LTI) to improve cellular infiltration and attachment: carboxymethylcellulose was added as a porogen to increase permeability and interconnectivity (CMC), and plasma treatment was applied to decrease the hydrophobicity of the scaffold surface (Plasma). Addition of carboxymethylcellulose increased the permeability of the scaffolds 2.5-fold, and plasma treatment decreased the contact angle by 20°. The permeability of the scaffolds was comparable to that of rigid open-cell foams reported elsewhere (10^{-12} – 10^{-10} m^2) [10]. Consistent with the rat excisional wound study described in Chapter III, PUR scaffolds stented porcine excisional wounds and resulted in significantly less contraction than untreated wounds at day 15. All three versions of the scaffolds supported tissue infiltration and showed significant biodegradation between day 8 and day 15. In untreated wounds, the number of $MAC387^+$ macrophages decreased from day 8 to day 15, consistent with wounds moving into resolution in the absence of scaffold material that promotes a typical foreign body

response [11]. As the scaffolds underwent degradation between day 8 and day 15, the number of macrophages increased in the CMC and Plasma groups, suggesting that carboxymethylcellulose treatment influenced the innate immune response. This transient increase in macrophages in scaffold treatment groups is consistent with an oxidative degradation mechanism mediated by macrophages [12]. All treatment groups had significantly fewer $Ki67^+$ cells at day 15 than at day 8, an indication that all wounds were moving from the proliferative phase of wound healing to the remodeling phase by day 15 [11]. Furthermore, the number of $TUNEL^+$ cells and the blood vessel area density in scaffold-treated wounds were not significantly different from untreated wounds at either time point. These data suggest that the PUR scaffolds did not adversely affect the wound healing process in porcine excisional wounds. To our knowledge, this is the first study demonstrating that single-layer void-filling scaffolds support wound healing in a porcine excisional model.

Since implantable PUR scaffolds achieved promising results in a porcine model, injectable PUR scaffolds were compared to implants in their ability to support cellular infiltration and facilitate wound healing in a porcine excisional model. Sucrose was added to the scaffolds as a porogen to prevent excessive foaming by absorbing moisture in the wound environment. The physical, mechanical, and rheological properties of the scaffolds were characterized *in vitro*. After leaching sucrose from the scaffolds, porosity and permeability increased, and density and compressive modulus decreased. The working and setting times of the scaffolds (4.8 ± 1.2 min and 16 ± 3 min, respectively) were appropriate for the clinical setting. In the porcine excisional wound study, implants had significantly less contraction than untreated wounds at days 9, 13, and 30, and

injectable scaffolds had significantly less contraction than untreated wounds at day 9. There were no significant differences between implants and injectables in wound contraction or cross-sectional area at any of the time points, suggesting that injectable scaffolds stented the wounds and delayed contraction as well as implants. Both the number of $Ki67^+$ cells and the proliferation/apoptosis ratio decreased from day 9 to day 13 in all treatment groups, and there were no significant differences in apoptosis among scaffold treatment groups. Implants had more macrophages than injectables at day 9, but macrophage presence declined from day 9 to day 13 in all treatment groups. Blood vessel density also decreased from day 9 to day 13 in all treatment groups. The patterns of proliferation, apoptosis, macrophage presence, and blood vessel formation provide evidence that the wounds were moving into the remodeling phase of healing by day 13. This study suggests that applying PUR scaffolds by injection rather than implantation did not adversely affect the wound healing process and that both injectable and implantable PUR scaffolds were biocompatible and reduced wound contraction in a porcine excisional model. Injectable scaffolds have not been tested previously in porcine excisional wounds. This research lays the groundwork for the use of injectable PUR scaffolds in tissue engineering applications to provide mechanical support and deliver biologics at the point of care.

Chapter VI described the development of a PUR plasmid delivery system for local gene therapy applications. This delivery system also has potential for use as a screening tool to test the performance of regenerative factors in animal models. Since many traditional transfection reagents such as polyethylenimine (PEI) suffer from instability [13, 14], a library of novel poly(ethylene glycol-*b*-(dimethylaminoethyl methacrylate-*co*-

butyl methacrylate)) polymers was developed to stabilize plasmid DNA (pDNA) during lyophilization and incorporation into PUR scaffolds. These polymers were designed such that dimethylaminoethyl methacrylate initiates electrostatic interactions with pDNA to trigger formation of polyplexes that are further stabilized by hydrophobic interactions of the butyl methacrylate in the core and steric shielding by the PEG corona. The butyl methacrylate content was tuned to achieve pH-dependent membrane disruption to promote endosomal escape. In this study, several diblock copolymers were shown to have higher stability and transfection efficiency than PEI before and after lyophilization. The diblock copolymer polyplexes had high stability ratios in physiologic conditions, leading to slow reaction-limited aggregation. In contrast, PEI polyplexes had a low stability ratio and fast diffusion-limited aggregation. The best performing diblock copolymer, 40L, had significantly higher transfection than PEI after lyophilization at N/P ratios of 5, 10, and 20. 40L polyplexes that were incorporated into PUR scaffolds as a lyophilized powder achieved higher transfection than polyplexes injected into the scaffold pores for up to three days after cell seeding. These results suggest that PUR scaffolds incorporating diblock copolymer-pDNA polyplexes as a lyophilized powder have high potential for use in local gene therapy applications. Injectable PUR scaffolds can deliver therapeutic pDNA at the point of care. Furthermore, a PUR delivery system for pDNA can be used as a screening tool to test the ability of newly discovered regenerative factors to enhance wound healing in animal models. In summary, the findings described in this dissertation indicate that an injectable PUR delivery system for plasmid DNA is a promising approach to healing skin wounds.

References

[1] Guelcher SA, Li B, Davidson JM. The effect of the local delivery of platelet-derived growth factor from reactive two-component polyurethane scaffolds on the healing in rat skin excisional wounds. Biomaterials 2009;30:3486-94.
[2] Dumas JE, BrownBaer PB, Prieto EM, Guda T, Hale RG, Wenke JC, et al. Injectable reactive biocomposites for bone healing in critical-size rabbit calvarial defects. Biomedical materials (Bristol, England) 2012;7:024112.
[3] Guelcher SA, Li B, Brown KV, Wenke JC. Sustained release of vancomycin from polyurethane scaffolds inhibits infection of bone wounds in a rat femoral segmental defect model. Journal of Controlled Release 2010;145:221-30.
[4] Guelcher SA, Dumas JE, Zienkiewicz K, Tanner SA, Prieto EM, Bhattacharyya S. Synthesis and Characterization of an Injectable Allograft Bone/Polymer Composite Bone Void Filler with Tunable Mechanical Properties. Tissue Engineering Part A 2010;16:2505-18.
[5] Guelcher SA, Dumas JE, Davis T, Holt GE, Yoshii T, Perrien DS, et al. Synthesis, characterization, and remodeling of weight-bearing allograft bone/polyurethane composites in the rabbit. Acta Biomaterialia 2010;6:2394-406.
[6] Adolph EJ, Hafeman AE, Davidson JM, Nanney LB, Guelcher SA. Injectable Polyurethane Composite Scaffolds Delay Wound Contraction and Support Cellular Infiltration and Remodeling in Rat Excisional Wounds. Wound Repair and Regeneration 2011;19:A9-A.
[7] Mikos AG, Kretlow JD, Klouda L. Injectable matrices and scaffolds for drug delivery in tissue engineering. Advanced Drug Delivery Reviews 2007;59:263-73.
[8] Laurencin CT, Khan Y, Yaszemski MJ, Mikos AG. Tissue engineering of bone: Material and matrix considerations. Journal of Bone and Joint Surgery-American Volume 2008;90A:36-42.
[9] Sullivan TP, Eaglstein WH, Davis SC, Mertz P. The pig as a model for human wound healing. Wound repair and regeneration : official publication of the Wound Healing Society [and] the European Tissue Repair Society 2001;9:66-76.
[10] Zhao W, Pizzi A, Fierro V, Du G, Celzard A. Effect of composition and processing parameters on the characteristics of tannin-based rigid foams. Part I: Cell structure. Materials Chemistry and Physics 2010;122:175-82.
[11] Braiman-Wiksman L, Solomonik I, Spira R, Tennenbaum T. Novel insights into wound healing sequence of events. Toxicologic pathology 2007;35:767-79.
[12] Guelcher SA, Hafeman AE, Zienkiewicz KJ, Zachman AL, Sung HJ, Nanney LB, et al. Characterization of the degradation mechanisms of lysine-derived aliphatic poly(ester urethane) scaffolds. Biomaterials 2011;32:419-29.
[13] Segura T, Lei YG, Huang SX, Sharif-Kashani P, Chen Y, Kavehpour P. Incorporation of active DNA/cationic polymer polyplexes into hydrogel scaffolds. Biomaterials 2010;31:9106-16.
[14] Mooney DJ, Hahn LD, Kong H. Polycation Structure Mediates Expression of Lyophilized Polycation/pDNA Complexes. Macromolecular Bioscience 2010;10:1210-5.

CHAPTER VIII

SUGGESTIONS FOR FUTURE WORK

The results of this dissertation have laid the groundwork for the use of injectable polyurethane (PUR) scaffolds with delivery of plasmid DNA (pDNA) for wound healing applications. This chapter presents suggestions for future studies on optimizing injectable PUR scaffolds and developing a PUR plasmid delivery system.

Improve rate of epithelialization

The studies on the use of injectable and implantable PUR scaffolds in rat and pig cutaneous wound models described in Chapters III – V provide evidence that wounds treated with PUR scaffolds have delayed re-epithelialization compared to untreated wounds. Although this delay is transient with no significant differences in epithelialization after 30 days, slow wound closure creates problems such as an increased probability of infection. To accelerate the rate of epithelialization, natural extracellular matrix (ECM) components such as fibrin, collagen, and hyaluronic acid can be applied as a gel or film to the top surface of the PUR scaffold. Fibrin is a major component of the blood clot that forms on the surface of a wound, collagen is the most common structural protein in the ECM, and hyaluronic acid is a glycosaminoglycan found in the ECM. Keratinocytes in the epidermis are more likely to attach to these natural biomaterials than to the more hydrophobic polyurethane. A rat excisional wound model should be used initially to test the effects of a variety of surface treatments on epithelialization in wounds treated with implantable or injectable PUR scaffolds. After the most effective treatments

have been identified in the small animal model, they should be applied to implantable and injectable PUR scaffolds in a porcine excisional wound model.

Use PUR scaffolds in an impaired porcine wound model

In Chapters IV and V, implantable and injectable PUR scaffolds were shown to be biocompatible and support tissue infiltration in porcine excisional wounds. However, with the exception of stenting wounds to reduce unwanted contraction, the scaffolds did not enhance healing. Untreated wound were fully epithelialized by day 30 after surgery. Testing the use of PUR scaffolds in an impaired healing model will better elucidate the capacity of the scaffolds to improve wound healing. One option for creating chronic wound conditions is using an ischemic flap model to restrict blood supply to the wound [1, 2]. Full-thickness excisional wounds developed in the middle of bipedicle flaps results in reduced epithelialization, delayed macrophage presence, and lower blood vessel density compared to non-ischemic wounds [1]. Another option for creating an impaired wound model is inducing diabetes in pigs using streptozotocin injections, but diabetes induction requires more time and higher cost than the ischemic flap model [3, 4]. A study comparing 40% sucrose implants, 40% sucrose injectables, and untreated wounds at days 8, 15, and 30 would require three pigs total with 12 wounds per pig (n = 4). Scaffold impact on epithelialization, wound contraction, cell proliferation and apoptosis, macrophage presence, and blood vessel formation should be assessed.

Optimize release kinetics of pDNA from PUR scaffolds *in vitro*

In Chaper VI, diblock copolymer-plasmid DNA polyplexes achieved transfection after release from PUR scaffolds *in vitro* for up to three days. Differences in transfection efficiency were observed when the wt% of solids (polyplexes + excipient) within the PUR scaffolds was increased from 2.5 to 5 wt%. Since transfection decreased over time and was higher for the 2.5 wt% scaffolds, it is likely that most of the polyplexes were delivered in a burst release within 1-2 days. In applications involving local delivery of therapeutic growth factors, a sustained release for several days after wound healing is desired. Decreasing the excipient wt% within PUR scaffolds has been shown to reduce the burst release and increase the sustained release of biologics [5, 6]. Therefore, the delivery of polyplexes from PUR scaffolds should be tested with lower excipient wt%. A range of excipient concentrations should be investigated (0.5 – 5 wt%). The release kinetics of polyplexes can be measured *in vitro* by labeling pDNA with a PromoFluor-500 fluorescent dye according to the manufacturer's instructions (Promokine, Heidelberg, Germany). PUR scaffolds incorporating polyplexes made with fluorescently labeled pDNA can be incubated in phosphate-buffered saline. The fluorescence in the releasate can be measured with an FL600 microplate reader (Bio-Tek Instruments, Winooski, Vermont), and the fluorescence in the scaffolds can be measured with a Xenogen IVIS imaging system (Perkin Elmer, Waltham, MA). The power law model or Weibull model can be used to characterize the polyplex release profile [5, 6]. After the release kinetics have been optimized, the transfection of cells seeded on PUR scaffolds incorporating pDNA polyplexes can be measured as described in Chapter VI.

Deliver pDNA from PUR scaffolds *in vivo*

Once the release kinetics and transfection efficiency of polyplexes delivered from PUR scaffolds have been optimized *in vitro*, the PUR plasmid delivery system can be tested *in vivo*. Scaffolds can be implanted subcutaneously in mice or rats, and transfection can be monitored by measuring luminescence with the IVIS imager. A wide range of pDNA doses has been used in previous studies investigating delivery of pDNA *in vivo* [7-10], so the dose will likely need to be optimized. A dose response experiment comparing PUR scaffolds incorporating 2-3 different doses of pDNA can be performed. Blank PUR scaffolds without pDNA should be included as a negative control. Polyplexes injected into the muscle of the hind limb can be included as a positive control.

After transfection of luciferase pDNA delivered from PUR scaffolds is confirmed, delivery of pDNA encoding genes for therapeutic proteins can be investigated. One regenerative factor that has potential to enhance wound healing is secreted Frizzled-related protein-2 (sFRP2). Young et al. discovered that sFRP2 is overexpressed in mesenchymal stem cells of MRL mice, a strain with remarkable healing capabilities [11, 12]. They have shown that sFRP2 inhibits the Wnt signaling pathway, leading to increased MSC proliferation and engraftment and decreased apoptosis, senescence, and differentiation to osteogenic and chondrogenic lineages in a subcutaneous wound model in mice [11, 12]. Another study by the Young group showed that daily injections of pyrvinium, a small-molecule Wnt inhibitor, in murine subcutaneous wounds resulted in enhanced granulation tissue formation, cell proliferation, and vascularization compared to wounds without pyrvinium treatment [13]. For delivery of sFRP2 pDNA, a small animal model should be used initially to test proof of concept. An excisional wound model in

diabetic rats would enable investigation of the effects of sFRP2 delivery in an impaired healing model. This model can be used to optimize the sFRP2 pDNA dose and release kinetics for future studies. Finally, an injectable PUR delivery system for sFRP2 pDNA can be investigated in a porcine excisional wound model. The effects of sFRP2 delivery from PUR scaffolds on stem cell recruitment, ECM production and organization, cell proliferation and apoptosis, and vascularization can be determined.

References

[1] Roy S, Biswas S, Khanna S, Gordillo G, Bergdall V, Green J, et al. Characterization of a preclinical model of chronic ischemic wound. Physiological genomics 2009;37:211-24.
[2] Contaldo C, Harder Y, Plock J, Banic A, Jakob SM, Erni D. The influence of local and systemic preconditioning on oxygenation, metabolism and survival in critically ischaemic skin flaps in pigs. Journal of Plastic, Reconstructive & Aesthetic Surgery 2007;60:1182-92.
[3] von Wilmowsky C, Stockmann P, Harsch I, Amann K, Metzler P, Lutz R, et al. Diabetes mellitus negatively affects peri-implant bone formation in the diabetic domestic pig. Journal of clinical periodontology 2011;38:771-9.
[4] Mendes JJ, Leandro C, Corte-Real S, Barbosa R, Cavaco-Silva P, Melo-Cristino J, et al. Wound healing potential of topical bacteriophage therapy on diabetic cutaneous wounds. Wound repair and regeneration : official publication of the Wound Healing Society [and] the European Tissue Repair Society 2013;21:595-603.
[5] Guelcher SA, Li B, Davidson JM. The effect of the local delivery of platelet-derived growth factor from reactive two-component polyurethane scaffolds on the healing in rat skin excisional wounds. Biomaterials 2009;30:3486-94.
[6] Nelson CE, Gupta MK, Adolph EJ, Shannon JM, Guelcher SA, Duvall CL. Sustained local delivery of siRNA from an injectable scaffold. Biomaterials 2012;33:1154-61.
[7] Lei Y, Rahim M, Ng Q, Segura T. Hyaluronic acid and fibrin hydrogels with concentrated DNA/PEI polyplexes for local gene delivery. Journal of controlled release : official journal of the Controlled Release Society 2011;153:255-61.
[8] Segura T, Lei YG, Huang SX, Sharif-Kashani P, Chen Y, Kavehpour P. Incorporation of active DNA/cationic polymer polyplexes into hydrogel scaffolds. Biomaterials 2010;31:9106-16.
[9] Kong HJ, Kim ES, Huang YC, Mooney DJ. Design of biodegradable hydrogel for the local and sustained delivery of angiogenic plasmid DNA. Pharmaceutical research 2008;25:1230-8.
[10] Storrie H, Mooney DJ. Sustained delivery of plasmid DNA from polymeric scaffolds for tissue engineering. Advanced drug delivery reviews 2006;58:500-14.
[11] Alfaro MP, Pagni M, Vincent A, Hill MF, Lee E, Young P. The Wnt Inhibitor sFRP2 Enhances Mesenchymal Stem Cell Engraftment, Granulation Tissue Formation and Myocardial Repair. Blood 2008;112:491-.
[12] Young PP, Alfaro MP, Vincent A, Saraswati S, Thorne CA, Hong CC, et al. sFRP2 Suppression of Bone Morphogenic Protein (BMP) and Wnt Signaling Mediates Mesenchymal Stem Cell (MSC) Self-renewal Promoting Engraftment and Myocardial Repair. Journal of Biological Chemistry 2010;285:35645-53.
[13] Saraswati S, Alfaro MP, Thorne CA, Atkinson J, Lee E, Young PP. Pyrvinium, a Potent Small Molecule Wnt Inhibitor, Promotes Wound Repair and Post-MI Cardiac Remodeling. Plos One 2010;5.

APPENDIX

EXPERIMENTAL PROTOCOLS

General PUR Scaffold Synthesis

Principle:

Procedure for making polyurethane scaffolds for skin wound healing projects.

Before starting:

- Read and understand the MSDS of the reagents listed below
- Personal Protective and Safety Equipment required:
    - Disposable nitrile gloves
    - Appropriate attire according to the Chemical Hygiene Plan (shoes, labcoat, goggles, etc.)

Reagents:

- Polyester triol
- Isocyanate (LTI, LTIPEG, HDIt, etc)
- Turkey red oil
- Calcium stearate
- TEGOAMIN catalyst

Materials and Equipment:

- Water
- Mixing cups
- Spatulas
- Mixer
- Kimwipes
- Pipettes
- Pipette tips
- Balance

Procedure:

1. If delivering biologic such as protein or nucleic acid, lyophilize in mixing cup overnight
    a. **Note:** if lyophilized solids are clumpy, break up with spatula
2. Combine polyol, catalyst(s), water, calcium stearate, and turkey red oil in mixing cup
3. Mix in mixer at high speed (3400 rpm) for 30 sec
    a. **Note:** increase time to 1 min for high molecular weight (>900) polyols

4. Add porogen (salt, sugar, CMC) if applicable and mix 30 sec
5. Add isocyanate and mix 30 sec
    a. **Note:** start timer when mixing begins
6. Let scaffold rise freely in open mixing cup

Clean-up:

1. Collect all glass waste (pipettes, vials, or broken glass) and dispose in the broken glass container (blue cardboard box)
2. Collect all solid waste and dispose in the biohazard waste container (red trash can)

Developing or Modifying PUR Scaffold Formulation

Principle:

Procedure for changing the formulation of polyurethane scaffolds for skin wound healing projects if scaffolds are not forming correctly. Typical problems that are encountered are listed below followed by suggestions for solving them.

Before starting:

- Read and understand the MSDS of the reagents listed below
- Personal Protective and Safety Equipment required:
    - Disposable nitrile gloves
    - Appropriate attire according to the Chemical Hygiene Plan (shoes, labcoat, goggles, etc.)

Reagents:

- Polyester triol
- Isocyanate (LTI, LTIPEG, HDIt, etc)
- Turkey red oil
- Calcium stearate
- TEGOAMIN catalyst

Materials and Equipment:

- Water
- Mixing cups
- Spatulas
- Mixer
- Kimwipes
- Pipettes
- Pipette tips
- Balance

Procedure:

1. High polyol molecular weight
    a. Increase catalyst pphp
    b. Increase water pphp
2. Low polyol molecular weight
    a. Decrease catalyst pphp
    b. Decrease water pphp
    c. Decrease turkey red oil (these foams have a greater tendency to shrink)
3. Mechanical properties are too low
    a. Add or increase gelling catalyst (COSCAT or iron catalyst)
    b. Decrease porosity (see below)

4. Porosity/pore size is too high
    a. Decrease water
    b. Increase turkey red oil
    c. Decrease blowing catalyst (DMAEE or TEGOAMIN33)
5. Porosity/pore size is too low
    a. Increase water
    b. Decrease turkey red oil
    c. Increase blowing catalyst (DMAEE or TEGOAMIN33)
6. Interconnectivity is too low
    a. Increase calcium stearate
    b. Increase water
    c. Decrease turkey red oil
    d. Increase blowing catalyst (DMAEE or TEGOAMIN33)
    e. Add or increase leachable porogen (salt, sugar, CMC)
7. Results are not reproducible
    a. Check humidity
    b. If possible make scaffolds on same day
8. Foams shrink/collapse after some time (minutes to days)
    a. Decrease or eliminate turkey red oil
    b. Increase water
9. Incomplete or slow gelling reaction
    a. Increase catalyst
    b. Add or increase gelling catalyst (COSCAT or iron catalyst)
10. When adding filler, scaffold does not solidy or does not form pores
    a. Decrease filler concentration
    b. Use granular form of filler (larger particles: >100 um) rather than fine powder
11. Filler aggregates or is not evenly distributed throughout scaffold
    a. Break up filler into smaller pieces before adding to scaffold
    b. Instead of mixing in mechanical mixer, mix by hand with spatula and put in mixer briefly (~15 sec) to concentrate PUR mixture at bottom

Clean-up:

1. Collect all glass waste (pipettes, vials, or broken glass) and dispose in the broken glass container (blue cardboard box)
2. Collect all solid waste and dispose in the biohazard waste container (red trash can)

Pig Study Protocol

Principle:

Protocol for preparing implantable and injectable PUR scaffolds for use in pig skin wound healing studies.

Before starting:

- Read and understand the MSDS of the reagents listed below
- Personal Protective and Safety Equipment required:
    - Disposable nitrile gloves
    - Appropriate attire according to the Chemical Hygiene Plan (shoes, labcoat, goggles, etc.)

Reagents:

- Polyester triol (T6C3G1L900)
- LTIPEG
- TEGOAMIN catalyst
- Sucrose (300-500 um)

Materials and Equipment:

- Water
- Mixing cups
- Spatulas
- Syringes
- Mixer
- Kimwipes
- Pipettes
- Pipette tips
- Balance
- Manilla folder
- Razor blades
- Meat slices
- DPBS

Procedure:

Implants

1. Make implants at least 5 days before surgery
2. Make 3.5x3.5x7 cm box out of manila folder
3. Combine T6C3G1L900 polyol, TEGOAMIN33 catalyst (5.46 pphp), and water (5 pphp) in mixing cup
4. Mix in mixer at high speed (3400 rpm) for 30 sec

5. Add sugar beads (300-500 um) at desired concentration (40% or 70%) and mix by hand with spatula for 30 sec
6. Add Ricerca LTIPEG (index = 115) to mixing cup and mix by hand with spatula for 30 sec
7. Use spatula to transfer PUR mixture to manila folder box (this must be done quickly – working time is ~5 min)
8. Allow scaffold to cure overnight
9. Cut scaffold into 2-3 mm thick slices using meat slicer
10. Cut 3x3 cm squares using razor blade
    a. Note: these can be slightly bigger than wound size to allow for adjustments at the surgery
11. Sterilize implants using ethylene oxide
12. Soak in DPBS for 3 days prior to surgery (keep in sterile environment)
13. Immediately before surgery, blot with Kimwipes and place in wounds

Injectables

14. Sterilize liquids with gamma irradiation, sucrose beads with ethylene oxide, and syringes and mixing cups in autoclave
15. Combine T6C3G1L900 polyol and TEGOAMIN33 catalyst (5.46 pphp) in mixing cup
16. Mix in mixer at high speed (3400 rpm) for 30 sec
17. Aliquot enough polyol+TEDA for 1 g batches (or desired batch size) in sterile syringes
18. Aliquot LTIPEG for 1 g batches (or desired batch size) in sterile syringes
19. Aliquot sucrose for 1 g batches (or desired batch size) in sterile mixing cups
20. On day of surgery, add polyol+TEDA to mixing cup with sucrose beads
21. Pipette in water (5 pphp) and mix for 30 sec with spatula
22. Add LTIPEG syringe and mix 30 sec
23. Spread onto wound with spatula

Clean-up:

1. Collect all glass waste (pipettes, vials, or broken glass) and dispose in the broken glass container (blue cardboard box)
2. Collect all sharps (razor blades, needles) and dispose in sharps container (red plastic box)
3. Collect all solid waste and dispose in the biohazard waste container (red trash can)

Histological Analysis Procedures

Principle:

Protocol for taking images of tissue sections, analyzing immunostaining, and performing histomorphometry.

Taking images

1. Check filter, condenser, shutter, and brightness settings on microscope
2. Use Infinity Analyze
3. Use "Area WB" (white balance) under "Capture Control" (select empty area on slide)
4. Adjust exposure, gain, gamma, light source, saturation, hue, brightness, and contrast in the "Imaging control" panel
5. Record these settings for future use to improve image consistency
6. Capture image (camera icon)
7. Save as .bmp to use in Metamorph

Metamorph analysis (histology and histomorphometry)

Applying a threshold

1. Go to Measure > Threshold image
2. Draw a region around area with desired color
3. Click "Add to threshold" in "Threshold Image" window
4. Save threshold for use in other images with same stain/threshold color

Counting cells/objects

1. Load or create a threshold
2. Set threshold state to "Inclusive"
3. Go to Measure > Integrated Morphometry Analysis
4. Adjust filter sizes as desired (note: if limits are not automatically adjusted in results, uncheck and check "Filter" box)
5. Click "Measure" and go to "Summary" tab for results

Measure wound area

1. Draw a "trace region" around desired area
2. Measure granulation tissue area (pink and/or light green) and possibly scaffold area – white)
3. Do not include fibrin clot (dark red) above wound or fat (white) or muscle (reddish brown) below wound
4. Go to Measure > Region Measurements

5. Select/enable “Area” in “Configure” tab
6. Area will be listed in “Measurements” tab

Measure wound length

1. Use trichrome images
2. Draw 3-4 “single lines” horizontally across wound
3. Use mature collagen (dark green) as limits
4. Go to Measure > Region Measurements
5. Select/enable “Distance” in “Configure” tab
6. Distance will be listed in “Measurements” tab

Measure wound thickness

1. Use trichrome images
2. Draw 8-10 “single lines” vertically across wound
3. Measure granulation tissue thickness – do not include fibrin clot (dark red) above wound or fat (white) or muscle (reddish brown) below wound
4. Go to Measure > Region Measurements
5. Select/enable “Distance” in “Configure” tab
6. Distance will be listed in “Measurements” tab

Measure reepithelialization

1. Use trichrome images
2. Draw “traced lines” horizontally across top surface of wound
3. Use separate lines for portions of the surface with and without epithelium
4. Use mature collagen (dark green) as limits
5. Go to Measure > Region Measurements
6. Select/enable “Distance” in “Configure” tab
7. Distance will be listed in “Measurements” tab

In vitro Transfection Experiment Protocol

Principle:

Steps for performing *in vitro* transfection experiments. This protocol can be used to optimize transfection efficiency or compare transfection reagents.

Before starting:

- Read and understand the MSDS of the reagents listed below
- Disinfect surfaces of Biosafety Cabinet with ethanol
- Personal Protective and Safety Equipment required:
    - Disposable nitrile gloves
    - Biosafety cabinet
    - Appropriate attire according to the Chemical Hygiene Plan (shoes, labcoat, goggles, etc.)

Reagents:

- Poly(ethylene glycol)-b-(dimethylaminoethyl methacrylate-co-butyl methacrylate)
- Polyethylenimine (PEI)
- Lipofectamine2000
- Plasmid DNA (ex: pPK-Luc-R3)

Materials and Equipment:

- PEG-b-(DMAEMA-co-BMA)
- Polyethylenimine
- Lipofectamine2000
- Plasmid DNA (ex: pPK-Luc-R3)
- Ethanol
- Citrate buffer (pH 4)
- Carbonate buffer (pH 10.8)
- 2 ml Eppendorf tubes
- 15 ml centrifuge tubes
- 50 ml centrifuge tubes
- Costar 96 well plate (black walls, clear bottom)
- D-luciferin potassium salt
- OPTIMEM
- DPBS
- DMEM

Procedure:

Day 1

1. Plate cells in 100 ul complete media in 96-well plate (see Cell Splitting protocols)
    - IMDF: 10,000 cells/well
    - MDA-MB-231: 20,000 cells/well

Day 2

2. Make polymer-DNA complexes in pH 4 citric acid/sodium citrate buffer
    - Calculate concentrations of plasmid and polymer needed in dilutions based on desired N/P ratio and amount of DNA added per well
        i. Note: I typically use a final DNA concentration of 25 ng/ml and determine the polymer concentration from the N/P ratio
    - Add polymer dilutions to plasmid dilutions in equal volumes and mix gently with pipette
    - Incubate complexes at room temperature for 15 min
    - Add pH 10.8 carbonate buffer to raise pH to 7.4
    - Aspirate media in designated wells and add 100 µL transfection media (ex: complete DMEM, serum-free DMEM, OPTI-MEM, OPTI-MEM + 2% FBS)
        i. Note: serum-free media achieves highest transfection, but serum-containing media is more similar to *in vivo* environment
    - Add complex solution containing 150-300 ng DNA to cells in 96-well plate

3. Make Lipofectamine 2000 positive control
    - Make plasmid dilution in OPTI-MEM
    - Make Lipofectamine 2000 dilution in OPTI-MEM (2.5-5 ul lipo/ug DNA)
    - Add lipo dilution to plasmid dilution and mix well
    - Incubate complexes at room temperature for 20 min
    - Aspirate media in designated wells and add 100 µL OPTI-MEM
    - Add lipo complexes to designated wells

4. Make PEI positive control
    - Calculate concentrations of plasmid and polymer needed in dilutions based on desired N/P ratio and amount of DNA added per well
    - Dilute PEI and plasmid in equal volumes of water
    - Add PEI dilution to plasmid dilution drop wise while vortexing
    - Aspirate media and add 100 µL PEI complexes to designated wells

Day 3

5. 24 h after transfection, aspirate transfection media and replace with complete media
    - Note: this time can be adjusted
6. Add 20 µL of 5 mg/mL luciferin to each well
7. Read luminescence signal on IVIS imager in VUIIS (wait 10 min after adding luciferin)
    - Read time of 5-30 sec depending on intensity
    - Field of view C
    - Use 8x12 grid to quantify signal
8. Immediately after reading luminescence, perform BCA assay following manufacturer's instructions (use RIPA buffer to lyse cells)

Clean-up:

3. Collect all glass waste (pipettes, vials, or broken glass) and dispose in the broken glass container (red box)
4. Collect all solid waste and dispose in the biohazard waste container (red trash can)
5. Aspirate all liquid waste into the liquid waste container
6. Disinfect surfaces of biosafety cabinet with ethanol

PUR Scaffold Synthesis for Plasmid Delivery

Principle:

Protocol for making PUR scaffolds incorporating plasmid for delivery *in vitro* or *in vivo*.

Before starting:

- Read and understand the MSDS of the reagents listed below
- Personal Protective and Safety Equipment required:
    - Disposable nitrile gloves
    - Appropriate attire according to the Chemical Hygiene Plan (shoes, labcoat, goggles, etc.)

Reagents:

- Polyester triol (T6C3G1L900)
- LTIPEG
- TEGOAMIN catalyst
- Calcium stearate
- Poly(ethylene glycol)-b-(dimethylaminoethyl methacrylate-co-butyl methacrylate)
- Plasmid DNA

Materials and Equipment:

- Water
- Mixing cups
- Spatulas
- Mixer
- Kimwipes
- Pipettes
- Pipette tips
- 0.2 um filter
- Balance

1. Sterilize all materials (autoclave mixing cups and spatulas; sterilize calcium stearate with ethylene oxide; filter water with 0.2 um filter; and sterilize polyol, LTIPEG, and TEGOAMIN33 by gamma irradiation)
2. Lyophilize pDNA polyplexes in mixing cup overnight
3. Break lyophilized solids up with spatula (so they will be well dispersed throughout scaffold)
4. Prepare polyol mix by combining T6C3G1L900 polyol, TEGOAMIN33 catalyst (2.73 pphp), water (10 pphp), and calcium stearate (2 pphp) in separate mixing cup
5. Mix in mixer at high speed (3400 rpm) for 30 sec

6. Add Ricerca LTIPEG (index = 115) to mixing cup containing polyplexes
7. Mix in mixer at high speed (3400 rpm) for 30 sec
    a. If solids are not well dispersed, break up with spatula
8. Add polyol mix to LTIPEG and polyplexes
9. Mix in mixer at high speed (3400 rpm) for 30 sec
10. Let scaffold rise freely in open mixing cup in sterile hood

Clean-up:

1. Collect all glass waste (pipettes, vials, or broken glass) and dispose in the broken glass container (red box)
2. Collect all solid waste and dispose in the biohazard waste container (red trash can)
3. Aspirate all liquid waste into the liquid waste container
4. Disinfect surfaces of biosafety cabinet with ethanol

Transfection on PUR Scaffolds *In Vitro*

Principle:

Steps for determining transfection of plasmid DNA incorporated into PUR scaffolds *in vitro*. Cells are seeded on the scaffolds, and luminescence is measured daily.

Before starting:

- Read and understand the MSDS of the reagents listed below
- Disinfect surfaces of Biosafety Cabinet with ethanol
- Personal Protective and Safety Equipment required:
    - Disposable nitrile gloves
    - Biosafety cabinet
    - Appropriate attire according to the Chemical Hygiene Plan (shoes, labcoat, goggles, etc.)

Reagents:

- Poly(ethylene glycol)-b-(dimethylaminoethyl methacrylate-co-butyl methacrylate)
- Plasmid DNA (pDNA)
- Hydroxyprolyl beta-cyclodextrin (HPBCD)
- Polyurethane

Materials and Equipment:

- PEG-b-(DMAEMA-co-BMA)
- Plasmid DNA (ex: pPK-Luc-R3)
- Hydroxyprolyl beta-cyclodextrin (HPBCD)
- PUR scaffolds
- Ethanol
- Citrate buffer (pH 4)
- Carbonate buffer (pH 10.8)
- 2 ml Eppendorf tubes
- 15 ml centrifuge tubes
- 50 ml centrifuge tubes
- Non-tissue culture treated 24-well plates
- D-luciferin potassium salt
- OPTIMEM
- DPBS
- DMEM

Procedure:

Making polyplexes and incorporating into scaffolds

1. Make a 10 mg/ml solution of 40% long (40L) PEG-b-(DMAEMA-co-BMA) in citrate buffer (pH 4)
    - Dissolve polymer in 100% ethanol with a concentration of 100 mg/ml
    - Slowly add citrate buffer until concentration reaches 10 mg/ml
    - Filter polymer solution with a 0.2 μm sterile filter
2. Make a 1 mg/ml solution of pDNA in citrate buffer (pH 4)
3. Add 40L solution to pDNA solution to achieve N/P = 10 (or desired ratio) and mix by pipetting
4. After incubating 15 min at room temp, add carbonate buffer (pH 10.8) to bring pH to 7.4
5. Desalt by filtering with GE Sephadex G-25 Nap-5 columns
    - Note: Larger columns may be required depending on sample volume. NAP-5 columns have maximum sample volume of 0.5 ml.
6. Transfer desalted polyplexes to 2 mL Eppendorf tubes (9 mm diameter) or 1 mL cylindrical Fisher vials (6 mm diameter)
    - If polyplex solution does not fit in vial, use higher polymer and pDNA concentration in steps 1 and 2. Precipitate may form in polyplex solution at high concentrations.
7. Add sterile 10 mg/ml HPBCD to achieve desired HPBCD:40L ratio
8. Freeze at -1 C/min in -80 C freezer (use pink freezing container or Nalgene container with isopropyl alcohol)
9. Lyophilize overnight and incorporate into PUR scaffold as lyophilized powder (see protocol for making PUR scaffolds for detailed instructions)
    - Note: make scaffolds in sterile hood with sterile materials. Polyplex activity is decreased by ethylene oxide exposure, so all components must be sterile prior to scaffold incorporation.
10. After curing, cut scaffolds into pieces with 1-2 mm thickness using razor blades
11. Measure total scaffold mass and mass of each piece to estimate amount of plasmid in each piece
12. Place PUR scaffold pieces in untreated 24-well plate (one piece per well)
13. Store in refrigerator until cell seeding

Seeding cells on PUR scaffolds

14. Begin splitting IMDF cells following instructions IMDF Cell Splitting protocol
15. After aspirating trypsin, disperse cells in 1 mL OPTI-MEM + 2% FBS (instead of 5 mL complete media)
16. Make 1:10 dilution of cells to add to hemocytometer and count cells as described in cell splitting protocol
17. Dilute cells to a concentration of 4,000,000 cells/mL
18. Add cells to PUR scaffolds in untreated 24-well plate
    - For 6 mm diameter scaffolds, add 25 ul (100,000 cells)
    - For 9 mm diameter scaffolds, add 50 ul (200,000 cells)
19. Place plate in 37 C incubator for 30 min
20. Add 1 ml OPTI-MEM + 2% FBS to each well
21. If possible, place plate on shaker in incubator

Measuring luminescence

22. Every 24 h, aspirate transfection media and replace fresh OPTIMEM + 2% FBS + 1 mg/ml luciferin
23. Read luminescence signal on IVIS imager in VUIIS (wait 10 min after adding luciferin)
    - Read time of 0.5-2 min depending on intensity
    - Field of view C
    - Use 4x6 grid to quantify signal

Clean-up:

7. Collect all glass waste (pipettes, vials, or broken glass) and dispose in the broken glass container (red box)
8. Collect all solid waste and dispose in the biohazard waste container (red trash can)
9. Aspirate all liquid waste into the liquid waste container
10. Disinfect surfaces of biosafety cabinet with ethanol

Transfection on PUR Scaffolds *In Vivo*

Principle:

Steps for incorporating plasmid DNA into PUR scaffolds and measuring luminescence produced in animals (mice or rats) containing PUR implants.

Before starting:

- Read and understand the MSDS of the reagents listed below
- Disinfect surfaces of Biosafety Cabinet with ethanol
- Personal Protective and Safety Equipment required:
    - Disposable nitrile gloves
    - Biosafety cabinet
    - Appropriate attire according to the Chemical Hygiene Plan (shoes, labcoat, goggles, etc.)

Reagents:

- Poly(ethylene glycol)-b-(dimethylaminoethyl methacrylate-co-butyl methacrylate)
- Plasmid DNA (pDNA)
- Hydroxyprolyl beta-cyclodextrin (HPBCD)
- Polyurethane

Materials and Equipment:

- PEG-b-(DMAEMA-co-BMA)
- Plasmid DNA (ex: pPK-Luc-R3)
- Hydroxyprolyl beta-cyclodextrin (HPBCD)
- PUR scaffolds
- Ethanol
- Citrate buffer (pH 4)
- Carbonate buffer (pH 10.8)
- 2 ml Eppendorf tubes
- D-luciferin potassium salt
- DPBS
- 1 ml insulin syringes (sterile)
- Nalgene tubing and connector
- 60 ml syringe

Procedure:

Making polyplexes and incorporating into scaffolds

1. Make a 10 mg/ml solution of 40% long (40L) PEG-b-(DMAEMA-co-BMA) in citrate buffer (pH 4)
    - Dissolve polymer in 100% ethanol with a concentration of 100 mg/ml
    - Slowly add citrate buffer until concentration reaches 10 mg/ml
    - Filter polymer solution with a 0.2 μm sterile filter
2. Make a 1 mg/ml solution of pDNA in citrate buffer (pH 4)
3. Add 40L solution to pDNA solution to achieve N/P = 10 (or desired ratio) and mix by pipetting
4. After incubating 15 min at room temp, add carbonate buffer (pH 10.8) to bring pH to 7.4
5. Desalt by filtering with GE Sephadex G-25 Nap-5 columns
    - Note: Larger columns may be required depending on sample volume. NAP-5 columns have maximum sample volume of 0.5 ml.
6. Transfer desalted polyplexes to 2 mL Eppendorf tubes (9 mm diameter – for rat study) or 1 mL cylindrical Fisher vials (6 mm diameter – for mouse study)
    - If polyplex solution does not fit in vial, use higher polymer and pDNA concentration in steps 1 and 2. Precipitate may form in polyplex solution at high concentrations.
7. Add sterile 10 mg/ml HPBCD to achieve desired HPBCD:40L ratio
8. Freeze at -1 C/min in -80 C freezer (use pink freezing container or Nalgene container with isopropyl alcohol)
9. Lyophilize overnight and incorporate into PUR scaffold as lyophilized powder (see protocol for making PUR scaffolds for detailed instructions)
    - Note: make scaffolds in sterile hood with sterile materials. Polyplex activity is decreased by ethylene oxide exposure, so all components must be sterile prior to scaffold incorporation.
10. After curing, cut scaffolds into pieces with 1-2 mm thickness using razor blades
11. Measure total scaffold mass and mass of each piece to estimate amount of plasmid in each piece
12. Store in refrigerator until surgery
13. Implant in subcutaneous pockets or excisional wounds

Measuring luminescence

14. Measure luminescence using IVIS imager in VUIIS at defined time points
15. Make solution of 15 mg/ml luciferin in DPBS (enough to inject 10 ul/g animal)
16. Anesthetize animals using isoflurane setting of 1.5-2 and oxygen flow rate of 2
    - Note: image up to 5 mice or 1 rat at a time
17. Place animal in IVIS with mouth connected to isoflurane
    - Note: make sure both valves from isoflurane dispenser to IVIS are open and any unused openings in IVIS are plugged
    - Note: rat mouths are too big for openings available in IVIS. Connect a Nalgene connector (one side 7/16", on side 5/16") with flexible tubing (5/16"). Connect the other end of the tubing to the opening of a 60 ml syringe. Cut the syringe at the 20 ml mark, and place the rat's mouth in the syringe. Tubing length and position will need to be adjusted to get rat in field of view.
18. Inject luciferin solution i.p. using 1 mL insulin syringe
19. If desired, tape animals' legs down to get better view of scaffolds
20. Read luminescence signal on IVIS (wait 5 min after adding luciferin)
    - Read time of 1-5 min depending on intensity
    - Adjust field of view so all scaffolds are in view
    - Use individual circles to quantify signal

Clean-up:

11. Collect all glass waste (pipettes, vials, or broken glass) and dispose in the broken glass container (red box)
12. Collect all solid waste and dispose in the biohazard waste container (red trash can)
13. Aspirate all liquid waste into the liquid waste container
14. Disinfect surfaces of biosafety cabinet with ethanol
15. Disinfect IVIS and anesthesia box

Splitting Immortalized Murine Dermal Fibroblasts (IMDF)

Principle:

Steps for splitting IMDF cells, plating flasks and well plates, and freezing cells.

Before starting:

1. Aliquot the required amount of media (αMEM or DMEM, 10% FBS, 1% pen-strep)
2. Warm up the DPBS, 0.25% trypsin and media to 37C using the water bath
3. Check cells using the inverted microscope
    - Healthy cells are spindle shaped and branched
    - If cells are rounded, change media or check water in incubator
    - If media is cloudy, cells are contaminated – add bleach and dispose
4. Get out pipettes (10 and 5 ml)
5. If you are freezing cells: prepare a 2 ml freezing tube (screw top with O-ring) and the freezing media (10% DMSO in FBS)

Materials and Equipment:

- Complete media
- DPBS
- Trypsin
- 5 and 10 ml pipettes
- Hemocytometer
- Inverted microscope
- Centrifuge
- Incubator

Procedure:

1. Aspirate old media – discard
2. Add 5-10 mL PBS and rock softly
3. Aspirate PBS
4. Add 1-2 mL trypsin and rock to make sure that its covering all the surface
    a. Incubate at room temp for 1-2 min
    b. While waiting- set up centrifuge
    c. Tap flask sideways to promote detachment of cells
5. Verify that cells are detached
    a. Use the inverted microscope to check morphology – the cells should be round and moving when the flask is tilted
    b. Look at the flask from underneath and rock it – the cells should be seen moving (cloudy)
6. Add 3-4 mL media, mix well
    a. Pipette up the mixture and use it to wash the surface of the flask. This will help remove the cells that are still attached. Repeat this several times.

7. Transfer to a 15 ml centrifuge tube
8. Centrifuge at **500 rpm** for 5 min
    a. While waiting- set up hemocytometer (small coverslip on top- S.G.)
9. Aspirate all supernatant - discard

TO FREEZE:

10. Add DMSO media (~2 mL) – [10% DMSO in FBS]
11. Release cells from tube, suspend
12. Transfer into 2 mL freezing tube
13. Freeze at -80C (leave in freezer overnight)
14. Transfer to vapor phase of nitrogen storage tank (current cells stored in box 4-2)

TO PLATE:

15. Add 5 mL fresh complete media
16. Thoroughly resuspend cell pellet by pipetting up/down
17. Inject 10 uL cell suspension into hemocytometer
18. Count # of cells in 1 mm squares (top, bottom, left, right)
    a. Cells/mL = (average # of cells per square)*(10^4)
19. Seed appropriate density into individual flasks and/or well plates (required cell #/(# of cells/mL))
    b. 1:10 split will reach confluency in 3-4 days
20. Fill flasks to 12 mL complete media (total)

Clean-up:

1. Collect all glass waste (pipettes, vials, or broken glass) and dispose in the broken glass container (red box)
2. Collect all solid waste and dispose in the biohazard waste container (red trash can)
3. Aspirate all liquid waste into the liquid waste container
4. Disinfect surfaces of biosafety cabinet with ethanol

Splitting MDA-MB-231 Cells

Principle:

Steps for splitting MDA-MB-231 cells, plating flasks and well plates, and freezing cells.

Before starting:

1. Aliquot the required amount of media (αMEM or DMEM, 10% FBS, 1% pen-strep)
2. Warm up the DPBS, 0.25% trypsin and media to 37C using the water bath
3. Check cells using the inverted microscope
    - Healthy cells are spindle shaped or triangular (smaller than fibroblasts and MC3T3)
    - If cells are rounded, change media or check water in incubator
    - If media is cloudy, cells are contaminated – add bleach and dispose
4. Get out pipettes (10 and 5 ml)
5. If you are freezing cells: prepare 2 ml freezing tubes (screw top with O-ring) and the freezing media (70% DMEM, 20% FBS, 10% DMSO)

Materials and Equipment:

- Complete media
- DPBS
- Trypsin
- 5 and 10 ml pipettes
- Hemocytometer
- Inverted microscope
- Centrifuge
- Incubator

Procedure:

1. Aspirate old media – discard
2. Add 5-10 mL PBS and rock softly
3. Aspirate PBS
4. Add 2 mL trypsin and rock to make sure that its covering all the surface
    a. Incubate at 37C for 3-5 min
    b. While waiting- set up centrifuge
    c. Tap flask sideways to promote detachment of cells
5. Verify that cells are detached
    a. Use the inverted microscope to check morphology – the cells should be round and moving when the flask is tilted
    b. Look at the flask from underneath and rock it – the cells should be seen moving (cloudy)
6. Add 3 mL media, mix well
    a. Pipette up the mixture and use it to wash the surface of the flask. This will help remove the cells that are still attached. Repeat this a couple of times.

7. Transfer to a 15 ml centrifuge tube
8. Centrifuge at **1000 rpm** for 5 min
    a. While waiting- set up hemocytometer (small coverslip on top- S.G.)
9. Aspirate all supernatant - discard

TO FREEZE:

10. Add DMSO media (~2 mL) – [70% DMEM, 20% FBS, 10% DMSO]
11. Transfer into 2 mL freezing tubes
12. Freeze at -80C (leave in freezer overnight)
13. Transfer to vapor phase of nitrogen storage tank (current cells stored in box 4-2)

TO PLATE:

14. Add 5 mL fresh complete media
15. Thoroughly resuspend cell pellet by pipetting up/down
16. Inject 10 uL cell suspension into hemocytometer
17. Count # of cells in 1 mm squares (top, bottom, left, right)
    c. Cells/mL = (average # of cells per square)*(10^4)
18. Seed appropriate density into individual flasks and/or well plates (required cell #/(# of cells/mL))
    d. 1:10 split will reach confluency in 3-4 days
19. Fill flasks to 12 mL complete media (total)

Clean-up:

1. Collect all glass waste (pipettes, vials, or broken glass) and dispose in the broken glass container (red box)
2. Collect all solid waste and dispose in the biohazard waste container (red trash can)
3. Aspirate all liquid waste into the liquid waste container
4. Disinfect surfaces of biosafety cabinet with ethanol